REPUBLIC OF TURKEY

FIRAT UNIVERSITY

GRADUATE SCHOOL OF NATURAL AND APPLIED SCIENCES

THE EFFECT OF AGEING AND QUENCHING MEDIA ON THERMODYNAMIC PARAMETERS AND STRUCTURE IN Cu-BASED SMAS

MASTER THESIS

Sivar Aziz Baiz

171114106

Department: Physics

Program: General Physics

Supervisor: Assoc. Prof. Dr. Canan Aksu CANBAY

July - 2019

REPUBLIC OF TURKEY

FIRAT UNIVERSITY

GRADUATE SCHOOL OF NATURAL AND APPLIED SCIENCES

THE EFFECT OF AGEING AND QUENCHING MEDIA ON THERMODYNAMIC PARAMETERS AND STRUCTURE IN Cu-BASED SMAS

Sivar Aziz Baiz

Master Thesis

Department: Physics

Supervisor: Assoc. Prof. Dr. Canan Aksu CANBAY

July – 2019

REPUBLIC OF TURKEY

FIRAT UNIVERSITY

GRADUATE SCHOOL OF NATURAL AND APPLIED SCIENCES

FACULTY OF SCIENCE

DEPARTMENT OF PHYSICS

The Effect of Ageing and Quenching Media on Thermodynamic Parameters and Structure in Cu-based SMAs

MASTER THESIS

SIVAR AZIZ BAIZ

(171114106)

Submission Date to the Institute: 27 / 06 / 2019

Thesis Presentation Date: 30 / 7 / 2019

Supervisor: Assoc. Prof. Dr. Canan Aksu CANBAY (FIRAT UNIVERSITY)

Committee: Prof. Fahrettin YAKUPHANOĞLU (FIRAT UNIVERSITY)

Committee: Prof. Enver AYDIN (DICLE UNIVERSITY)

July-2019

DECLARATION

I am presenting the thesis entitled “Production, Characterization, and Improvement of High Temperature Shape Memory Alloys” for fulfilling the requirements of a master’s degree in faculty of sciences, department of Physics. I declare that the presented content of this thesis is my own work with all experimental work, data, graphs, and results.

Sivar Aziz Baiz

ELAZIG - 2019

ACKNOWLEDGMENT

First, I would like to thank my beloved family members, my Father, my mother, and all the others family members for their support throughout my whole life, they encouraged me in the first step for this study and helped me in all the possible ways to succeed. I would like to thank my lovely fiancée "Bahra Arkan" she supported as much as she can and always motivated me to make this happen.

I also would like to express my gratitude to all the friends who supported me with a word or motivation, very especially Mr. Harmand Ali who always stand by me in needs.

Thanks to all the others for their continuous motivation, they supported me so I could achieve my goals with a positive result.

I also would like to express my gratitude to supervisor Assoc. Prof. Dr. Canan Aksu CANBAY who has helped me a lot and guided me along the way towards finalizing this project, her exist made the things easier and she always encouraged me to work hard, learn more and to do better in everything, thanks to all the other lab members who helped even if it was a small contribution.

I would like to thank **FUBAP** (Firat University Scientific Research Projects Unit)**,** for financially support of this research thesis under project **NO: FF 18.21.**

Regards to all…

Thank you all.

Sivar Aziz Baiz

Elazig-2019

TABLE OF CONTENTS

ÖZET

BAKIR BAZLI ŞEKİL HAFIZALI ALAŞIMLARDA YAŞLANDIRMA VE SÖNDÜRME ORTAMININ TERMODİNAMİK PARAMETRELER VE YAPI ÜZERİNDEKİ ETKİSİ

Bu tez çalışmasında, sırasıyla SI 1, SI 2, SI 3 ve SI 4 şeklinde kısa adlandırmaları yapılan Cu-22.22Al-3Fe (at%), Cu-22.79Al-2.59Fe-2.44Mn (at%), Cu-22.79Al-5.42Fe-0.98Mn (at%) ve Cu-21.52Al-3.49Fe-1.95Mn (at%) şeklindeki dört farklı kompozisyona sahip üç ve dört elementli şekil hafızalı alaşımlar (SMAs) ark eritme yöntemi ile üretildiler. Alaşımlardan SI 2 ve SI 4 alaşım numunelerinin bir kısmına ısıl yaşlandırma da yapılıp farklı soğutucu akışkan madde (tuzlu buzlu su, sıvı azot, kaynar su, oda sıcaklığındaki hava) ortamlarına koyularak soğutuldular. Bütün elde edilen farklı SMA numunelerinin karakteristik martensitik dönüşüm sıcaklıkları ile diğer termodinamik parametreleri farklı ısıtma/soğutma hızlarında alınan diferansiyel taramalı kalorimetri (DSC) ve diferansiyel termal analiz (DTA) ölçümlerinin analizleri yapılarak incelendi. Numunelerin hepsinin farklı ısıtma/soğutma hızlarında elde edilen bütün ileri (ısıtma) ve geri (soğutma) eğrileri üzerinde karakteristik martensitik faz dönüşüm pikleri gözlendi. Bu alaşımlardan çoğunun ileri dönüşüm piklerinin 100 °C'nin üzerinde olduğu ve dolayısıyla yüksek sıcaklık şekil hafızalı alaşımı (HTSMA) oldukları belirlendi. Dörtlü-sistem alaşımlarının homojen ve yaşlandırılmış tüm farklı numunelerinin yapısal özellikleri, difraksiyon düzlemleri ve karşılık geldikleri fazlar oda sıcaklığında yapılan X-ışını ölçümlerinin analizleri yoluyla belirlenerek tüm numunelerin oda sıcaklığında β1′(18R) tip martensit faz yapısına sahip oldukları anlaşıldı ve her bir numunenin ortalama kristalit büyüklüğü Debye-Scherrer formülü kullanılarak hesaplandı. Sonuç itibariyle, dört adet homojenize (SI-1, SI-2, SI-3 ve SI-4) ve sekiz adet (dörder adet yaşlandırılmış ve farklı ortamlarda soğutulmuş SI-2 ve SI-4 numuneleri) olmak üzere toplam on iki farklı numune birbirleriyle kıyaslanarak incelenmiş ve aralarında kompozisyon, ısıl yaşlandırma ve farklı ortam soğutmalarına dayalı olarak yapısal özellik ve termodinamik parametrelerinde önemli oranda farklılıklar oluştuğu gözlenmiştir. Özellikle farklı soğutucu ortamların yaşlandırılmış alaşım numuneler üzerine etkileri muazzam seviyelerde olmuştur. Ayrıca, yaşlandırılmış alaşımlar üzerine etkileri birbirine yakın bulunan sıvı azot ve kaynar suyun geleneksel tuzlu buzlu sudan daha hızlı soğutma özelliğine sahip olmaları nedeniyle SMA parametrelerinin modifikasyonu işlemlerinde tuzlu buzlu sudan daha iyi sonuçlar verebileceği görülmüştür.

Anahtar Kelimeler: Şekil hafızalı alaşımlar, Yaşlandırma, Karakteristik dönüşüm, Termal Analiz, Yapısal Analiz.

SUMMARY

THE EFFECT OF AGEING AND QUENCHING MEDIA ON THERMODYNAMIC PARAMETERS AND STRUCTURE IN Cu-BASED SMAS

In this study, four samples of different ternary and quaternary composition SMA as SI-1,SI-2, SI-3 and SI-4 of Cu-22.22Al-3Fe(at%), Cu-22.79Al-2.59Fe-2.44Mn(at%), Cu-22.79Al-5.42Fe-0.98Mn(at%) and Cu-21.52Al-3.49Fe-1.95Mn(at%) was produced respectively by arc melting. The SI-2 and SI-4 samples responded. Quenching the samples were made in four different media (Iced water, boiling water, liquid nitrogen, and room temperature). The characteristic martensitic transformation temperatures and thermodynamic parameters of all the samples investigated by differential scanning calorimetry (DSC) and differential thermal analysis (DTA) are taken at different heating/cooling rates. The characteristic direct martensitic phase transitions of most of the samples occurred at high temperature in heating/cooling DSC curves. Austenite starts the temperature of the samples are above 100°C and that's why these SMAs samples are called high-temperature shape memory alloys (HTSMAs). The X-ray analyses were made at room temperature to determine the structural features, the diffraction planes and their corresponding phases of all the samples. The martensite planes were observed for all the samples resulted from β1′(18R) planes and the average crystallite size was determined for the alloy samples using Debey-Scherrer equation. The results of the new quaternary HTSMAs of different composition (SI-1, SI-2, SI-3, and SI-4) were investigated along with SI-2 and SI-4 treated samples. Quenched samples in different media results were amazing, as the effect of these different media on the thermodynamic and structural properties of the samples were not as it was expected and it is very obvious that the effect of boiling water and liquid nitrogen quenching medium were very close to each other and mostly better than the result of usual iced water quenching medium on the treated samples.

Keywords: Shape memory alloys, Ageing, Characteristic Transformation, Thermal analysis, Structural analysis.

LIST OF FIGURES

Page no.

LIST OF TABLES

Page no.

LIST OF SYMBOLS AND ABBREVIATIONS

Symbols	Meaning
MR	Magneto-rheological
OWSMA	One Way Shape Memory Alloy
TWSMA	Two Way Shape Memory Alloy
T_g	Glass Transition temperature
BCC	Body-Centered Cubic
FCC	Face Centered Cubic
SE	Superelasticity
SME	Shape Memory Effect
SMA(s)	Shape Memory Alloy(s)
SMM(s)	Shape Memory Material(s)
MEMS	micro-electromechanical systems
HTSMAs	High-Temperature Shape Memory Alloys
PSMAs	Polymer Shape Memory Alloys
MSMAs	Magnetic Shape Memory Alloys
SEM	Scanning Electron Microscopy
α	alpha phase
β	Beta phase
G	Gibbs free energy
A_s	Austenite Start
A_f	Austenite Finish
M_s	Martensite Start
M_f	Martensite Finish
T	Temperature
S	Entropy
H	Enthalpy
T_{bend}	The temperature of bended shape film
T_{flat}	The temperature of the flatted shape of the film
E	Total energy
P	pressure
V	volume
Q	Activation energy
LTP	Low-temperature phase
HTP	High-temperature phase
T_o	Equilibrium temperature
SIM	Stress-induced martensite
TIM	Thermally-induced martensite
DSC	Differential scanning calorimetry
M_d	The temperature at the maximum point of the martensite peak
DTA	Differential Thermal Analysis
TGA	Thermogravimetric analysis
EDX	Energy-dispersive X-ray
XRD	X-ray diffraction
FWHM	Full width half maximum

1. INTRODUCTION

The world development pushes toward the smart system. Unique features of smart materials led to the rapid growth of these types of materials and made it very noticeable due to their instant reaction to the environment as it changes, which led to wide use in different areas and applications. This intelligent function of smart materials increased the necessity of micro-controllers, sensors, and actuators to help in decreasing the weight and volume of the components and parts in machines. Magneto-rheological (MR) fluids, shape memory alloys (SMAs), piezoceramics, and electrorheological (ER) fluids are some examples of smart materials [1]. Shape Memory Alloys (SMAs) or Shape Memory Materials (SMM) are a type of Smart Materials, these smart alloys have a special ability to take two different shapes or phases at two different temperatures. Shape memory alloys are metals that have many characteristics like; returning to their original shapes even after several deformations and superelasticity, they can take their first shape after deforming by heating [2], the response of SMA actuators mainly depends upon the way by which heat is added and removed.

SMAs was first found in 1932 by Arne Olander [3] who noticed the reversible transformation of cadmium–gold alloy based on resistivity changes and metallurgical observations, in 1938 Gruninger and Mouradian observed (Cu–Zn) similar changes as in (Cd–Au) brass under thermal fluctuations. ‘‘Shape-Memory’’ for a polymeric dental material term first was described by Vernon in 1941 [4]. Later, Chang and Read in 1951 describe the thermoelastic behavior of Cu–Zn for the first time using the term ‘shape memory effect’. In 1962 the shape memory effect (SME) of Nickel-Titanium (NiTi) alloy exposed the importance of shape memory materials (SMMs) by William Buehler and Frederick Wang [5]. Shape Memory Alloys can have several types according to applications that they are used in such as High-Temperature Shape Memory Alloys (HTSMAs), SMM thin films, Polymer Shape Memory Alloys (PSMAs), Magnetic Shape Memory Alloys (MSMAs). The most used alloys between all the shape memory alloys are NiTi (Nickel-Titanium) due to their effective properties compared to other SMAs, CuZnAl, and CuAlNi due to their low cost as SMA. Adding elements to these SMAs can change properties and characteristics by an increase or a decrease in the Martensite (M_s and M_f) and Austenite (A_s and A_f) temperature or to progress its material properties such as high fatigue life, corrosion resistance, and ductility. martensite phase as the low-temperature phase and austenite as a high-temperature phase in alloys that shows shape memory effect [6]. SMAs have been used in many areas due to high damping capacity, high-power density, solid-state actuation,

fatigue resistance, and durability; they are divided into sections based on their uses in applications as aerospace, automotive, robotics, and biomedical, etc. SMAs are used in micro-electromechanical systems (MEMS), structures and composites [7], mini actuators and even in fashions. In shape memory alloys there are some parameters that we should consider, structural and thermodynamic parameters are needed to see if a sample gave a good shape memory effect or not.

The main thermodynamic parameters in SMAs are M_s and M_f which are the martensite phase start and finish temperature and the austenite start, and finish temperatures are abbreviated as A_s and A_f , the maximum peak temperature is A_{max} and the equilibrium temperature which the temperature that gibs free energy of both phases is in equilibrium. The calculation of hysteresis value shows the austenite finish temperature o martensite start temperature or in another word it shows the range of temperature for the phase transformation to happen. Enthalpy (ΔH) value is to see how difficult a sample is to transform and the entropy (ΔS) value is to see the degree of order and disorder, activation energy calculation is to show if the investigated sample is suitable to what application because higher activation energy shows that this sample needs more energy to transform and vice versa while to know this it is important for the SMAs to be applied. Crystallite size (D) which is calculated through the XRD analysis results is also important to see the SME in an alloy

In this study, new composition Cu-based shape memory was produced, characterized and then improved to have modified futures and to investigate the effect of different media that used for quenching the samples. The effect of each media was studied, and results were unexpected as it showed that using iced water is less effective compared to boiling water or liquid nitrogen. These results may change the aspect of the way of quenching the samples.

2. ALLOYS

2.1. Introduction to Alloys

Earth planet contains most of the materials that we could ever want in somewhere. Earth's store of amazing materials can supply virtually every need. From the Iron and copper that are used for building our civilization, gold we wear like jewelry or the oil that powers machines. More than 90 naturally occurring elements existed and most of them are metals. In their pure forms, they are not always suitable for our needs. For example, iron is amazingly strong, but it can be quite brittle at the same time, and it loses weight as it reacts with its environment. Or aluminum, when it is pure, it's very light but it's too weak and soft to be of much use. That's why most of the "metals" we use are not actually pure at all but alloys: more than one pure metal is combined with other substances to improve their material characteristics like mechanical, thermal, electrical, magnetic properties and so on. They are added to make them harder, stronger, resist more to corrosion, lighter, or advance in their melting temperature. Alloys are widely used in our daily life around from house stuff to the car that we ride even in our body like as it is used in filling teeth (Dental amalgam) to the satellites above and so many others. Alloys are a content of two or more metals or sometimes in some instance, it can contain non-metals even[8]. Alloys produced by manufacturers, mixing molten base metals (the elements that will make up the most significant portions of the needed alloy) with molten supplemental elements. We might express the word alloy as “mixture of metals” but this might be not always true or correct because some alloys contain only a metal which manufactured with a non-metallic material like in cast Iron for example, which can be made from Iron as a basic metal material and carbon which is a non-metallic material[9]. So, the better way to explain alloy is as a two-different chemical element that combined but one should be metal. An alloy is made out of the main metal, the parent metal, or the base metal that most of the alloy is made of. The rest material can be called as an alloying agent, it can be metallic or non-metallic. The agent alloy present in much smaller amount compared to the base material sometimes even less than 1 percent but still makes an alloy and can change the properties of alloy material. Alloys can be sometimes compound (chemically bonded elements) it is mostly atoms of the elements intermixed called solid solutions[10].

2.2. Substitutional alloys

Alloys that consist of more than one chemical element, when the atoms of the base metal alloy are replaced by the agent atoms of the alloy which it can be of the same size as the parent metal or bigger. Usually, the substitution occurs between the nearby element on the periodic table. As in brass which is composite of copper and zinc and 10 to 35 percent of the copper atoms are replaced substitutionally by the atoms of the agent (zinc). Copper and zinc are close on the periodic table and their atom sizes are almost the same as each other [11, 12]. As it is shown in Figure 2.1, the blacks are the main metal and the reds are the agent substitutions among the parent metals in the alloy.

Figure 2.1 Substitution alloy (replacement of the base metal atoms by the agent atoms) [10].

2.3. Interstitial alloys

In this type of alloy, the size of atoms of the base metal should not be the same as the size of the agent atoms, so that the atoms to fit in the spaces between atoms (gaps or interstices) of the parent atoms and we call this interstation alloy[13]. An example of this type of alloy is Steels; as the small numbers of carbon atoms go in between the spaces of the large size atoms of the iron crystalline lattice. This type is shown as figure below in Figure 2.2.

Figure 2.2 Interstitial alloy (as the reds are smaller size agent atoms in between the black base atoms) [10].

3. PHASE TRANSFORMATIONS

Changes in the crystal structure or state in solids to the stable state underneath definite conditions are phase transformations. Phase transformations can be divided into two categories as a result of microstructure change in solids:

a. A new phase replaces the original phase completely
b. Small fractions of the original phase develops, one or more new small phases inside the main phase (minor phases).

3.1. Phase Transformation Energy

As the development of technology in progress, one of the most important tools so that to easier control the process of changing the structural features of materials is phase transformation. Actually, for a phase to transform from one to another, then the phase condition should be very deeply studied so that to predict if any transformation of phases takes place or not. The first (origin) phase should be in more unstable phase as compared to the transformed phase [14]. This can be the key concept for the transformation to occur. Measuring the stability of a material phase can find out throughout mathematical equation in thermodynamics. Gibbs free energy is the one that can measure the stability of a material phase under constant temperature and pressure.

$$G = H - TS \tag{3.1}$$

Where the chemical-free energy (Gibbs free energy) is equal to the difference between the enthalpy(H) of the system and the product of the absolute temperature(T) and the entropy(S) of the system [15]. As the enthalpy (H) is the measure of the system's heat content which can be shown as;

$$H = E + PV \tag{3.2}$$

where (E) is the addition of both the kinetic and the potential energy of the system's atoms (total internal energy of the system) with the product of pressure (P) and system's volume (V).

If there is no opportunity for any change or transformation to happen, then we can say that the system is in its equilibrium condition or the most-stable condition. In a closed system (no change in the system's composition and weight) at constant pressure and

temperature it will stay the same, and in such condition, it has the lowest quantity of Gibbs free energy as it is in stable equilibrium situation;

$$dG = 0 \tag{3.3}$$

As it is shown in Figure 3.1, various atomic configurations of the system are shown along the x-axis to present a graphic explanation for the equilibrium state. The stable equilibrium state represented by the A configuration. Yet, a few more configurations could feature the system, the metastable equilibrium state located at the local minimum area of the Gibbs free energy by B configuration [16].

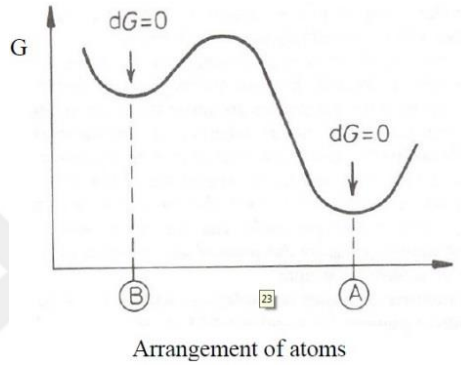

Figure 3.1 Change of Gibbs free energy provoked by different arrangements of atoms. The (A) configuration represents a stable equilibrium with the lowest G), whereas the (B) configuration matches the metastable condition [17].

According to thermodynamics bases, a reaction can take place when there is a possibility of the difference of the Gibbs free energy;

$$\Delta G = G2 - G1 \tag{3.4}$$

As G1 and G2 are the initial and resultant state of the systems Gibbs free energy, this equation is shown as figure below in Figure 3.2. Mostly the system is in an entire range of the metastable state and after the transformation, it is in a stable equilibrium state.

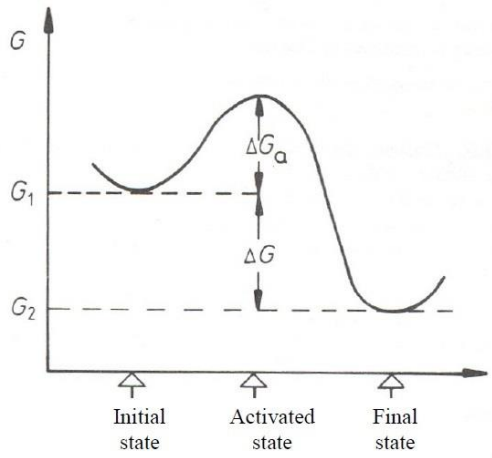

Figure 3.2 Transfer the initial state to the final state via the activated state having greater energy [17].

Due to the difference between the maximum Gibbs free energy between the stable and metastable conditions respectively, some metastable life cycles can be very short in a period while other cases can even show as an infinite period. The rate of transformation can be reduced by this maximum Gibbs free energy representing an energy barrier for the transformation to happen.

The related atom should undergo its activated situation corresponding by the amount of Gibbs energy expressed as (G1 + Ga), before the amount of free energy per atom drops from the level of (G1) to (G2) as (G = G2 – G1) then the driving force for a transformation to occur. The energy is shown in (Figure 3.2) shows a substantial number of atoms in average energy. A non-planed thermal shift of atoms will bring a change of energy per atom as a matter of time and it may be sometimes adequate to permit the atom to reach its activated state. This process is called thermal activation.

In metal alloys, phase transformation may occur via changing temperature, composition or applying external load or pressure. The most effective one between the above ways for a phase to change in metal alloys is changing the temperature by the mean to heat treat it. This means to pass the boundaries of the weight or atomic percentage to temperature phase diagram (Figure 3.3 phase diagrams) of the alloys while heating or cooling. Phase transformation can be one of the ways to gain a more desirable characterized material as it produced, or heat treated. Two of the main dependent factors in the heat-treating process is time and temperature. In some types of phase transformation development in a microstructure of both one- and two-phase alloys have seen a change in the character or number of phases.

3.2. Phases and Phase Transformations Diagrams

The phase of an alloy can be defined as a unique chemical and/or physical characteristic of a part in a system. Each phase in a system has different chemical and/or physical characteristics that it can define some properties of the system at a certain temperature and percentage of the alloys either it is an atomic percentage or weight percentage. A phase of material can contain one or more than one component, a phase with one component is called homogenous system (single-phase) and a phase with multi-component is known as a heterogeneous system (mixture phase).

Phase diagrams are a graphical representation of the combination of pressure, temperature, and composition at equilibrium. In order to design a heat treatment for an alloy to gain some desired mechanical properties, it is important to know how to use these diagrams. According to the number of components, phase diagrams can be divided into groups as shown in the table below:

Table 3.1 The diagram categories on the no. of elements.

Name of System (Diagram)	**Unary**	**Binary**	**Ternary**	**Quaternary**	**Quinary**
No. of Components	One element	Two elements	Tree elements	Four elements	Five elements

As the number of the content elements increase in the diagram goes to more complicated, that why we will explain some about phase diagrams general information on binary phase diagram as an example [18]. Two solid elements as the mixed both can solve one into another or sometimes both into each other and make a solid solution. These solid solution regions on the phase diagram are separated by a line starts on the 100% of the solvent elements side. The diagram is basically between the atomic percentage or weight percentage of the elements on the X-axis and temperature scale on the Y-axis of the diagram. Each element melting point is indicated on the Y-axis cross line of each element aside (Figure 3.3). When the materials are in the liquid region (molten) they are separated from the second region of the diagram which is liquid + solid region, this line called “Liquidus line” as it also is shown in Figure 3.3. As well as the liquid + solid region is separated from the complete solid region with a “Solidus line” and the line that separates the solid solution from the two materials solid-phase called “Solvus line”. A rapid transformation of the liquid phase of both materials to the solid phase of both the materials

goes through a point called Eutectic point (shown as point (a) in Figure 3.3). While point (b) and (c) on the same figure (Figure 3.3) shows the maximum amount one element to solve in the element. The other point reactions on the phase diagram are shown in the table below:

Table 3.2 Point reaction on the phase diagrams

Name of the point conversion phases on the phase diagram	Phases transform
Eutectic	Liquid → Solid (L → A+B element in solid form)
Monotectic	Liquid 1 → Liquid 2 + Solid phase
Peritectic	Liquid + Solid Phase → Another solid phase
Eutectoid	One solid-phase → Two different solid phase
Monotectoid	One solid-phase → Two different solid phase
Peritectoid	Two different solid phases → One solid phase

Note: Eutectoid differs from monotectoid is that includes two phases separated by a miscibility slit or gap, and that why it has different compositions but the same crystal structure.

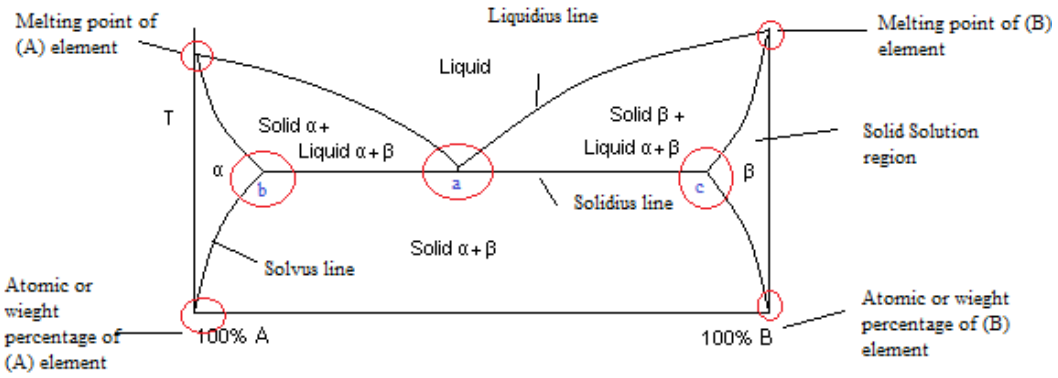

Figure 3.3 A phase diagram sample with some explanation of the diagram[19].

3.3. Phase Transformation Types

Several phase transformations in the processing of materials are important to be achieved, and normally they contain some modification of the micro-level structure. For more clarifying these transformations, it can be divided into three categories. The first classification is the diffusion-dependent transformation where no change in neither the number nor structural composition of the presented phase. Allotropic transformations, recrystallization and grain growth, and solidification of a pure metal include in this type. The second classification phase transformation is also diffusion-dependent transformation but what differs it with the previous one is that there might be some change in the composition and most number of phases: the last microstructure contains two distinct phases [20]. The third type of transformation is diffusionless, a metastable phase is produced.

Martensite phase is in this category of transformation. Martensite is very important in many productions of alloys.

In transforming a phase, usually at least one different phase occurs which is completely different from the previous transformed phase in physical or chemical characteristic and properties or even both. Moreover, phase transformation mostly doesn't happen suddenly, but it starts with the formation of a considerable number of small particles of the new phase(s). This formation increases more and more until it will be completed along with all the new phase(s). The transformation of phases can be divided into two stages: **nucleation** and **growth** [21]. The nucleation name came from the nuclei particle (small particles) of the transformation ongoing phase, which often these particle number is in the range of a few hundred atoms.

3.3.1. Nucleation

There are two types of nucleation, named as homogenous type and heterogeneous type. The difference between these two types can be made as maintained by, the site at which nucleating takes place. Nuclei of the transformed phase form uniformly through the pre-transformed phase for the homogeneous type, while for the heterogeneous type, nuclei form differently at structural inhomogeneities, such as insoluble impurities, container surfaces, dislocations, grain boundaries, and so on [22]. See the nucleation time-dependent graph (Figure 3.4).

3.3.2. Growth

In a phase transformation, the growth step starts once an embryo(nuclei) has run over the (r*), critical size, and turn out to be a stable nucleus. Note that with the growth of the new phase particles, nucleation will continue to arise simultaneously; obviously, nucleation cannot happen in districts that have already transformed into the new phase. Additionally, where particles of the new phase meet, the growth process will terminate in any region meanwhile here the transformation will have got completion. Particle growth happens by long-range atomic diffusion, which normally involves several steps e.g., across a phase boundary, diffusion through the parent phase, and then into the nucleus. Subsequently, the rate of growth G is determined by the diffusion rate, and its temperature dependence is the same as for the diffusion coefficient[23].

$$G = C \exp(-\frac{Q}{kT}) \tag{3.5}$$

C (a preexponential) is independent of temperature and where Q (the activation energy).

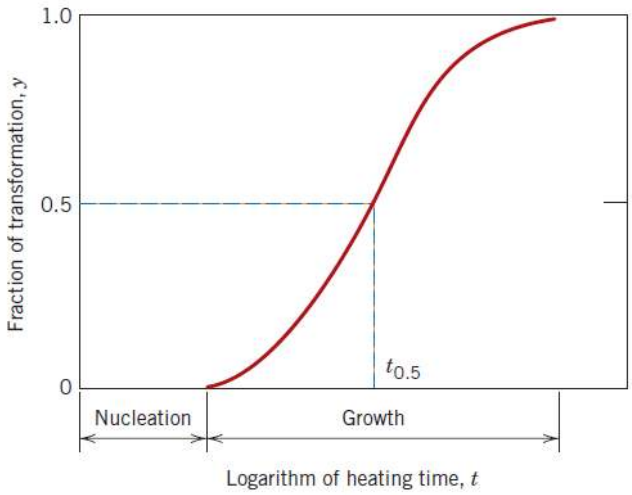

Figure 3.4 Fraction of transformation, nucleation, and growth time-dependent graph [24].

3.4. The General Characteristics of Martensite Phase and Electron Concentration:

The transformations that accompanying with distinct movements of the atoms less than that of one interatomic spacing are called diffusionless transformations. These types of transformations are usually defined as martensite. In materials that are in a non-stable or metastable phase called austenite phase, this type of phase transformation occurs and in steels, it can be seen by rapidly cooling the material after it was heated above the critical temperature in austenite. Owing to the coordinated movement of atoms resembling a shear deformation, this transformation is often defined as a shear or military transformation [25]. This kind of reaction involves a type known as the martensitic transformation, in honor of the German scientist in metallography “Adolf Martens” this transformation named martensite. Those phase changes that involve no long-range diffusion are known as diffusionless transformation. For a period of time, it has been well known that certain metallic systems undergo solid-state phase transformations which involve a change in crystal structure but none in chemical composition or content. The formation of a new phase at such extremely high transformation rates as found in steel and several of other alloys have been observed. The formation of a martensitic structure is instant through a shearing motion of atoms. Martensite is a metastable low-temperature phase (LTP) that forms when a phase

is stable at high temperature (HTP), austenite in steel, is cooled at certain rate thereby suppressing the formation of diffusion-controlled phases [26].

It is often possible to completely suppress the formation of the low-temperature equilibrium phase or the formation of any metastable low-temperature phases whenever an alloy is quenched very rapidly through a solid-state phase transformation range to a low temperature. If a low-temperature phase forms a martensitic alloy, however, it is not possible to suppress its formation even at the highest possible quench rates. Martensite is an equilibrium phase for many alloy systems. Without the need for rapid cooling as in steel, the transformation in these alloys just befalls naturally with very slow cooling rates. Since it is a stable phase, it will not decompose into equilibrium structure upon heating like metastable martensite in steel. Martensite starts to form at cooling in a temperature termed as M_s and the temperature at which the HTP (Austenite) has been completely transformed into martensite finish, termed as M_f. The martensitic reaction reverses to HTP on a heating temperature which is referred to as austenite start temperature; A_s. The reverse reaction is completed at a higher temperature which is termed the austenite finish temperature; A_f, as shown in Figure 3.5.

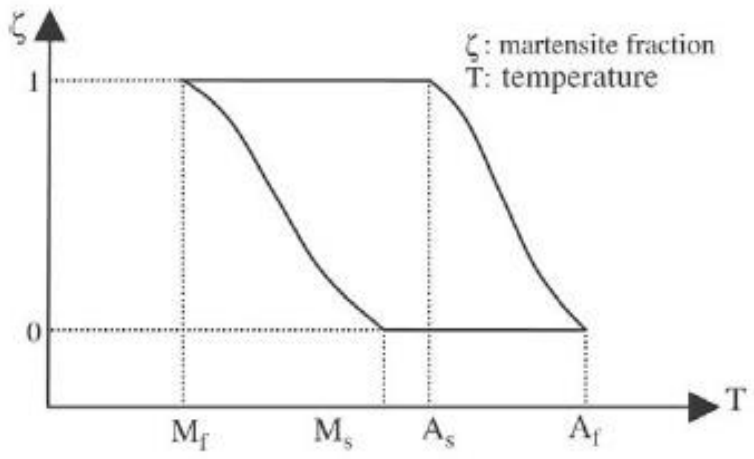

Figure 3.5 Martensitic transformation and it is HTP reverse transformation starts and finish graph temperature [27].

There are generally three different types of kinetics for martensite formation [28]:

a) ***Thermal transformation,*** the reliance of martensite fraction on the transformation temperature is of sigmoidal shape and the portion of austenite transformed depends on the transformation temperature only.

b) ***Athermal transformation*** begins with a fast formation of an important portion of martensite ("burst") – this martensite fraction forms isothermally. Additional formation of martensite upon temperature drop occurs a thermally.

c) ***Isothermal transformation***: Transformations of this type occur in carbon-free iron-based alloys. The martensite fraction at a temperature is proportionate to the time of transformation.

In martensitic transformations, the structure change is produced by a cooperative movement of all atoms. Each crystal transforms into a new crystal of the same composition.. The structure of the HTP and LTP change with each alloy and varies from a simple base center cubic (BCC) to a more complicated face center cubic (FCC) or even more complicated structure which may have as many as 18 atomic layers to define the unit cell. Figure 3.6 clears the above statement. This complexity of crystal structure makes it difficult to describe the relative movements of atoms, often described as shuffling and shear. Probably the most important aspect in martensitic reactions involves a special crystallographic relationship between the martensite and HTP, a semi-coherent interface, which allows a fast growth mechanism to operate. The martensitic transformation involves a simple shear combined with uniaxial tension or compression normal to the habit plane, the plane of lattice on which they are formed [29]. The martensite plane shows two different structure to accommodate the shear of the transformation. These are internally twined and internally slipped substructure.

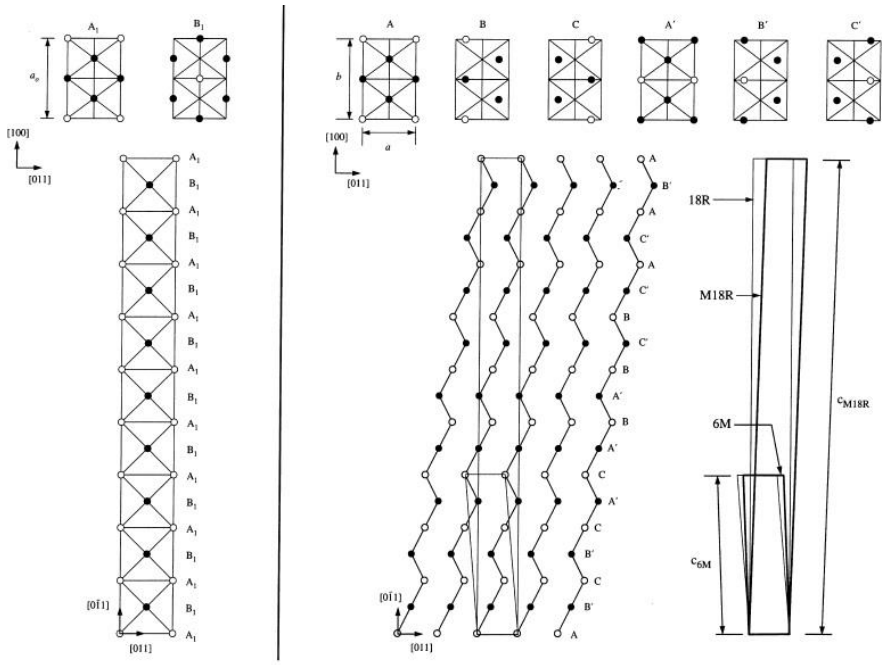

Figure 3.6 BCC transfer to a more complicated atomic structure of 18 layers [25].

3.4.1. Thermoelastic and non-Thermoelastic Martensite Phase

Thermoelastic martensite transformation, as contrasted with non-thermoelastic transformation such as those occurring in most ferrous alloys, are characterized by a comparatively small transformation hysteresis and a small shear component of the transformation. If martensite forms and grows continuously as the temperature decreased and vanish continuously by the exact contrary path as the temperature raised, then thermoelastic martensitic transformation is realized. Transformation is defined as being elastic if during the growth with the resistive energy. As a small shear component, free energy required to start the martensite reaction is low. Upon farther lowering of the temperature extra or additional transformation occurs by both the growth of the old plates and nucleation of new plates. The continued growth of the old plated occurs by a jerky motion. Growth arises over short-range of the area as on the lowering the temperature freer energy becomes available. When free energy available to drive the reaction is counterbalanced by the strain energy generated in then HTP, the growth is terminated. More free energy becomes accessible to form martensite and the plates grow till sufficient strain energy is generated to achieve a new balance, as the temperature is lowered. This type of martensite is called thermoelastic martensite [30]. The increase in elastic limit resulting from the ordered atomic arrangement is closely related to the thermoelastic behavior (Figure 3.7).

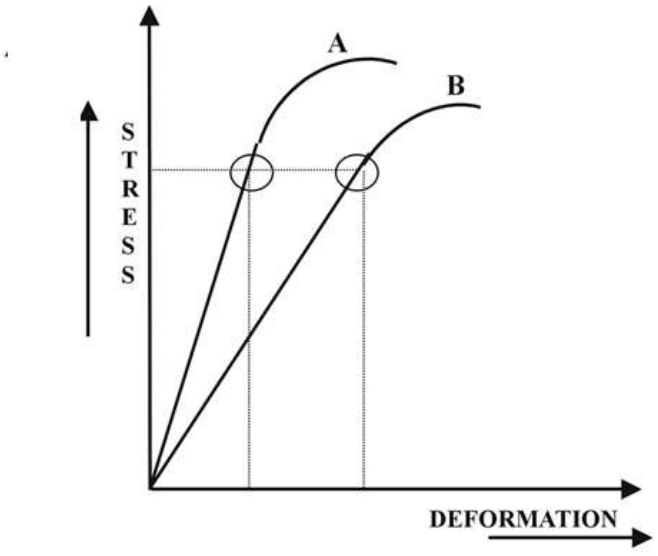

Figure 3.7 Effect of ordering on hypothetical stress-strain curves [31].

Additional stiffness imparted by the ordering inhibits ordinary plastic deformation due to the martensite shape strain and permits the HTP / LTP interface to remain elastically coherent. The parent phase and martensite phase ordering arrangement is important because of the reverse transformation that takes place on heating.

3.4.2. Thermodynamical and Morphological Characters of Martensite Phase

The needed energy to start martensitic transformation can be expressed as T_o–M_s, where T_o is the equilibrium temperature, at which the free energy of martensite and austenite is the same, see Figure 3.8., the point is also shown in the figure when martensite starts transforming back into austenite during annealing. The deformation energy following the development of a small martensitic plate has an important role in the process of nucleation. A thermal reaction may be handled with application of the classical theory of homogeneous nucleation, where;

a) nuclei develop fast upon achievement of *M*s.

b) subcritical nuclei exist in the initial lattice and these become supercritical upon achievement of *M*s temperature.

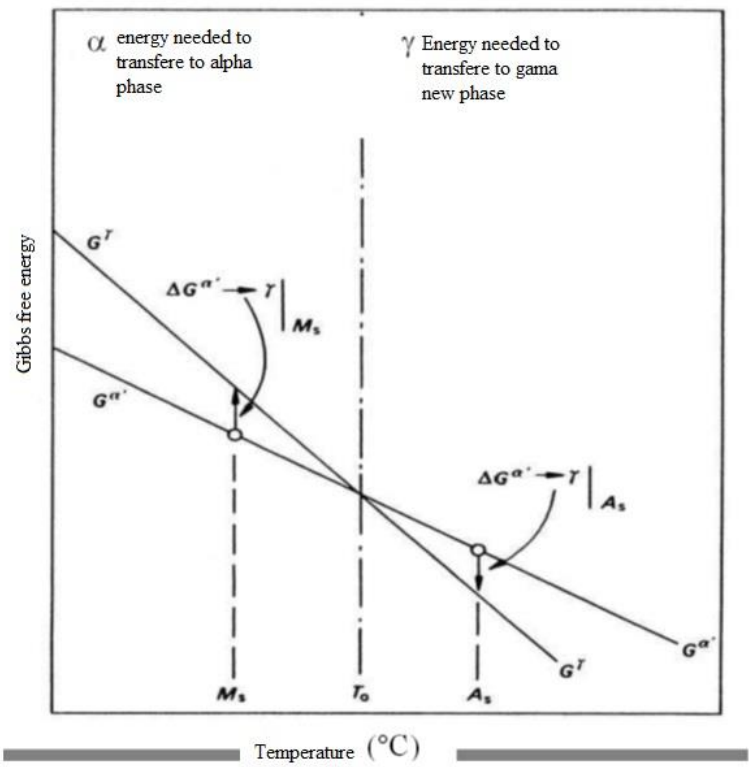

Figure 3.8 Thermodynamic driving force during martensitic transformation (M_s) and reverse transformation (A_s) [27].

The martensite-to-austenite transformation is represented in the isothermal transformation diagram (Figure 3.5). The starting of this transformation is signified by a

horizontal line defined as Martensite start. Two other horizontal and dashed lines, labeled as *M*(d) and *M*(f), indicate (%50) and (%90-%100) percentages of the austenite-to-martensite transformation, Figure 3.8, whereas the temperature increased the growth of the new (β) phase which can be shown as a martensite phase between the austenite parent phase. The change in alloy composition leads to varying in temperatures at which these lines are located and that's due to the difference in their free energy barrier. In the same time, Figure 3.9 explains the morphological phase of martensite. The martensitic transformation is independent of time indicated by the horizontal and linear character of these lines, it is a function only of the temperature to which the alloy is quenched or rapidly cooled. This type of transformation is known as **athermal transformation.** The two main factors for this type of transformation are temperature and external stress. Hence, there are two types of martensite transformations which leads to two different characters; the temperature-induced transformation which causes the SME and the stress-induced transformation which results in the superelasticity.

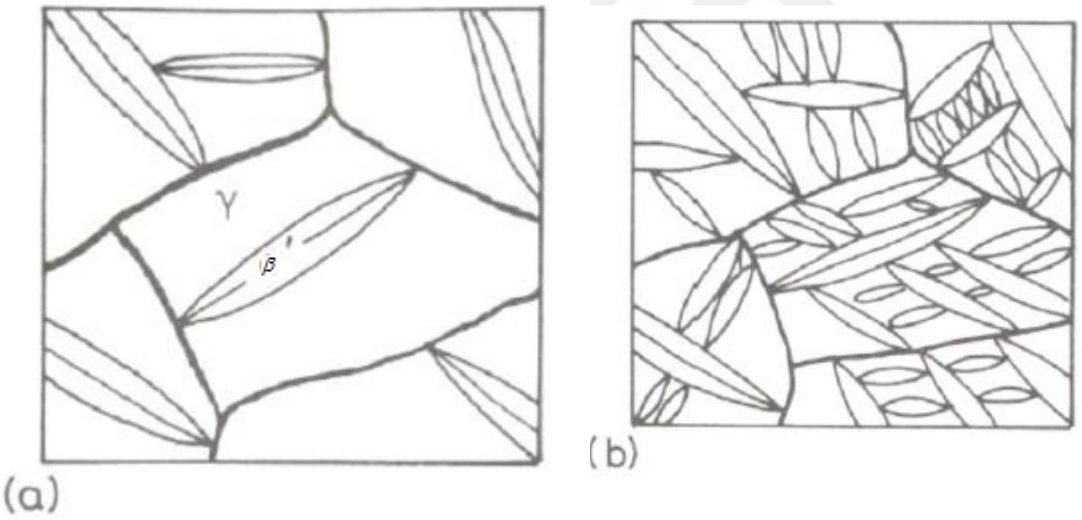

Figure 3.9. (a) Growth of martensitic plates in high-carbon austenite above the M_s temperature. (b) Growth of martensitic plates in high-carbon austenite above the M_d temperature [32].

As the transformation of the martensite phase finish and at this point, we talk about the temperature of the material behind the M_f, we see that under optical micrograph all the nuclei completely grew and show a seed-shaped phase or like a leaf of a tree which is sharped at the ends. The orientation of these leaf-shaped, sometimes Z -shaped, or needle-shaped phase in one grain may change with the other grain, see Figure 3.10.

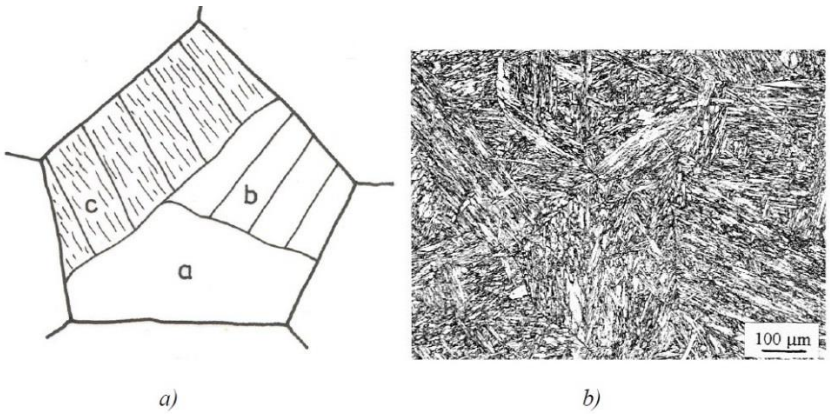

Figure 3.10 An optical micrograph of the martensite shape phase, (a) Different shapes inside one grain. (b) The optical micrograph of more than one grains[32].

3.4.3. Electron Concentration in Martensite Phase

Electrons inside materials play a great role conducting energy inside the materials, alloys which are mostly metallic materials are needed to conduct or sometimes to change their phase due to the amount of energy that is given to the alloys. The martensitic phase of alloys when they go under phase transition by heating or cooling like changing in vibrational entropy is first order, and diffusionless. The entropy change ΔS of the average periodic lattice formation very closely to depend on the number of electrons to a number of atoms or what is called electron concentration (e/a) [8]. Shape memory alloys or better to say Cu-based SMAs undergo martensitic transformation too and they obey Hume Rothery Rules [1]. This rule states that an average number of conduction (valence) electron, electro-negativity, and the atomic size factors, can dominantly control the behavior of alloys. Although impurities reduce the electron mean free path in impure solid materials at high temperature due to collisions and that make the contribution of conduction electrons to small and negligible to the entropy of Cu-based SMAs, effects on a number of physical properties of the alloy and stabilize the phase of close-packet structured alloy. In a study by E. Obrador et al. in 1997 a Cu-Al-Mn shape memory alloy at a particular e/a rate of1.46 value that transforms from 18R to 2H martensitic phases where this value is very close to the eutectoid point's e/a rate and corresponds to the composition for which the bcc phase is stable in the largest temperature range and dependence on this particular e/a value in martensitic transformation gives shape memory effect to alloy [6]. In general, the e/a value for SME to be seen should be between 1.45-1.49 [7].

4. SHAPE MEMORY EFFECT

Shape memory effect is a property that gives a type of material unique characteristics which is reverting to original shape after their shape was deformed as they are heated. It is a diffusionless phase transformation between two different phases. One of the phases occur at a low temperature which is a metastable phase and the other phase arises at high temperature and it is a stable phase [33]. The low-temperature metastable phase is called martensite that gives the main character of shape memory effect. The high-temperature phase which is more stable called austenite (parent phase) of the material. As it was explained in the previous section (section 2. Phase Transformation) stress-induced to the material can also transform the shape, in this case, there is another unique character arise called superelasticity, and when there is a thermal change in the temperature of the material then shape memory effect can be seen. Also, it was explained in the same section pointed to above that when we change the temperature of the materials that show shape memory effect, transformation starts from the austenite parent phase to metastable martensite phase by growing the nuclei of the new phase instantly and this growing continue till all the phase changes to the new phase (Figure 4.1).

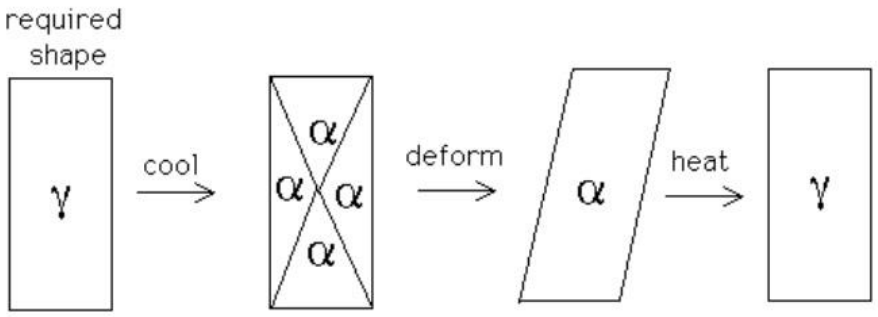

Figure 4.1 Shape memory effect [34].

Note that remembering the original shape can be lost by introducing defects during transformation, like by repeated cycling. The ability of different materials for this cycle changes and this also play a rule in the applications. Critical temperature points in starting the martensite phase and ending of the phase are known as martensite start (M_s) and martensite finish (M_f) as with the austenite start (A_s) and austenite finish (A_f) are important to be known so that the shape memory effect of the material to be ordered as low-temperature shape memory or high-temperature shape memory. Besides that, they show the existence of shape memory effect in material or not. A measure of the difference in the transition temperatures between heating and cooling is called hysteresis (i.e. DT = A_f - M_s),

which is generally defined between the temperatures at which the material is in 50% transformed to austenite upon heating and in 50% transformed to martensite upon cooling [35]. During the choose of SMA material for aimed technical applications, knowing the hysteresis of the material is important, e.g. a small hysteresis is required for fast actuation applications (such as MEMSs and robotics). Larger hysteresis is essential to recall the predefined shape within a large temperature range (such as in pipe joining) [36]. So, this property is important and requires careful consideration. In addition, the transition temperatures referred to identify the operating range of an application. The composition of SMA material, the thermomechanical processing tailored to the SMA and the working environment of the application itself (e.g. applied stress) influence these transition temperatures and the hysteresis loop behavior [37].These transition temperatures can be measured directly or indirectly, with numerous techniques such as differential scanning calorimetry (DSC), electrical resistivity measurement as a function of temperature it can be determined directly and can be indirectly measured from a series of constant stress thermal cycling experiments. These two phases that can be seen in shape memory effect show some different and other times the same properties in different measurements like specific heat capacity and thermal conductivity. The martensite structure is softer and more malleable; i.e. can be readily deformed by application of an external force; whereas the austenite structure is relatively hard and has a much higher Young's modulus [38] (Table 4.1).

Table 4.1 Commercial NiTi SMA physical properties [38].

Property	Symbol	Units	Value	
			Martensite	Austenite
Corrosion Resistance	–	–	Similar to 300 series SS or Ti-alloy	
Density	ρ_D	kg/m^3	6450–6500	
Electrical Resistivity (approx.)	ρ_R	μΩ cm	76–80	82–100
Specific Heat Capacity	c	J/kg K	836.8	836.8
Thermal Conductivity	k	W/m K	8.6–10	18
Thermal Expansion Coefficient	α	m/m K^{-1}	6.6×10^{-6}	11.0×10^{-6}
Ultimate Tensile Strength	σ_{UTS}	MPa	895 (Fully annealed)/1900 (Hardened)	
Young's Modulus (approx.)	E	GPa	28–41	75–83
Yield Strength	σ_Y	MPa	70–140	195–690
Poisson's Ratio	ν	–	0.33	
Magnetic Susceptibility	χ	μemu g	2.5	3.8

4.1. Shape Memory Alloys

Materials that possess shape memory effect are called shape memory alloys, they are a group of metallic alloys that can remember their form (shape and size). They can be back to their original shape via thermal or magnetically effect on the materials that lead to a change in the parent phase of the materials and its shape can be changed.

The material can return to its original form when heated beyond a defined temperature by external or internal heating or magnetic field for MSMAs after it was deformed by loading with an external force. Practically, SMAs can exist in six possible transformations, three different crystal structures (twinned martensite, detwinned martensite, and austenite) and in two distinct phases [39] (see Figure 4.2).

During the process of cooling, the transformation starts to revert to the martensite at martensite start-temperature (M_s) and it completes when it reaches the martensite-finish-temperature (M_f) (Figure 4.3). (M_d) is the maximum temperature at the point above A_f which martensite can no more be induced with stress, and the SMA is like any ordinary metallic material above this temperature permanently deformed. The effect of shape memory in alloys was first discovered by Arne Olander in 1932, and the ‘‘shape-memory’’ term was described first by Vernon in 1941 for his work on polymeric dental material. The importance of shape memory materials (SMMs) was not documented until in 1962 when the shape memory effect (SME) in a nickel-titanium (NiTi) alloy revealed by William Buehler and Frederick Wang [40], which is also known as nitinol (NOL) at the end of the materials name (NiTi) is an abbreviation of the place that the discovery took place in. Since then, the discovery of nitinol, applications of SMAs have been increasing in numerous commercial fields; such as in aerospace, mini actuators and micro-electromechanical systems (MEMS), robotics, industrial applications, and consumer products, structures and composites, automotive, biomedical, and even in fashion. Iron-based and copper-based SMAs, are low-cost and commercially available, but due to they're no stability, brittleness and poor thermo-mechanic performance compared with NiTi alloys, Iron-based and copper-based SMAs are not so preferred in application [41]. The unique properties of SMAs that makes these alloys to be such useful in many areas are more than just recovery of the original shape but properties like large stroke length per weight ratio, electrical actuation and small voltages, noise-free operation, compact and lightweight, rapid reaction at a specified temperature, large recoverable strain per stroke and also it is very intensive to a wide variety of environmental conditions. Based on the application domains, SMAs use can be divided into categories as military use, aerospace, robotics, medical use, etc. Based on starts and finish temperature, input effect on the material to change their shape, chemical compositions and elements that they are made of, as well as the way that they are used in, we can categories shape memory alloys (*e.g.* high-temperature shape memory alloys that they change their phases at high temperature, magnetic shape memory alloys that they can change their shape

as the magnetic field is induced, polymer shape memory alloys that they consist of polymer elements and SMM thin films in which they are produced and used as thin films like NiTi thin films). Compared to other materials SMAs behavior is much more complex and actually, this complicity made it to be so useful in many applications, (Figure 4.4). The various effect was observed through their thermomechanical loading path and their hysteresis loading path. There are many areas that SMAs used in here are two given applications:

First, in aerospace, it is used in actuators structural connectors, vibration-dampers, sealers, release or deployment mechanisms, inflatable structures, manipulators, and the Pathfinder application [42]. If we take electrical actuators (VEASE™, SMArt Clamp™), thermal actuators (Memory safe, circuit breaker, window or louver opener, valves), and heat engines for example actuator or work production, there is motion against a stress and thus work is being done by the memory element on the applications.

Second, the use of SMAs in for implants in dentistry, and a few years later, the first superelastic braces made from a NiTi alloy. SMA made important progress in biomedical after its use in minimally invasive surgery (MIS) [43], and further biomedical applications are industrialized and introduced after the approval of the Mitek surgical product (i.e. Mitek Anchor) for orthopedic surgery.

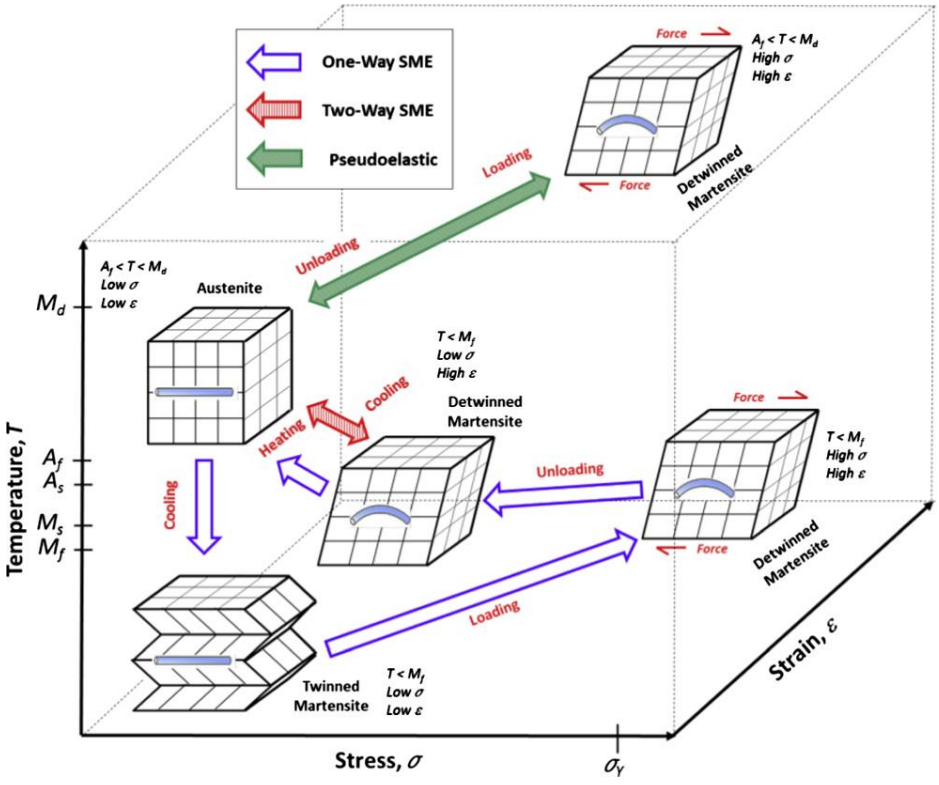

Figure 4.2 SMA phases and crystal structures [39].

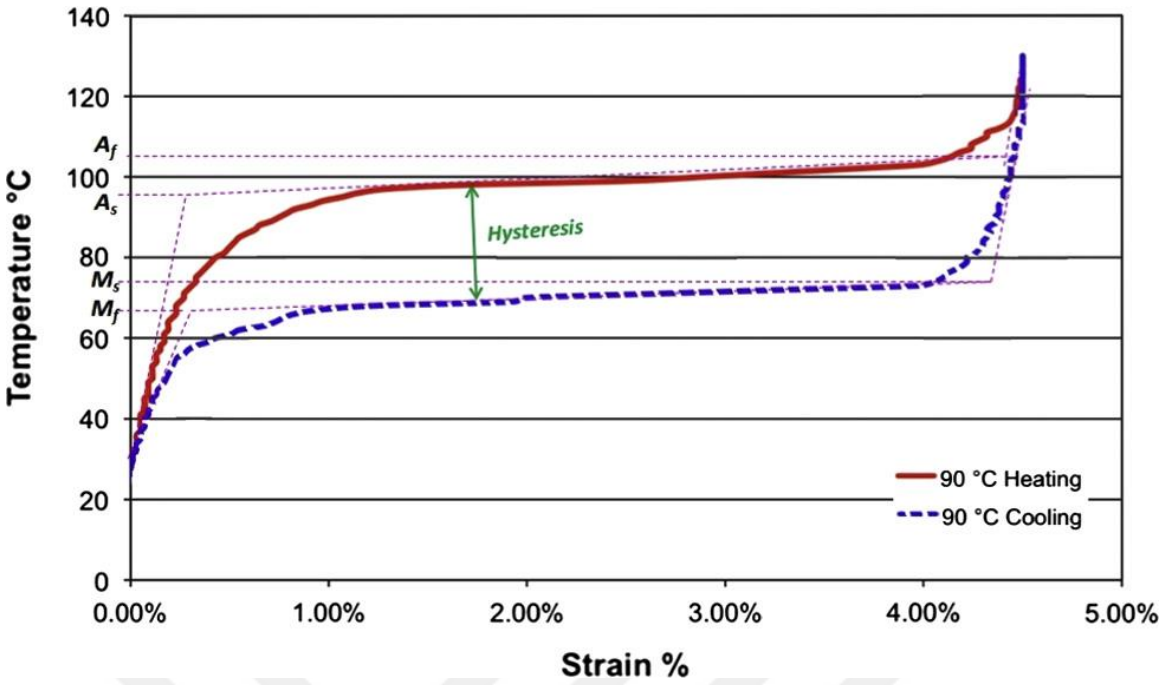

Figure 4.3 Flexinol NiTi SMA (HT) phase transformation [44].

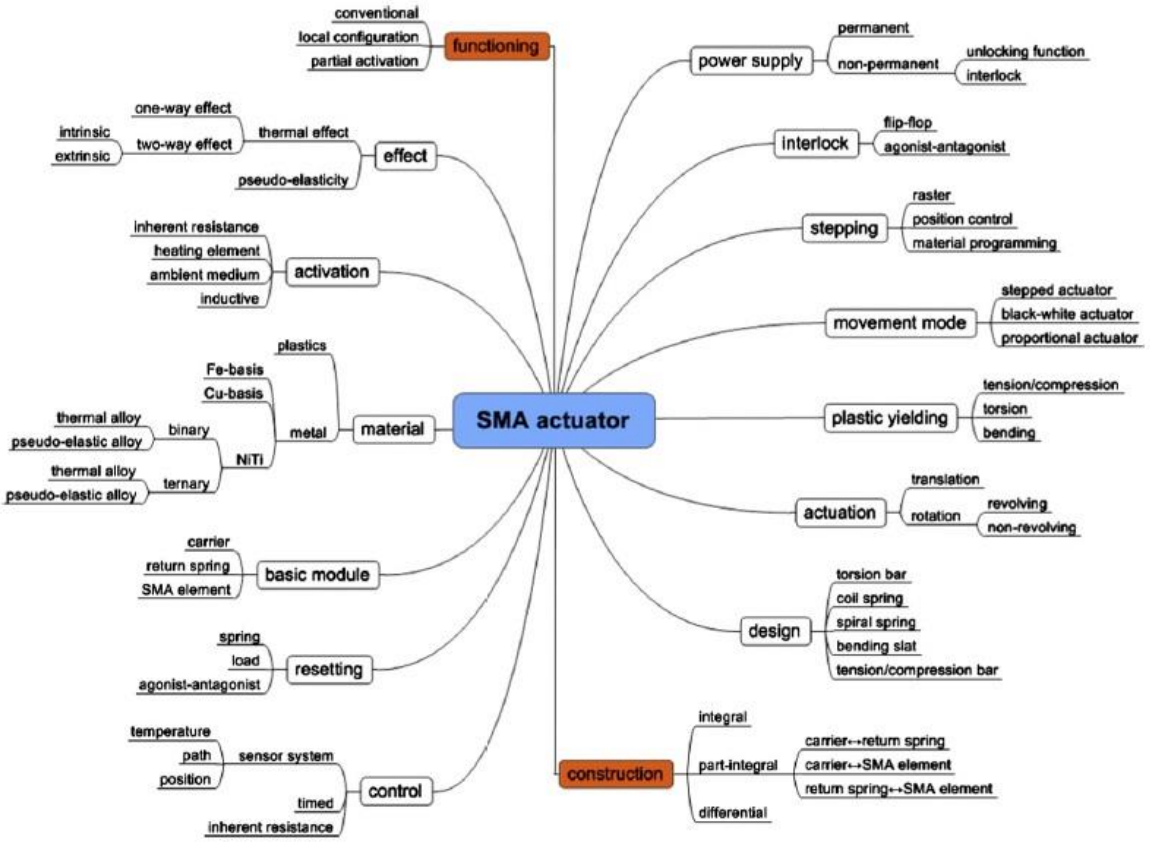

Figure 4.4 SMA actuator element features [45].

4.1.1. One-way Shape Memory Alloys

One-way shape memory effect (OWSME) are those shape memory alloys that in their cold state or low temperature, can be bent and change its shape as it loaded with an external force. They remain in their deformed shape till they are heated above (A_s) where the material's phase from deformed martensite to original austenite. As we decrease the temperature below the (A_f) and the material temperature reaches the (M_s) it takes the other phase but not deformed, in other words, it goes back to the pre-deformed martensite phase. Normally one-way shape-memory materials or alloys are soft, easily deformable when they are in their low temperature and applied with a load, ductile and they stay in the deformed shape as they were deformed, means they don't have the elasticity to return to the pre-deformed shape, but regain its original shape, rigidity or stiffness only after heating it to the high-temperature phase (austenite)[46]. If we looked at Figure 4.2, we can see the one-way shape memory effect path. As it is shown with the blue arrow. The process is four stages in general. Stage one is when the material is in the low-temperature phase and loaded. As the external force or load induces on the material, they start to a twin which means that their atom position changes and that lead to a change in the macroscopic structure of the material. Then when the load is removed, we can name it as the second stage, the materials take a more ordered shape close to the original pre-deformed shape, but still it is in low-temperature mode and can be induced with stress to change the shape macroscopically and this is called detwinning which stands for the reverse process of twining that the material experienced when it was induced with external load in the first stage. In this stage of again loading the material to give it a close pre-deformed shape but not original, and reverse the twinning process, the elastic strain of the material develops [47]. In the third stage, upon unloading the material which is now in detwinned form, again no shape change occurs so that to say it goes elastically to the twinning form. The fourth stage of one-way shape memory alloys is when the material is in detwinned form and then thermally induced. As the temperature of the material increases microstructure of the material due to the thermal energy starts to change and we can see the material goes into the other phase that shape memory alloys obtain in high-temperature condition. The material's phase transforms to austenite and the transformation starts when the temperature is in (A_s) and when the temperature increases and reaches (A_f) the phase completes and retain the original pre-deformed shape. So, heating is the only way to give back the material then pre-deformed shape. The self-accommodating growth of the martensitic variants occurs as the stress-free

cooling of austenite induced. The morphology of the self-accommodate is a characteristic of the alloy's crystallography. Actually, no macroscopic transformation strain produces as those groups' growth, but the multiple interfaces exist in these structures (boundaries between the twinning interface and martensite variants) are really mobile. The heart of shape memory effect is due to this great mobility. The stress level that the detwinning can arise in is far lower than the plastic yield point of the martensite. We can name this deformation as a reorientation of the variants, and it should be at a temperature lower than the (M_f), by this, we mean that the material has to be completely in martensite phase when the load is induced to deform it or twin it [48].

4.1.2. Two-way Shape Memory Alloys

Reversible SME or two-way shape memory alloy (TWSMA) differs with the one-way shape memory alloy in that it can remember two different shapes at two various temperatures while in one-way shape memory alloy it was just one shape, but we could change the shape with external force or load when the material was in martensite and then through heating it regained the original shape. In two-way shape memory alloy, there is no load or external force on the material to give it a differing shape, but the material takes a shape in two different temperature levels (this explained in Figure 4.2 where the red arrow shows this two-way property). The reason that this type of shape memory effect is so unique relies on what is so-called "training" [49]. Training means that to make the material to remember both shapes at different temperatures because when the material is in low-temperature phase "martensite" it has a shape but as it transforms to "austenite" when the temperature increases it instantly forgets the previous shape that it had in martensite. By leaving some marks of the martensite shape in the high-temperature shape, the material can "learn" to reverse back to the original shape of martensite upon cooling.

TWSMA is less applied commercially due to the 'training' requirements and to the fact that it usually produces about half of the recovery strain provided by OWSMA for the same material and it strain tends to deteriorate quickly, especially at high temperatures [44]. Therefore, OWSMA provides a more reliable and economical solution. Various training methods have been proposed and two of them are spontaneous and external load-assisted induction [50]. In two-way shape memory effect, transformation strain is produced during the heating and cooling of the material. This magic was first observed in 1974 by Perkins. Training can be found in so many ways like heat treating the material, inducing a non-homogenous plastic strain at low temperature or even high-temperature phase, aging under

applied stress in austenite, thermomechanical cycling either thermal cycling or isothermal loading mechanically are also possible to progress the TWSME. All these trainings based on repeating the process of deformation and transformation cycle between martensite and austenite phase that makes dislocation in the matrix structure. This mechanism is not completely explained yet and there is no general acceptance about the exact way that facilitates the TWSME. The closest one to be accepted is that this structure makes an anisotropic stress field that supports the formation of the oriented martensite variants. This results in a possible shape change between the phase transformation temperature. It is important to certain the way of training and how long to be done on a material to give it the exact TWSME and not to affect in the opposite in the properties of the material like a non-stabilized two-way memory effect and reduce in the efficiency of training. Sometimes even considering the way and the duration of training but still, it can have some secondary effect like a change in hysteresis size, decrease in the macroscopic transformation strain and change in the transformation temperature. With those secondary effects and other things still, TWSME is most suitable to be used in actuators because no resetting force needed to be considered in design [37].

4.2. Superelasticity

Pseudoelasticity or superelasticity is another magical character of SMAs. This character not like shape memory effect is not in any way related to thermally induced recover of the shape but shows recovery to the original shape after when stress is induced. It gives the material a great elastic property when the alloys are in austenite phase (A_f<T<M_d) and stressed to deform its shape or macrostructure via detwinning it to martensite phase and when it's unloaded, or the stress removed it instantly goes back to austenite parent phase (Figure **4.2**). As a result, up to 8 percent, these materials can reversibly be deformed. As this property is based on the formation of martensite by stress, so it is an isothermal transformation and involves potential energy storage. This property of SMAs gave it a great opportunity to be very widely used in so many applications, especially the elastic actuators and other high elastically strain parts that are very essential to so many applications in various areas like; aerospace, medical, robotics and etc.[51].

4.3. Copper-based Shape Memory Alloys

Cu-based SMAs are extensively studied group of shape memory alloys because of their easy manufacture and low cost. β-phase is the equilibrium-phase at high temperatures in Cu-based alloys, but at low temperatures, it can be booked as a metastable-phase, by means of quenching and throughout quenching, these alloys get more ordered. Below 565ºC the decomposition of the β-phase contains complex transformations. Easy fabrication, low cost together with a reasonable shape memory effect makes these materials to be very widely used in various application [52]. Cu-based alloys can be categorized into three divisions or types of alloys that exhibit shape memory effect in a binary system along with another element (Figure **4.5**);

- Cu-Zn.
- Cu-Al.
- Cu-Sn.

Cu-Zn SMAs are ductile due to their big grain size and a high degree of order that change the properties of the shape memory alloys from transformation temperature to hardness and ductility or toughness besides with other properties that also may change like magnetic, electrical, and so on. Cu-Al SMAs are ductile due to their big grain size and high degree of order, the shape memory effect, in general is due to the high β-phase martensitic transformation in Cu-based alloys., because of the ductility and high (M_s) temperature of this type of Cu-based SMAs, addition of elements in most of the times is prepared to give it a harder structure along with a lower martensite start temperature so that it can be more applicable to various areas. Addition of the third element is essential and choosing the elements should be precise, elements like Be, Mn, and Ni, is effective in stabilizing the β-phase and lowering the martensitic transformation start temperature (M_s) as it was supported by recent studies. Each 1 at. % of Be addition to the Cu–Al binary system resulted in an important decrease of M_s by the amount of -114 K without any change in martensitic transformation nature [53]. Exactly, what happens here is that the β-phase undergo a change in structure A2 to the DO3 structure. This addition which resulted in such a great amount of conserving energy made Cu–Al–Be suitable for many applications [54].

While when Mn is added to the binary Cu-Al differ with another element, it gives it different property and change [55]. Since 1960 Cu–Al–Ni and Cu–Al–Mn SMAs have been intensively studied. Some studies have focused on the effect of quaternary modifications for

the development of grain refinement and ductility of these materials. It was reported by "Sutou et. al and Mallik et. Al" that by adding a quaternary element to Cu–Al–Mn properties like the SME, superelasticity, and damping can be even more improved compared with the ternary Cu–Al–Mn. The grain size can be reduced by the addition of B, Ni, and Si in the alloy [55]. Other elements like cadmium or vanadium can affect the mechanical properties, if it was added to Cu–Al–Mn system an obvious change in thermal and structural variations can be observed such as;

(i) The phase changes caused by heating and cooling the structure.

(ii) The development of the structure analyzed by X-ray and optical microscope analysis was explored [56].

The Cu–Al–Mn–X (X = Ni, Ti) shape memory alloys at the range of 10–12 at. % of aluminum and 4–5 at. % manganese, effects of the alloying elements on the transformation temperatures, and the structural and the magnetic properties of the shape memory alloys. It was observed that due to the addition of nickel into the Cu–Al–Mn system the transformation temperature decreased while the addition of Ti caused an increase in the transformation temperatures [57]. For high-temperature applications owing to its transformation temperatures Cu–Al–Ni SMAs have been highly recommended. Depending on the Al and Ni contents in the alloy. The effect of Ni content is weaker than the effect of Al in CuAlNi SMAs which promote the formation of a different phase and change the transformation temperature.

The Cu-Sn martensitic transformation is not thermoelastic and annealing temperatures can make the shape memory effect to be disappeared. The table of these alloys is given in Figure 4.5 [58]. In the Cu-Sn system, face-centered cubic (fcc) structure is primary α-phase. In contrast, disordered A2 body-centered-cubic (bcc) is the structured content of the Peritectic β-phase. According to the phase diagram, the temperature of the Peritectic reaction α+liquid→β varies between 795.7 ºC and 798 ºC [59].

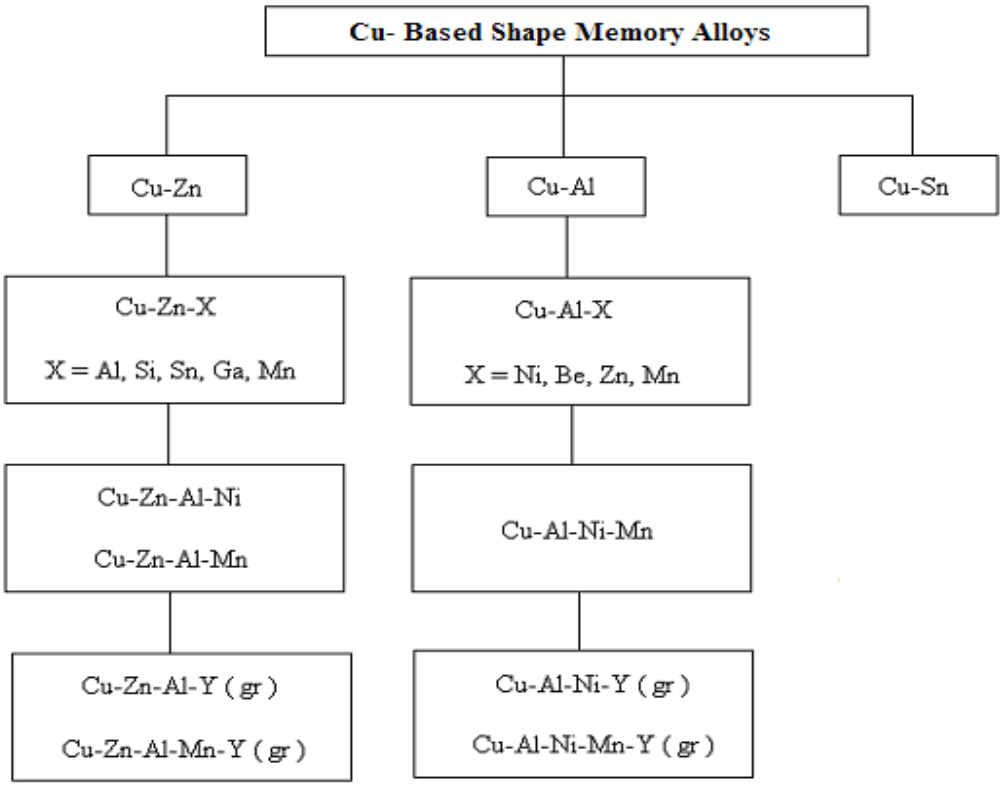

Figure 4.5 Cu based shape memory alloys [59].

5. MATERIALS AND METHODS

5.1. Materials

In this study, we prepared a ternary (Cu-Al-Fe) and 3 quaternary (Cu-Al-Fe-Mn) shape memory alloys with new compositions. These elements of Cu, Al, Fe and Mn powders of impurity of close to (99.99%) for each element in all the samples were measured with their specified percentages and then mixed together. After that the measured samples as powder we pressed with a compressing machine under 1 ton of pressure to have a pellet form, see Figure 5.1. These pellets were together melted under argon atmosphere with Edmund Buehler model arc melting machine, see Figure 5.2, and the results were hard ingot samples. To take the measurements of all the samples, we cut the casted ingots into small pieces of around 4×4x2 mm, 20–40mg of tablets and around 5x3x2 mm, 15-40 mg of flat tablets. After cutting, homogenization of samples was made for 1 hour in the β-phase field to refine atoms to take their original sits which might be affected due to the cutting process when the samples might heat up a little, in Figure 5.3 we can see the used furnace for homogenization process. The samples were briefly named as SI-1, SI-2, SI-3, and SI-4. Differential scanning calorimetry (Shimadzu DSC-60A calorimeter) measurements were taken for all the homogenized samples at heating/cooling rates of 5, 15, 25 and 35˚C/min to see the possibility of finding new shape memory alloys, (see Figure 5.4). All the samples were heat-treated (aged) and then quenched but only SI-2 and SI-4 responded while SI-1 and SI-3 did not show SME behavior on DSC curves and this is caused probably because aging plus quenching diminished the SME properties of SI-1 and SI-3. Heat-treatment (aging) of SI-2 and SI-4 were made at two different temperatures (SI-2 -200^{o}C and SI-4 -250^{o}C) for one hour due to their different DSC results taking martensite temperature in consideration and then quenched. We took four different ways to quench these two samples and from each, we kept a non-quenched reference. Iced water, boiling water, liquid nitrogen, and room temperature were the conditions or quenching media that we put the samples in. Quenching the aged samples rapidly helps in gaining β1′ martensite phase in the parent austenite phase and to avoid having precipitations. By utilizing a Shimadzu DSC-60A calorimeter and its TA-60 WS analysis equipage, the DSC (differential scanning calorimetry) measurements were taken at 5, 15, 25, and 35˚C/min of heating/cooling rates to determine the characteristic martensitic transformation temperatures of the samples. Additionally, the DTA (differential thermal analysis) measurements were taken from room

temperature to 900˚C at the single heating rate of 25˚C/min for each sample by using a Shimadzu DTG-60AH instrument to investigate the phase transitions of the samples at high temperatures, as it is shown in Figure 5.5. The microstructural X-ray (XRD) analysis measurement data of the samples were obtained by using a Rigaku RadB-DMAX II diffractometer with CuKα radiation room conditions to reveal the diffraction planes and determine the crystallite size of each sample, the used device for this purpose can be seen in Figure 5.6.

Figure 5.1 The pressing machine that we used to press the powered elements and make it as pellets.

-a- -b-

Figure 5.2 Edmund Buehler model arc melting machine**.** (a) The plane that we put the pelleted powder on to be melt. (b) The process of melting in the arc-melter.

Figure 5.3 The furnace that's used for homogenizing the samples

Figure 5.4 Shimadzu DSC-60A calorimeter used in this study

Figure 5.5 Shimadzu DTG-60AH that used for this study.

Figure 5.6 Rigaku RadB-DMAX II XRD device used in this study.

5.2. Methods

5.2.1. Energy Dispersive X-ray (EDX)

In this analyzing method, X-ray should be produced and the process of gaining X-ray goes through two steps. The first step is that there is a material and a high energy beam should hit the materials inner shell to get to the electrons on the shells of the material. The high energy makes the electron to be knocked-off to a higher energy level, till now this is one step of the process. The second step of X-ray to be produced starts when the knocked electron leaves a positive hole as a mark behind and that makes the negative electron from higher energy level shells to be attracted and instantly an electron jumps to fill this hole. Jumping from a higher energy level to a lower one means that there is some extra energy that should be released, this releasing comes in the form of some electromagnetic waves or more specifically X-ray (the process is illustrated in Figure 5.7). Each element got a different number of electrons and that makes them different in the production of X-ray [60].

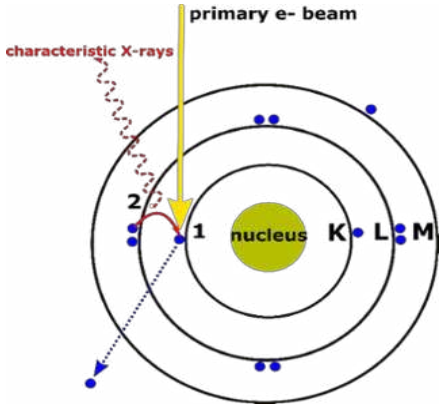

Figure 5.7 X-ray generation process: 1) The energy transferred to the atomic electron knocks it off leaving behind a hole, 2) Its position is filled by another electron from a higher energy shell and the characteristic X-ray is released [61].

A detector is placed at an angle close to the sample and can measure a different amount of photon energy ranges. The higher the solid angle between the sample and the detector, the higher the detection probability. EDX measurement can be qualitative and quantitative, it means it can predict or identify the element and the percentage of the element at the same time from the position and the height of the peaks. Figure 5.8 shows a measurement taken for a sample by EDX.

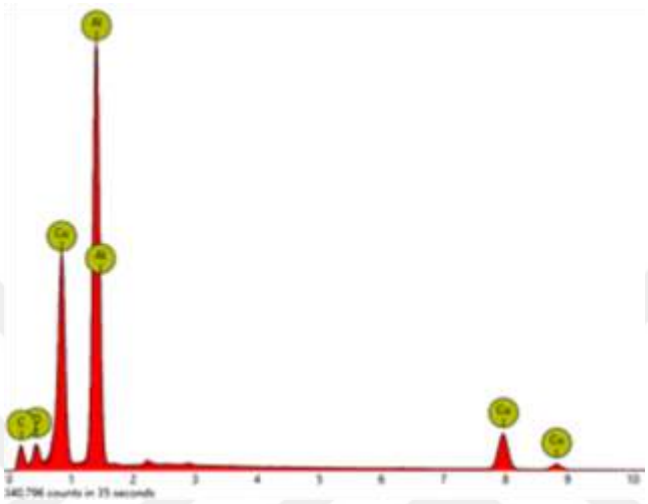

Figure 5.8 Typical EDX spectrum: y-axis depicts the number of counts and x-axis the energy of the X-rays[61].

5.2.2. X-Ray Diffraction (XRD)

X-ray diffraction is now a common technique for the study of atomic spacing and crystal structures. The main parts that consist XRD are three; X-ray tube, sample holder, and a detector to collect the diffracted X-ray. The generation of X-ray is by heating a filament in a cathode tube, as the filament is heated enough then electrons will start to be produced because they have the energy to escape from the atoms outer shell. After the electrons were produced it must be accelerated toward the target or a directed point by applying a voltage and bombarding the target material with electrons. When the electrons have sufficient energy to be able to penetrate the materials inner shell electrons, X-ray spectra are produced. These X-ray spectra consist of several components such as K_α and K_β. Characteristic of the material target (Cu, Al, Fe, Mn) is specified by specific wavelengths. Foils or crystal monochromatic is needed for filtering. CuK_α radiation = 1.5418Å makes copper the most common target material for single-crystal diffraction. Both the sample and the detector are rotated when the X-ray is directed toward the sample target. Constructive interference is produced between the target and the incident ray when conditions satisfy Bragg's

Law ($n\lambda=2d\sin\theta$) and also Figure **5.9** explains the scheme of Bragg's Law. This law explains the wavelength of electromagnetic radiation to the angle of diffraction and the space between the lattice planes in a crystalline sample. The identification of the mineral allowed to be specified by conversion of the diffraction peaks to d-spacing because each mineral has a set of unique d-spacing. To be more accurate this is achieved by comparing the d-spacing with standard patterns of references. This diffraction pattern can be thought of as a chemical fingerprint. What makes XRD be one of the most important non-distractive tools for analyzing almost all the kinds of materials (powder, fluid, and crystals)

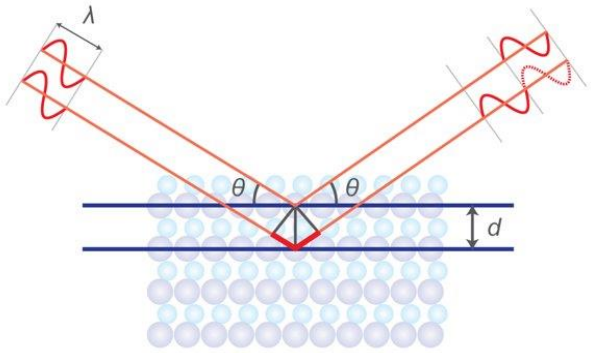

Figure 5.9 The diffraction of X-ray on the planes of the target material [61].

One of the keystones in understanding X-ray diffraction is the Bragg equation, $n\lambda = 2d\sin\theta$. n is an integer, λ is the characteristic wavelength of the X-rays, d is the rows of atoms interplanar spacing, and θ is the angle of the X-ray beam with respect to these planes. In the case of studying of shape memory alloys, there are more to be done with the XRD data. The data of peak intensity, full width half maximum wave, the angle of diffraction, and inter planer spacing (d-spacing) parameters can be provided by XRD analysis. The values of those parameters obtained from XRD analysis data, are used in Debye–Scherrer equation [62] to find the crystallite size of SMAs;

$$D = \frac{0.9\lambda}{B_{1/2}\cos\theta} \tag{5.1}$$

where D is the grain size, λ is the X-ray wavelength, $B_{1/2}$ is the full-width half maximum(FWHM), and $\cos\theta$ is the cosine of the diffracted angle. Among all the given data, the one which has the full intensity (100%) should be chosen because it is the one that has the maximum peak on, see Figure 5.10.

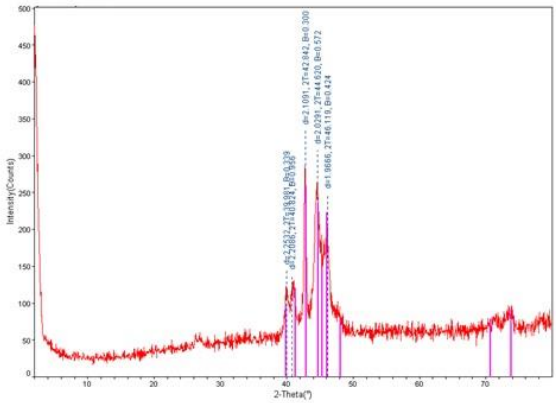

Figure 5.10 The Diffracted pattern of X-ray shown as peaks [63].

5.2.3. Differential Scanning Calorimetry (DSC)

DSC is a device that its measurement is a comparison between two things. The device consists of two places that the process will be applied on, one is the pan (the container or the holder of the sample that supposed to be measured) and the other place or pan contains a reference sample (Figure 5.11). The reason that the reference sample is needed is that the main process is a comparison between the amount of heat is needed to keep both the sample and the reference at the same temperature. The DSC programmed in a way that you must define the rate that you want the sample to heat up or cooled down, by this, we mean that the increase in temperature considered with time (°C/min). The heat capacity of the reference sample should have to be defined well over the range of temperatures to be scanned. This technique was first commercially introduced in 1963 at Pittsburgh Conference on Analytical Chemistry and Applied Spectroscopy, but it was developed before that in 1962 by Watson and M. J. O'Neill [64].

DSC analysis can be used for so many different purposes like to measure specific heat or heat capacity, crystalline phase transition temperature and energy, reaction energy and temperature, latent heat of melting, glass transition temperature, precipitation energy and temperature, oxidation induction times, and melting temperature. DSC analysis measures the abortion and the releasing amount of energy of a sample when it is heated or cooled, providing endothermic (heat absorption) and exothermic (heat evolution) processes data. The materials should be completely non-corrosive so that its data to be measured with DSC. The materials that are needed to be measured should be well studied and carefully properties and reaction of the materials to the sensitive parts of DSC should be taken into consideration.

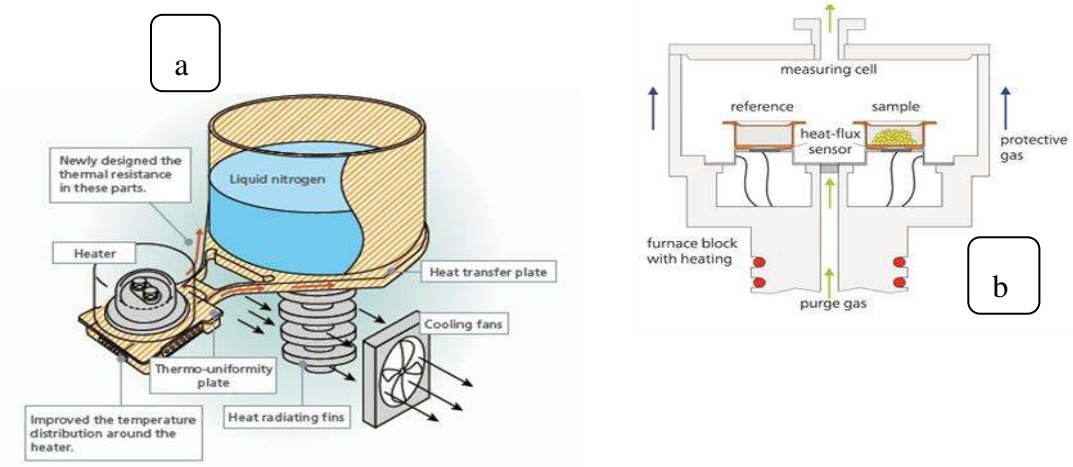

Figure 5.11. (a) DSC device structures and parts. (b) The inner structure of the sample and reference holder [65].

To avoid the reaction between the sample and the pan that sample will be put in one should choose the exact materials that the pans are made from. The range of the temperature is another issue that should be considered for the correct pan. Pans can be made of materials like Cu, Au, Pt, Al, and graphite. As the rate of heating and cooling can be controlled starting from room temperature to the evaluated temperature that is needed. In some cases, the process is needed to start or to go far below zero or the data might have to be taken in a different atmosphere and not air as in usual, in such cases other gases rather than air can be used for both purposes of different atmosphere needed rather than air or to be cooled down far below zero. Atmosphere gases rather than air can be: nitrogen, oxygen, argon, vacuum, and sometimes controlled mixed gases in some exceptional cases. Among all the application and detection that DSC can be used for like; metal alloy melting temperatures and heat of fusion, determine the thermal stability of a material, determine the reaction kinetics of a material, and so many others the one that we have to concentrate on according to shape memory alloys field is the transition of phases [66].

As the temperature of a sample increases it means that energy flows into the sample and this means that the sample is more closely to be activated to reaction or transformation of the phases to happen. The principle that DSC depends on is this. When the temperature increases as a matter of time or when the rate increase to a point equal to the free activation energy it means that the sample is more likely to change its structural form. Absorption of more energy process is called endothermic, and it shows on the DSC diagram as a peak up

sitting down. Emission or releasing energy process is called exothermic, and it's shown on the diagram as an up-word direction peak (to ward up). In this way, by detecting the difference in the amount of heat flow to the sample and the reference differential scanning calorimetry can analyze the absorption as the sample need more heat to stay at the same temperature or the release of heat as it needs less amount of heat to stay in equal temperature with the reference. Physical change (glass transition temperature T_g) is another thing that DSC can detect [64].

SMAs are materials that they can have two different shapes in two various temperature, that means as the temperature increases, they change their structure. This can be seen in DSC diagram measurement as two peaks of endothermic and exothermic. When the temperature increases to a point called A_s the structure starts to change, and the atoms seat changes as the temperature go up more till at a point called A_f the structure is completely different. This new phase is called austenite and it appears as an endothermic peak on the DSC diagram. While when the temperature goes down at a point called M_s the structure starts to change back to a lower metastable phase, this phase completes at a point called M_f and it appears as a release process of heat (exothermic) in shape of a peak on the DSC(Figure 5.12) diagram [67].

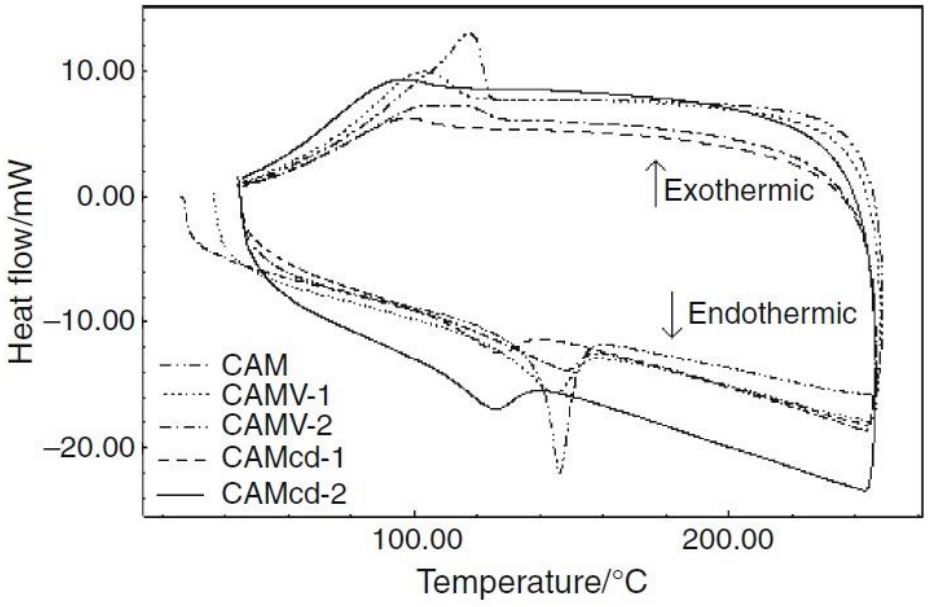

Figure 5.12 DSC curves of the alloys at a heating rate of 15 °C min^{-1} [56].

5.2.4. Thermogravimetric/ Differential Thermal Analysis (TG/DTA)

This is not only one device it is two devices that can measure the data at the same time. Thermogravimetric is the measurement of the loss of weight of the sample that changes with increasing temperature. The rate of the temperature per time is under control and the mass of the sample before measurement, during the measurement, and after the measurement is automatically measured by the equipment itself. The difference in the samples masses the main thing that is concentrated on by the device. Oxidation, crystallization, vaporization, and any other physical or chemical changes that result in sample weight loss or gain. The atmosphere can be nitrogen, helium, air, other gas, or in a vacuum. Varied materials like, metals, composite materials, polymers and plastics, ceramics, and glasses can be analyzed. The form of the material either powder or bulk makes no difference and can be measured [68]. The loss and the gain of mass in TGA measurements explained below;

$$\text{Reactant(s)} \rightarrow \text{Product(s)} + \text{Gas (a mass loss)}$$

$$\text{Gas} + \text{Reactant(s)} \rightarrow \text{Product(s) (a mass gain)}$$

Differential Thermal Analysis in almost the same in measurement with DSC. There is a difference in the technique between the DSC and the DTA. In this measurement, it is the heating flow of the sample and the reference that remains the same. As the temperature increases which leads to change in the structure of the and the thermal properties cause a change in the temperature between the sample and the reference. The maximum temperature that it can reach is 1000°C for most of the TG/DTA devices as it starts from room temperature. The weight of the sample should be between 1 to 150 mg, but the sample with more than 100 mg is preferred for the measurement accuracy while the sensitivity is up to 0.01mg [69]. In Figure 5.13 the endothermic and the exothermic of measurement is shown with DTA. See the illustration structure of TG/DTA in Figure 5.14.

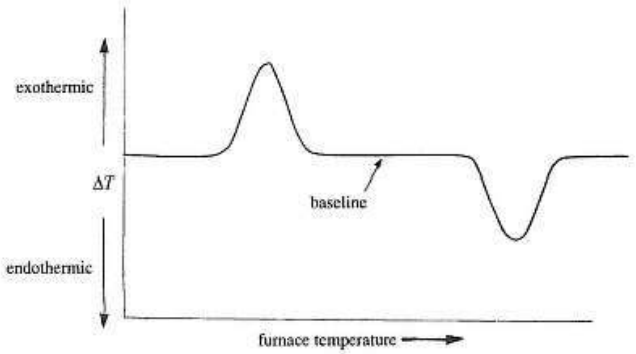

Figure 5.13 The endothermic and the exothermic of the reaction of a sample shown by DTA analysis [70].

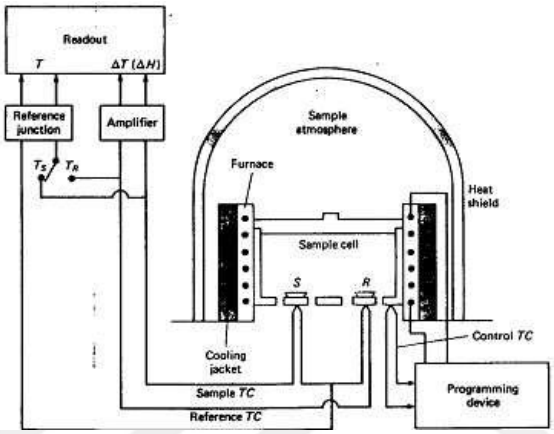

Figure 5.14 The TG/DTA analysis structure [70].

Figure 5.15 belongs to data measurement of a shape memory alloy sample with the analysis of the curves.

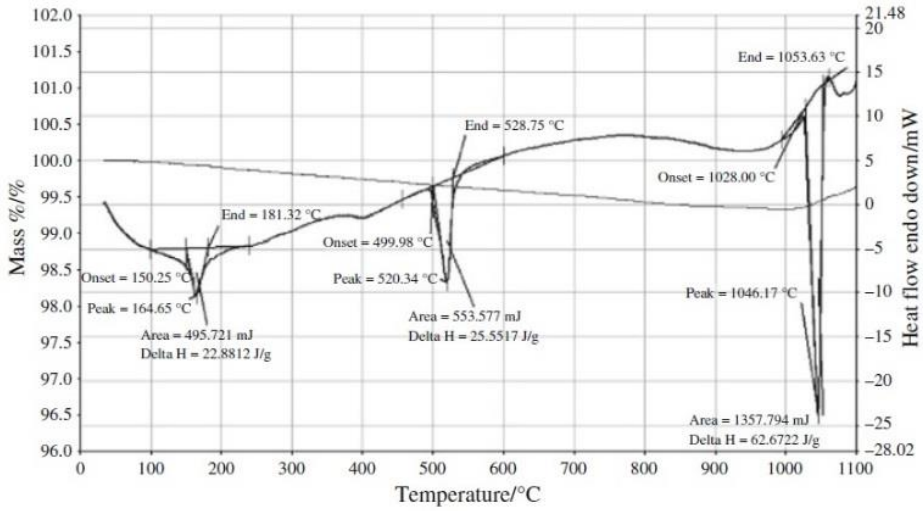

Figure 5.15 TG/DTA curve of the alloy at a heating rate of 20 _C min-1 [53].

6. RESULTS AND DISCUSSION

6.1. Energy Dispersive X-ray (EDX) Measurement Results

The percentages of the elements in each prepared sample were analyzed using Bruker Model energy dispersive X-ray (EDX) instrument at room temperature to detect the chemical composition of the alloy as atomic ratio percentages (at%). SI-2, SI-3, and SI-4 samples are quaternary shapes memory alloys (Cu-Al-Fe-Mn) and the table below shows the atomic percentage of both samples. All the alloys that we have to contain majority Cu percentage, more than 70 (at %) in both samples and that's why we call them Cu-based shape memory alloy. Secondary elements with Cu can be Cu-Zn, Cu-Al or Cu-Sn as shown in Figure 4.5 [60]. Here we have the most common secondary element which is Al with an atomic percentage of more 20 (at %) in all samples as it can be seen in Table 6.1.

Table 6.1 Chemical compositions of elements and electron concentrations.

Alloy ID	e/a	Chemical compositions (at %)			
		Cu	Al	Fe	Mn
SI-1	1.47	74.78	22.22	3	_
SI-2	1.50	72.19	22.79	2.59	2.44
SI-3	1.51	70.81	22.79	5.42	0.98
SI-4	1.48	73.04	21.52	3.49	1.95

6.2. X-Ray Diffraction (XRD) Measurement Results

The structure analyses of all the four pure non-quenching samples and both SI-2 and SI-4 quenched samples at different media were taken using X-ray diffraction. The X-ray measurements were all taken at room temperature by using Rigaku RadB-DMAX II diffractometer. The X-ray measurements can be seen in Figure 6.1 (a) and we can see that β1′(1210) is the highest diffraction peak in SI-1 and SI-2 sample while in SI-3 sample were β1′(122) is the highest and in SI-4 β1′(0022) is the highest peak. In SI-2 samples β1′(1210) peak with an intensity of 3840 a.u at $2\theta=44.54°$ is the highest compared to other samples

peaks, indicating the long period stacking ordered type of monoclinic martensite β1′(M18R). Other samples peaks are 2θ=42.799° with an intensity of 1053 a.u., 2θ=44.659° with an intensity of 913, 2θ=40.258° with an intensity of 671 a.u. for SI-3, SI-1 and SI-4 respectively. The sample with the highest intensity is the neatest and atomic ordered sample. From Figure 6.1 (a) all the peaks, β1′(122) β1′(1210), β1′(2012) and β1′(0022) for all the samples can be seen, except in SI-1 the β1′(0022) can't be seen.

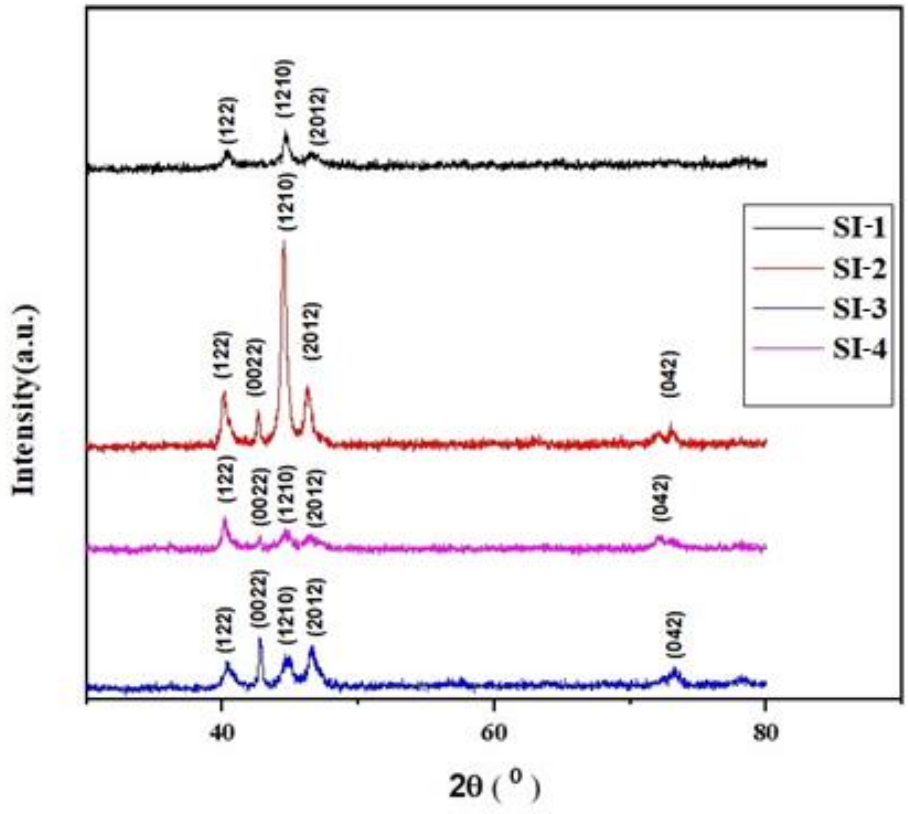

Figure 6.1 (a)X-Ray diffraction patterns of the pure non-quenched SI samples.

X-ray diffraction for both SI-2 and SI-4 quenched samples can be seen in Figure 6.1 (b) and Figure 6.1 (c) respectively. As for SI-2, the long period ordered type of monoclinic β1′(0022) martensite (M18R) plane can be seen very obviously in all the quenching type samples as the highest peak while in the non-quenched sample β1′(1210) is the main highest peak. The main diffracted planes in all the samples are β1′(122), β1′(1210), β1′(2012), γ1′(002) of 2H forms, β1′(042) and α(200)of copper-based precipitations [71, 72]. The intensity peaks of the samples are investigated and as it is noticed that SI-2 β1′(1210) peak with an intensity of 3840 a.u at 2θ=44.54° is the highest compared to other quenched samples peak, 2θ values of; 42.68°with 2325 a.u. iced water, 42.782°with 2300 a.u. liquid

nitrogen, 42.78° with 2080 a.u. room temperature, 42.779° with 1760 a.u. boiling water[28]. Again as well as it is explained that SI-2 homogenized non-quenched sample is the neatest and atomic ordered sample among the other pure homogenized non quenched samples, the same thing goes for SI-2 quenched samples as well.

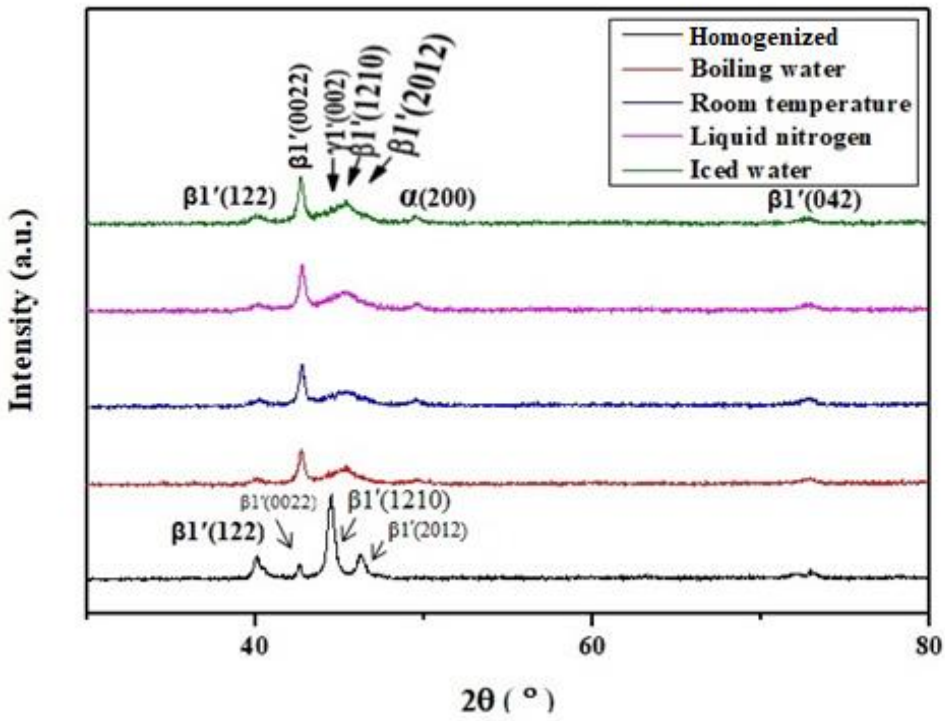

Figure 6.1 (b) X-ray diffraction patterns of SI-2 homogenized non-quenched and quenched samples.

SI-4 homogenized along with different SI-4 quenched samples XRD measurements can be seen in Figure 6.1 (c). The diffracted peaks in all SI-4 samples are the same diffraction planes as in SI-2 samples. 2θ=42.868° with 2990 a.u., 42.7° with 2770 a.u., 42.86° with the intensity of 2585 a.u., 42.82° with 1800 a.u. and 2θ=40.258° with an intensity of 671 a.u. are the located peaks with the intensity of liquid nitrogen, boiling water, iced water, room temperature, and homogenized non-quenched samples respectively. The highest diffracted peak is β1′(0022) for all the quenched samples and β1′(122) is the highest peak for homogenized SI-4 sample. The sample quenched in liquid nitrogen has the highest intensity value which makes it be the most ordered sample.

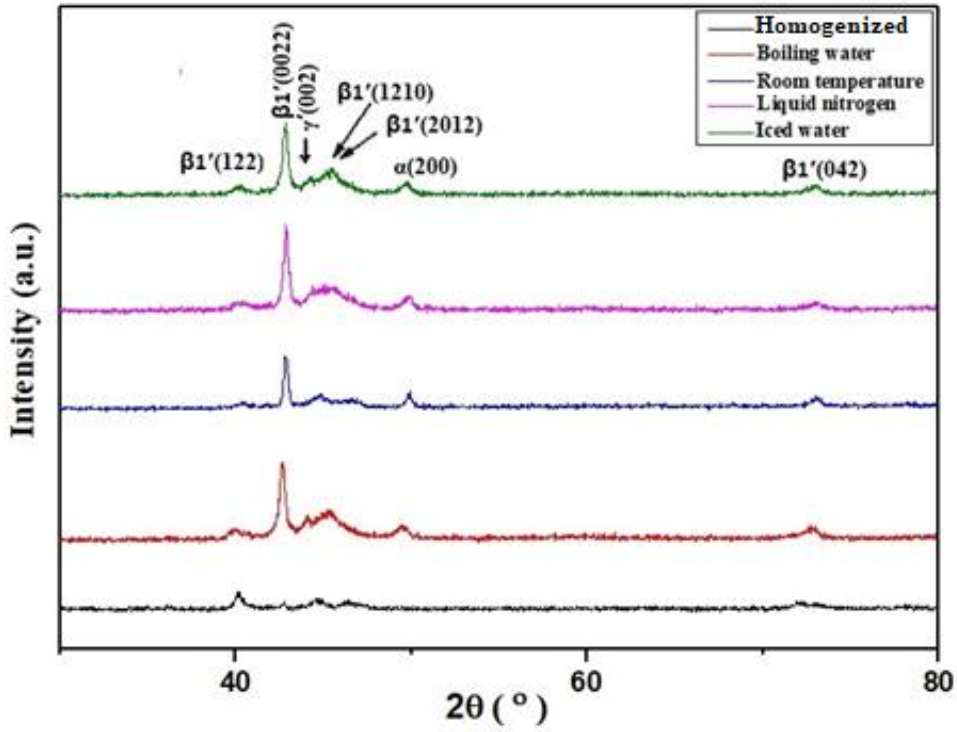

Figure 6.1 (c) X-ray diffraction patterns of SI-4 homogenized non-quenched and quenched samples.

The average crystallite size (D) values of the all samples were calculated by using the XRD data in Debye-Scherrer equation (5.1) [63] here; λ is the wavelength of the X-ray CuKα radiation (λ=0.15406nm), $B_{1/2}$ is the peak full width at half maximum (FWHM) and θ is the Bragg angle of diffraction. The crystallite size values were obtained for SI-1, SI-2, SI-3, and SI-4 samples are 16.21nm, 20.029nm, 14.43nm and, 16.84nm, respectively. As it is obvious that sample SI-2 has the largest crystallite size and smallest crystallite size belong to SI-3 which can be seen in Figure 6.2 (a).

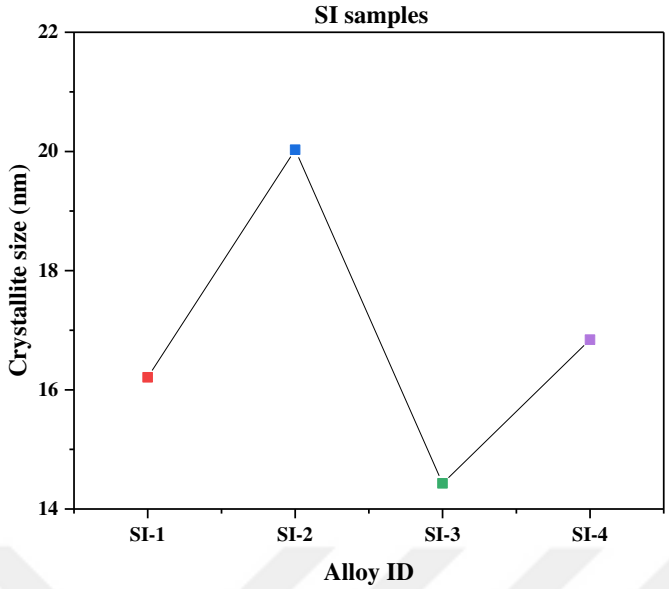

Figure 6.2 (a) Crystallite size of SI-1, SI-2, SI-3 and SI-4 samples.

For SI-2 quenched and non-quenched samples the crystallite size were all calculated, and the sample quenched at room temperature with crystallite size of 23.19 nm has the largest value and the smallest crystallite size belong to homogenized non-quenched sample 20.029 nm, 22.29 nm, 22.23nm and 22.88nm are the crystallite sizes for boiling water, iced water, and liquid nitrogen. The crystallite size for the samples can be seen in Figure 6.2 (b).

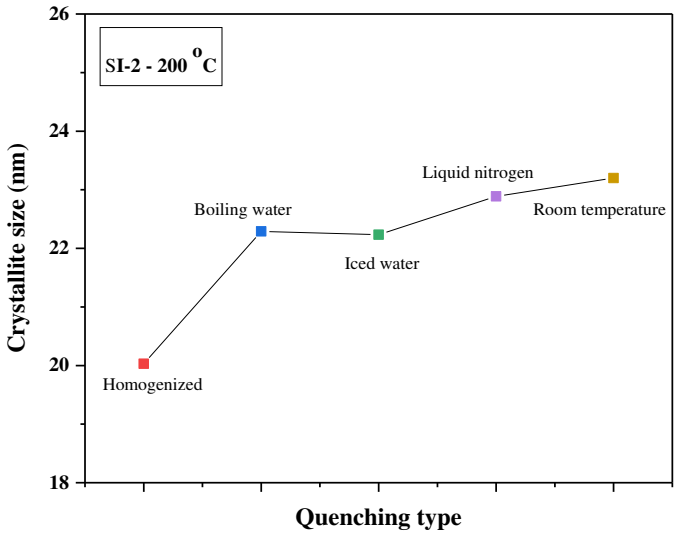

Figure 6.2 (b) Crystallite size of SI-2 quenched and non-quenched samples.

The same calculation was made for SI-4 quenched samples and as it is shown in Figure 6.2 (c), the largest crystallite size 24.55nm belongs to liquid nitrogen quenched sample and the lowest crystallite size 15.23nm is the boiling water samples value, 16.84nm, 16.87nm and 24.00nm are the values for homogenized, room temperature and iced water samples respectively.

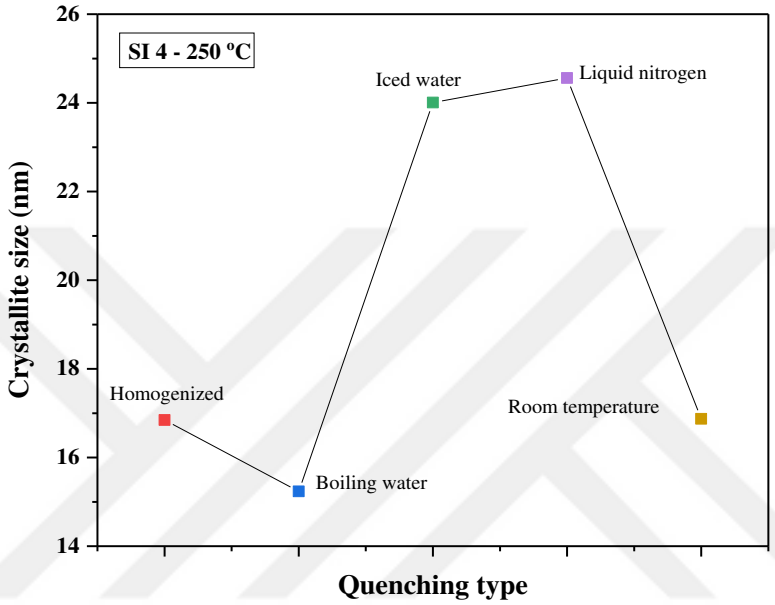

Figure 6.2 (c) Crystallite size of SI 4 quenched and non-quenched samples.

6.3. Differential Scanning Calorimetry (DSC) Measurement Results

The thermal DSC measurements of all the samples were taken at different heating/cooling rates, the obtained results showed martensite transformation peaks on DSC curves for each one of the SI samples (SI-1, SI-2, SI-3, and SI-4) and both (SI-2 and SI-4 quenched) samples at four different media. The SI samples curves made a downward endothermic peak that slightly varied in position at different temperatures for each sample of (SI-1, SI-2, SI-3, and SI-4) as it can be seen in Figure 6.3. These samples' DSC measurements were all made at rate of 25°C/min and each sample on a forward martensite (*M*) to austenite (*A*) phase shown an endothermic peak, each peak's temperature range is different from the others, as SI-1 endothermic peak is between 353.88°C to 381.00°C which is the highest temperature peak among the samples in Figure 6.3, and SI-2 is between 114.20°C to 144.75°C has the lowest endothermic temperature range. The upward cooling

of the samples from DSC curves an exothermic peak of reverse austenite (*A*) to martensite (*M*) appears and again samples showed different temperature ranges for the exothermic peak as between 86.74°C to 265.38°C, shifting the endothermic and exothermic peaks of the samples is due to the different percentages of different elements, as it can see from Table 6.1.

Table 6.1 that in SI-2 compared to SI-1 an addition of *Mn* element can be seen and that effect on the transformation temperature of the samples and other percentages of other samples as well can make a difference in transformation temperature and other thermodynamic parameters. These phase transformations start and finish at the temperatures of A_s (austenite start), A_f (austenite finish), M_s (martensite start), and M_f (martensite finish) during the heating and cooling processes of thermal analysis measurements. These thermodynamic parameters and the characteristic martensitic transformation temperatures from the analyses of these DSC curves were given for each one of the samples as heating/cooling rates in Table 6.2. In this table, the given values of characteristic A_s, A_f, M_s, M_f and the hysteresis of A_s-M_f temperatures for all the four samples can be seen. According to these values listed in that table, as in general and on the average of all heating/cooling rates the highest transformation temperatures were obtained for sample SI-1 and the lowest values are for the sample SI-2.

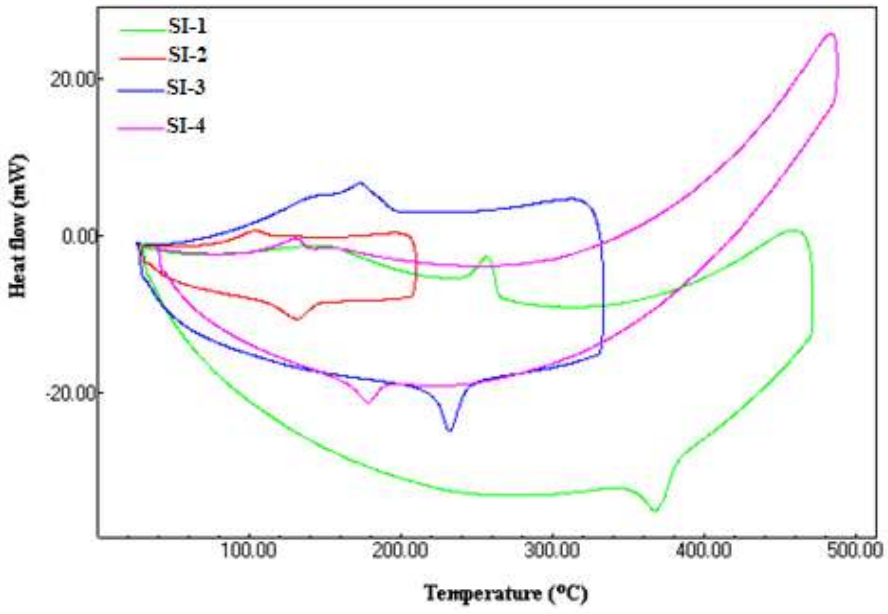

Figure 6.3 DSC curves of SI-1, SI-2, SI-3 and SI-4 samples with a heating/cooling rate of 25 ˚C/min

.

Table 6.2 Transformation temperatures, thermodynamic parameters and hysteresis values of SI samples with different heating/cooling rates (5, 15, 25 and 35 ˚C/min).

Alloy ID	Rate (ºC/min)	A_s (˚C)	A_f (˚C)	A_{max} (˚C)	M_s (˚C)	M_f (˚C)	T_o (˚C)	A_s-M_f (˚C)	A_f-M_s (˚C)	$\Delta H_{M\rightarrow A}$ (J/g)	$\Delta S_{M\rightarrow A}$ (J/g˚C)
SI 1	5	374.54	386.89	352.96	271.17	167.11	329.03	92.43	115.72	8.39	0.025
	15	359.58	380.57	368.49	266.43	244.96	323.50	114.62	114.14	8.91	0.027
	25	353.88	381.00	367.66	265.38	244.09	323.19	109.79	115.62	10.54	0.032
	35	348.47	381.14	365.00	263.90	238.57	322.52	109.9	117.24	11.96	0.037
	Average:	355.36	381.15	368.02	266.72	248.68	324.56	106.68	115.68	9.95	0.0302
Alloy ID	**Rate (ºC/min)**	**A_s (˚C)**	**A_f (˚C)**	**A_{max} (˚C)**	**M_s (˚C)**	**M_f (˚C)**	**T_o (˚C)**	**A_s-M_f (˚C)**	**A_f-M_s (˚C)**	**$\Delta H_{M\rightarrow A}$ (J/g)**	**$\Delta S_{M\rightarrow A}$ (J/g˚C)**
SI 2	5	114.03	139.78	129.43	119.67	77.57	129.72	36.46	19.85	4.36	0.0336
	15	113.29	141.87	129.79	119.05	76.33	130.46	36.90	22.44	7.24	0.0555
	25	114.42	144.65	131.59	115.46	87.16	130.05	27.26	29.13	7.02	0.0540
	35	115.6	147.49	133.74	116.03	89.16	131.76	26.44	31.01	7.5	0.0570
	Average:	114.33	143.45	131.14	117.55	86.55	130.49	31.78	25.60	6.20	0.0500
Alloy ID	**Rate (ºC/min)**	**A_s (˚C)**	**A_f (˚C)**	**A_{max} (˚C)**	**M_s (˚C)**	**M_f (˚C)**	**T_o (˚C)**	**A_s-M_f (˚C)**	**A_f-M_s (˚C)**	**$\Delta H_{M\rightarrow A}$ (J/g)**	**$\Delta S_{M\rightarrow A}$ (J/g˚C)**
SI 3	5	257.77	313.11	285.15	221.56	182.91	267.33	74.86	91.55	1.94	0.007
	15	223.87	240.73	231.25	196.64	157.58	218.68	66.29	44.09	7.62	0.034
	25	222.16	242.21	232.27	194.72	153.90	218.46	68.26	47.49	10.18	0.046
	35	222.84	247.42	234.94	192.69	144.29	220.05	78.55	54.73	10.46	0.047
	Average:	231.66	260.86	245.90	201.40	159.67	231.13	71.99	59.46	7.55	0.0335
Alloy ID	**Rate (ºC/min)**	**A_s (˚C)**	**A_f (˚C)**	**A_{max} (˚C)**	**M_s (˚C)**	**M_f (˚C)**	**T_o (˚C)**	**A_s-M_f (˚C)**	**A_f-M_s (˚C)**	**$\Delta H_{M\rightarrow A}$ (J/g)**	**$\Delta S_{M\rightarrow A}$ (J/g˚C)**
SI 4	5	186.97	204.47	188.86	135.61	120.09	170.04	66.88	68.86	5.09	0.0299
	15	169.92	191.96	181.7	139.22	96.46	165.59	73.46	52.74	5.41	0.0326
	25	167.22	188.98	178.79	139.36	118.98	164.17	48.24	49.62	4.78	0.0291
	35	158.27	183.7	172.6	139.14	117.53	161.42	40.74	44.56	5.63	0.0348
	Average:	170.59	192.27	180.48	138.33	113.26	165.30	57.33	53.94	5.22	0.031

For SI-2 quenched and non-quenched samples the DSC analysis peaks as it can be seen in Figure 6.4 (a, b, c, d and e) that on the way of heating the samples the direct transformation of martensite to austenite an endothermic peak of several size and positions, M (β1'; 18R)→A(β1(DO3; L21)) transition peaks could be seen in all the SI-2 quenched samples in the range of between 106-176 °C. On the way back of cooling the samples A→M transformations exothermic peaks placed between 44-119 °C. In Table 6.3 the other thermodynamic parameters and other analyzed values of DSC measurements can be seen like A_s, A_f, M_s, M_f and the hysteresis values of the samples.

Table 6.3 Transformation temperatures, thermodynamic parameters and hysteresis values of SI-2 -200ºC-quenched samples with different heating/cooling rates (5, 15, 25 and 35 ˚C/min).

	Rate (°C/min)	As (°C)	Af (°C)	Amax (°C)	Ms (°C)	Mf (°C)	T0 (°C)	ΔHM→A (J/g)	ΔSM→A (J/g°C)	As-Mf (°C)	Af-Ms (°C)
Homogenized	5	114.03	139.78	129.43	119.67	77.57	129.725	4.36	0.0336	36.46	20.11
	15	113.29	141.87	129.79	119.05	76.33	130.46	7.24	0.0554	36.96	22.82
	25	114.42	144.65	131.59	115.46	87.16	130.055	7.02	0.0540	27.26	29.19
	35	115.6	147.49	133.74	116.03	89.16	131.76	7.5	0.0570	26.44	31.46
	Average	114.33	143.45	131.14	117.55	82.555	130.5	6.53	0.0500	31.78	25.89
Boiling water	**Rate (°C/min)**	**As (°C)**	**Af (°C)**	**Amax (°C)**	**Ms (°C)**	**Mf (°C)**	**T0 (°C)**	**ΔHM→A (J/g)**	**ΔSM→A (J/g°C)**	**As-Mf (°C)**	**Af-Ms (°C)**
	5	115.29	139.38	128	80.56	44.34	109.97	6.6	0.0600	70.95	58.82
	15	117.54	149.82	135.09	77.19	60.98	113.505	6.87	0.0605	56.56	72.63
	25	117.7	156.87	139.48	75.63	60.49	116.25	7.29	0.0627	57.21	81.24
	35	112.27	176.2	159.15	76.46	59.49	126.33	5.05	0.0399	52.78	99.74
	Average	115.7	155.57	140.43	77.46	56.32	116.51	6.45	0.0558	59.37	78.10
Iced water	**Rate (°C/min)**	**As (°C)**	**Af (°C)**	**Amax (°C)**	**Ms (°C)**	**Mf (°C)**	**T0 (°C)**	**ΔHM→A (J/g)**	**ΔSM→A (J/g°C)**	**As-Mf (°C)**	**Af-Ms (°C)**
	5	114.61	136.66	128.74	81.34	70.6	109	5.17	0.0474	44.01	55.32
	15	118.35	142.68	132.2	78.63	67.69	110.65	6.29	0.0568	50.66	64.05
	25	116.08	148.03	136.06	77.79	65.39	112.91	6.69	0.0592	50.69	70.24
	35	120.55	154.19	139.68	77.83	65.83	116.01	7.42	0.0639	54.72	76.36
	Average	117.40	145.39	134.17	78.90	67.38	112.14	6.39	0.0569	50.02	66.49
Liquid nitrogen	**Rate (°C/min)**	**As (°C)**	**Af (°C)**	**Amax (°C)**	**Ms (°C)**	**Mf (°C)**	**T0 (°C)**	**ΔHM→A (J/g)**	**ΔSM→A (J/g°C)**	**As-Mf (°C)**	**Af-Ms (°C)**
	5	120.04	139.56	133.02	80.72	61.53	110.14	3.05	0.0277	58.51	58.84
	15	121.43	146.92	135.74	96.48	81.45	121.7	4.69	0.0385	39.98	50.44
	25	125.76	154.32	140.37	77.55	62.77	115.93	4.7	0.0405	62.99	76.77
	35	105.97	127.53	107.14	77.2	61.58	102.36	2.37	0.0231	44.39	50.33
	Average	118.3	142.08	129.06	82.99	66.83	112.53	3.70	0.0325	51.47	59.09
Room temperature	**Rate (°C/min)**	**As (°C)**	**Af (°C)**	**Amax (°C)**	**Ms (°C)**	**Mf (°C)**	**T0 (°C)**	**ΔHM→A (J/g)**	**ΔSM→A (J/g°C)**	**As-Mf (°C)**	**Af-Ms (°C)**
	5	120.16	135.03	128.19	80.44	67.11	107.73	1.14	0.0106	53.05	54.59
	15	121.79	145.34	129.63	77.31	66.81	111.32	3.16	0.0283	54.98	68.03
	25	120.59	153.71	134.85	75.47	61.28	114.59	4.31	0.0376	59.31	78.24
	35	124.83	163.13	139.91	75.31	61.3	119.22	4.82	0.0404	63.53	87.82
	Average	121.84	149.30	133.15	77.13	64.12	113.21	3.36	0.0292	57.72	72.17

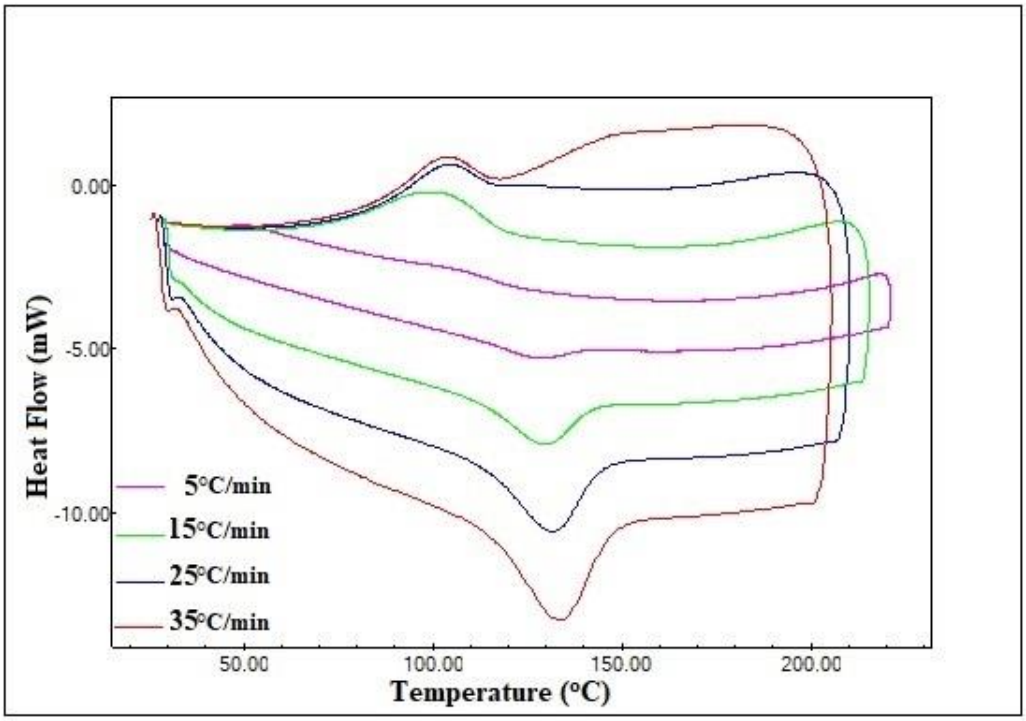

Figure 6.4 (a) DSC curves of SI-2 homogenized, non-quenched with heating/cooling rates of5,15, 25 and 35 ˚C/min.

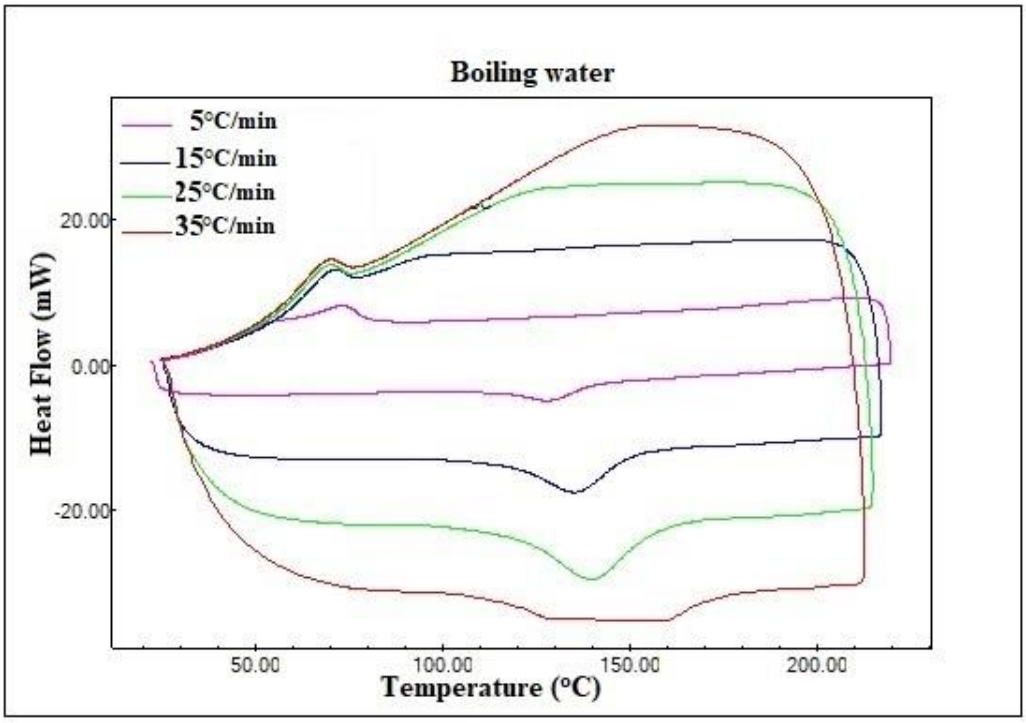

Figure 6.4 (b) DSC curves of SI-2 quenched in boiling water, with heating/cooling rates of5,15, 25 and 35 ˚C/min.

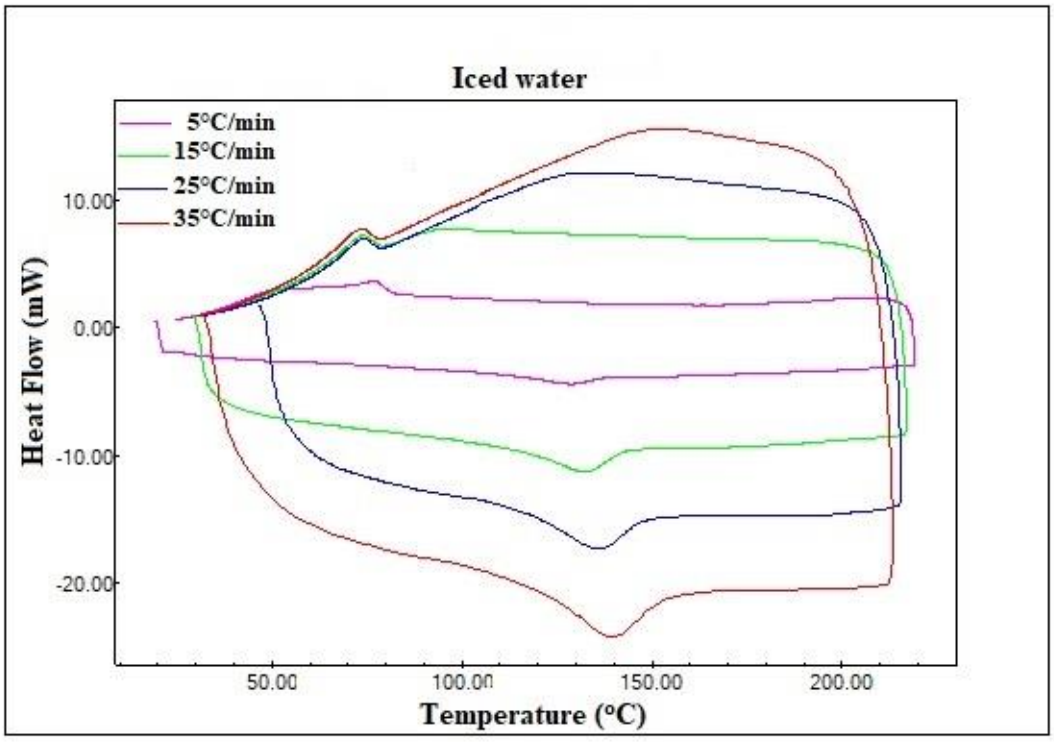

Figure 6.4 (c) DSC curves of SI-2 quenched in iced water with heating/cooling rates of5,15, 25 and 35 ˚C/min.

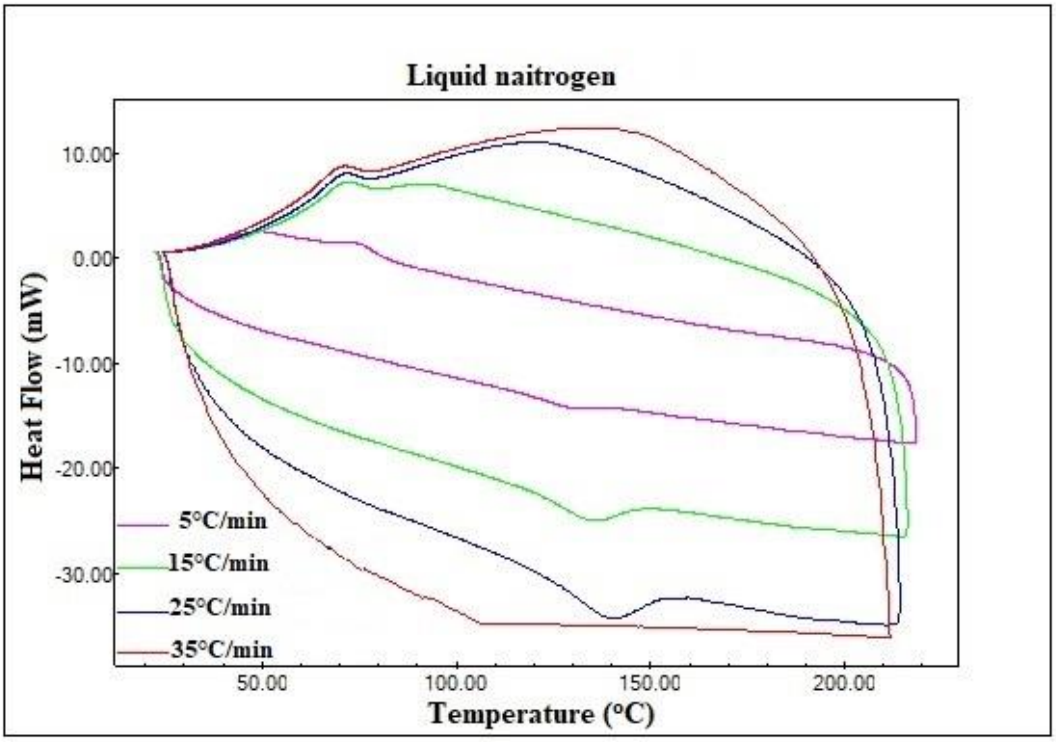

Figure 6.4 (d) DSC curves of SI-2 quenched in liquid nitrogen with heating/cooling rates of5,15, 25 and 35 ˚C/min.

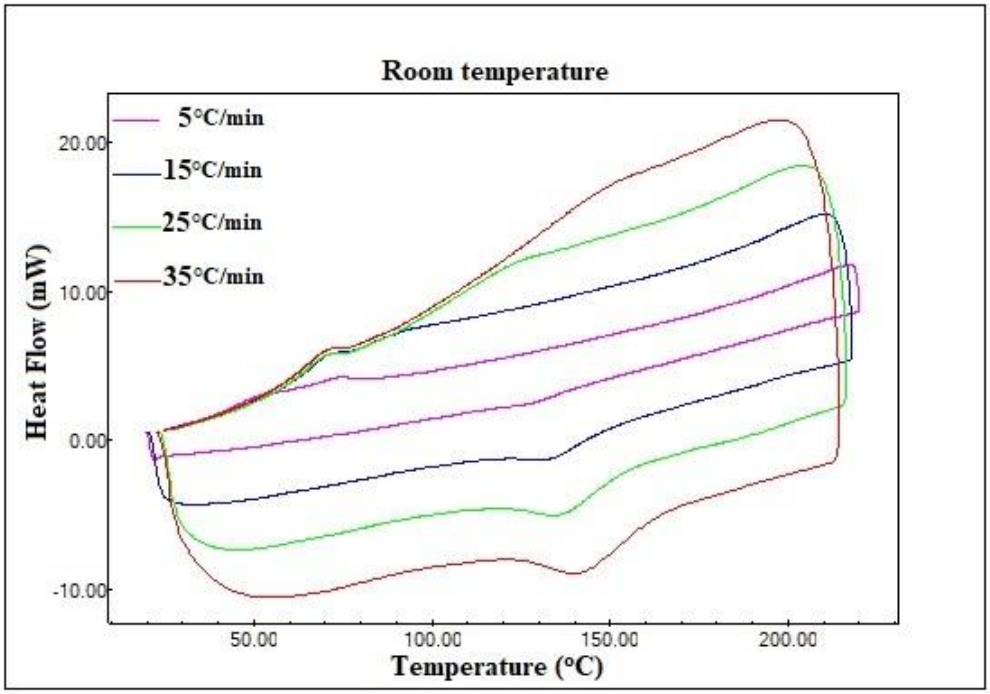

Figure 6.4 (e) DSC curves of SI-2 quenched in room temperature with heating/cooling rates of5,15, 25 and 35 ˚C/min.

For SI-4 quenched samples which all aged at 250ºC and quenched in four different media and non-quenched sample were investigated thermally using DSC measurements. The measurement at the rates of 5, 15, 25 and 35°C/min were taken and the displayed results show martensite peaks on DSC curves as it can be seen in Figure 6.5 (a, b, c, d, and e) for all the samples respectively. The first downward endothermic peaks that slightly varied in positions are the peaks indicate the direct martensitic transformations from β1′martensite (*M*) phase to β1(L21)austenite(*A*) phase at the temperature range of between 173°C and 207°C and then on the upward cooling parts of the curves at temperature between 95°C and 129°C, exothermic peaks exist of the reverse martensitic transformations of *A*(β1(L21)) to *M*(β1′). As we can see from Table 6.4 that shows the martensite characteristic temperatures of SI-4 quenched samples that the highest transformation temperatures were obtained for the sample quenched in boiling water and the lowest could be observed for the sample quenched in iced-brine water.

Table 6.4 Transformation temperatures, thermodynamic parameters and hysteresis values of SI-4 -250ºC-quenched samples with different heating/cooling rates (5, 15, 25 and 35 ˚C/min).

	Rate (°C/min)	As (°C)	Af (°C)	Amax (°C)	Ms (°C)	Mf (°C)	T_o (°C)	ΔHM→A (J/g)	ΔSM→A (J/g°C)	As-Mf (°C)	Af-Ms (°C)
Homogenized	5	186.98	204.47	188.86	135.61	120.09	170.04	5.09	0.0299	66.88	68.86
	15	169.92	191.96	181.7	139.22	96.46	165.59	5.41	0.0326	73.46	52.74
	25	167.22	188.98	178.79	139.36	118.98	164.17	4.78	0.0291	48.24	49.62
	35	158.27	183.7	172.6	139.14	117.53	161.42	5.63	0.0348	40.74	44.56
	Average	170.59	192.27	180.48	138.33	113.26	165.30	5.22	0.0316	57.33	53.94
Boiling water	**Rate (°C/min)**	**As (°C)**	**Af (°C)**	**Amax (°C)**	**Ms (°C)**	**Mf (°C)**	**T_o (°C)**	**ΔHM→A (J/g)**	**ΔSM→A (J/g°C)**	**As-Mf (°C)**	**Af-Ms (°C)**
	5	177.9	193.3	184.45	129.31	115.9	161.30	4.54	0.0283	62	63.99
	15	176.62	196.09	186.92	125.89	102.8	160.99	5.31	0.0330	73.82	70.2
	25	177.44	201.28	190.65	122.74	105.55	162.01	6.56	0.0405	71.89	78.54
	35	181.82	207.89	194.27	123.1	105.94	165.49	5.95	0.0360	75.88	84.79
	Average	178.44	199.64	189.07	125.26	107.55	162.45	5.59	0.0344	70.90	74.38
Iced water	**Rate (°C/min)**	**As (°C)**	**Af (°C)**	**Amax (°C)**	**Ms (°C)**	**Mf (°C)**	**T_o (°C)**	**ΔHM→A (J/g)**	**ΔSM→A (J/g°C)**	**As-Mf (°C)**	**Af-Ms (°C)**
	5	173.13	192.42	180.84	127.01	110.08	159.71	5.63	0.0352	63	65.15
	15	174.91	196.07	184.95	124.77	95.93	160.42	5.25	0.0327	78.98	71.3
	25	174.33	199.11	186.92	120.95	105.28	160.03	7.55	0.0471	69.05	78.16
	35	175.11	203.92	189.66	121.38	102.98	162.65	7.65	0.0470	72.13	82.53
	Average	174.37	197.88	185.59	123.53	103.57	160.70	6.52	0.0405	70.79	74.285
Liquid nitrogen	**Rate (°C/min)**	**As (°C)**	**Af (°C)**	**Amax (°C)**	**Ms (°C)**	**Mf (°C)**	**T_o (°C)**	**ΔHM→A (J/g)**	**ΔSM→A (J/g°C)**	**As-Mf (°C)**	**Af-Ms (°C)**
	5	175.63	189.34	183.12	127	113.42	158.17	4.21	0.0266	62.21	62.34
	15	176.21	195.43	186.35	123.79	95.55	159.61	4.22	0.0264	80.66	71.64
	25	176.76	199.59	188.4	121.09	106.38	160.34	6.69	0.0417	70.38	78.5
	35	173.81	204.93	191.81	120.74	105.38	162.83	6.96	0.0427	68.43	84.19
	Average	175.60	197.32	187.42	123.15	105.18	160.24	5.52	0.0343	70.42	74.16
Room temperature	**Rate (°C/min)**	**As (°C)**	**Af (°C)**	**Amax (°C)**	**Ms (°C)**	**Mf (°C)**	**T_o (°C)**	**ΔHM→A (J/g)**	**ΔSM→A (J/g°C)**	**As-Mf (°C)**	**Af-Ms (°C)**
	5	173.77	192.72	184.1	129.34	114	161.03	5.26	0.0326	59.77	63.38
	15	174.46	195.93	185.02	126.39	98.16	161.16	7.7	0.0477	76.3	69.54
	25	179	200.67	189.38	124.43	106.09	162.55	7.45	0.0458	72.91	76.24
	35	177.35	204.06	190.47	123.4	106.08	163.73	7.88	0.0481	71.27	80.66
	Average	176.14	198.34	187.24	125.89	106.08	162.12	7.07	0.0435	70.06	72.455

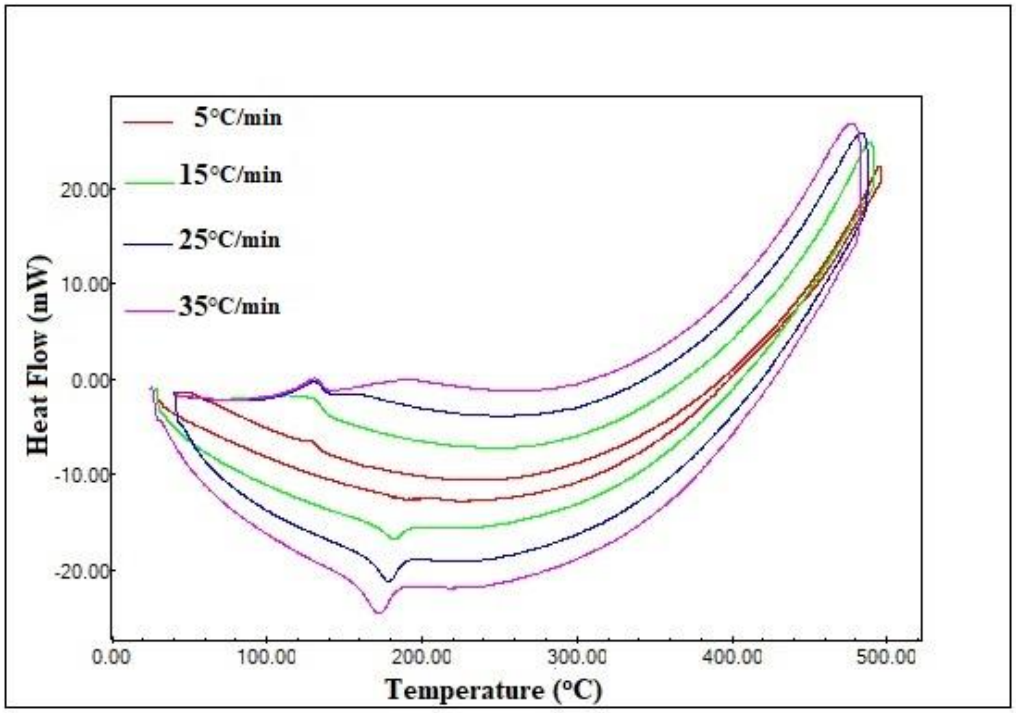

Figure 6.5 (a) DSC curves of SI-4 homogenized non-quenched sample with heating/cooling rates of 5,15, 25 and 35 ˚C/min.

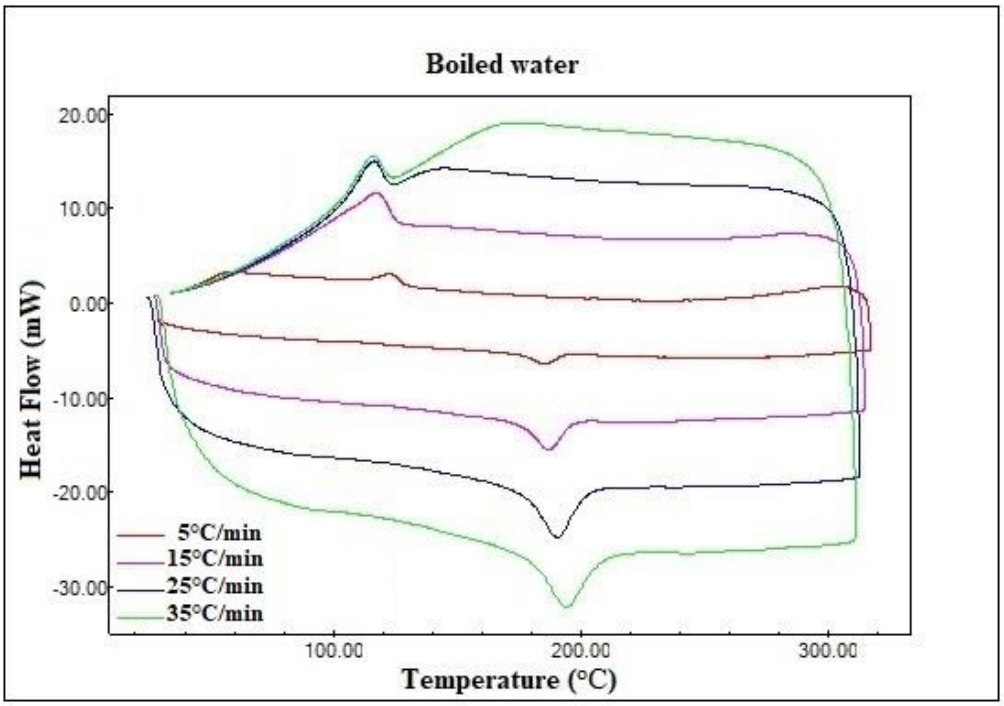

Figure 6.5 (b) DSC curves of SI-4 quenched in boiling water with heating/cooling rates of 5,15, 25 and 35 ˚C/min.

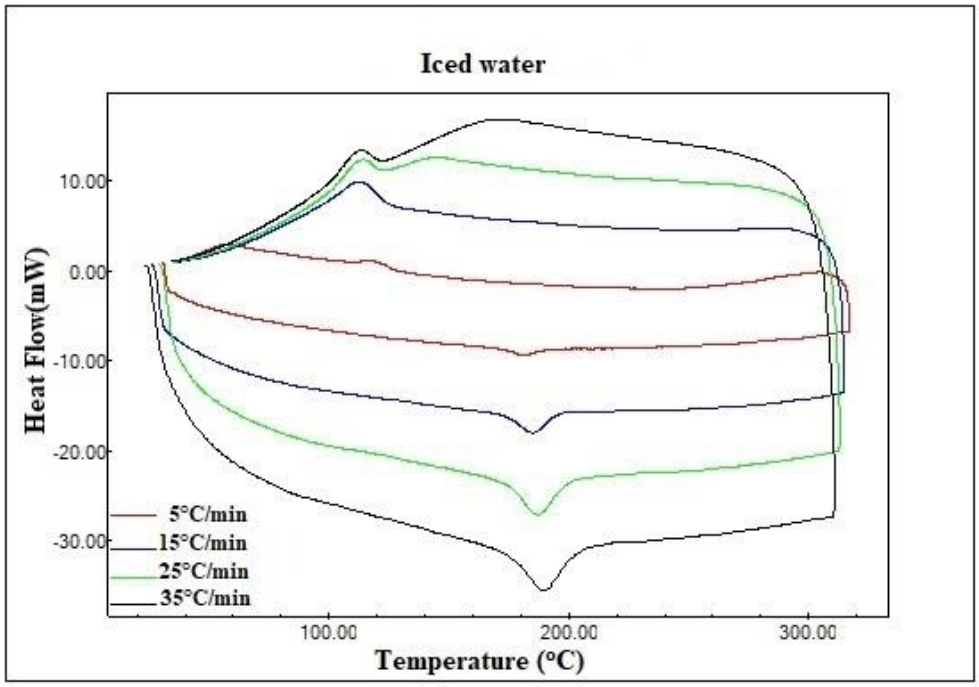

Figure 6.5 (c) DSC curves of SI-4 quenched in iced water with heating/cooling rates of 5,15, 25 and 35 ˚C/min.

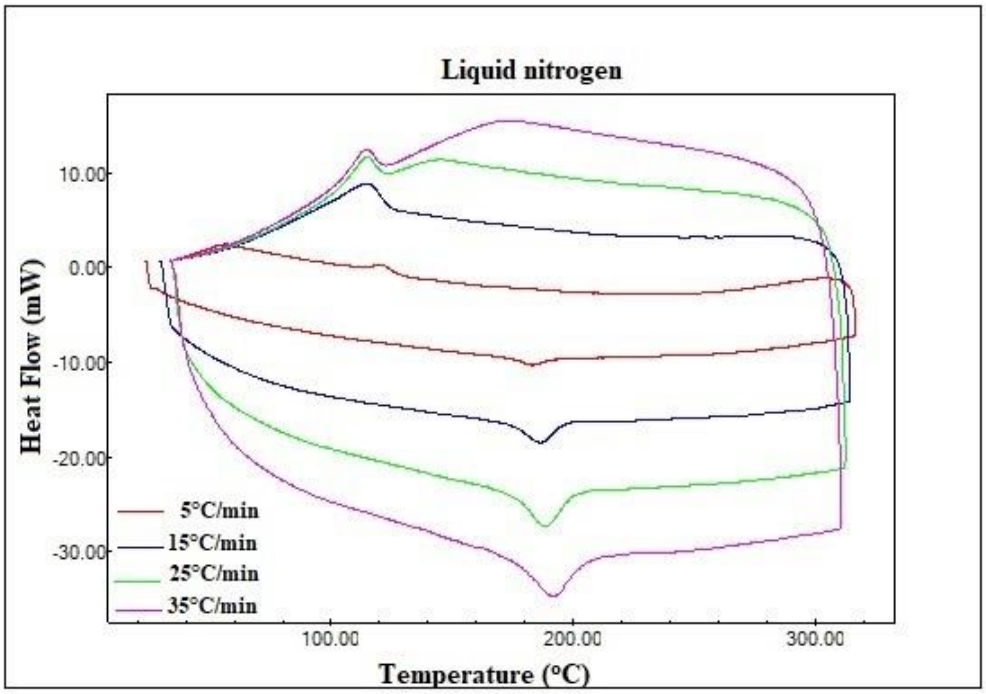

Figure 6.5 (d) DSC curves of SI-4 quenched in liquid nitrogen with heating/cooling rates of 5,15, 25 and 35 ˚C/min.

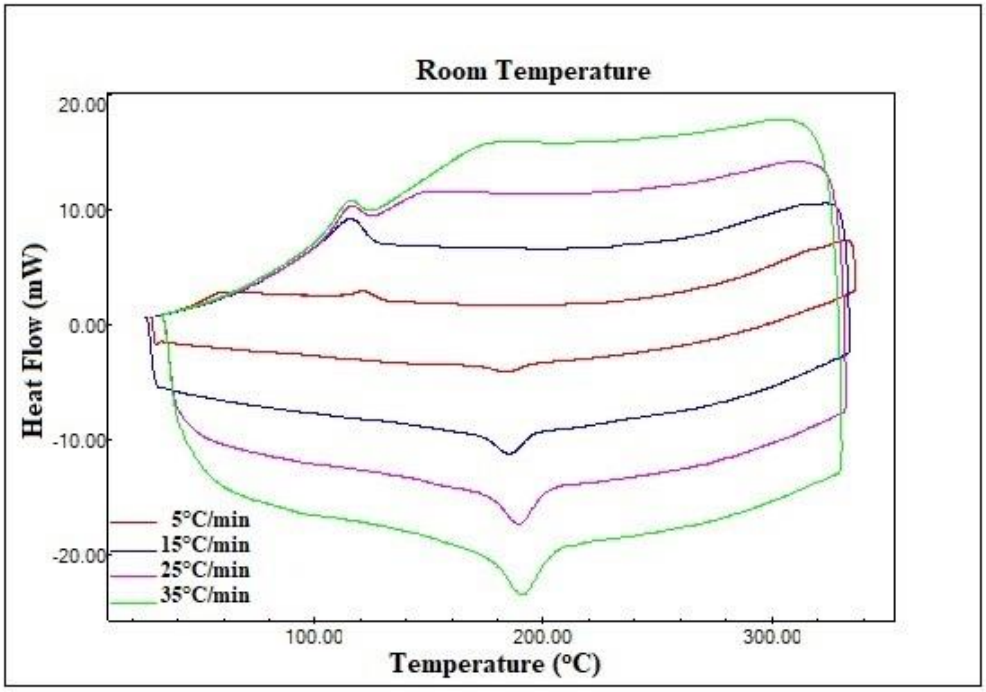

Figure 6.5 (e) DSC curves of SI-4 quenched at room temperature with heating/cooling rates of 5,15, 25 and 35 ˚C/min.

The average values of A_s-M_s, average A_s, A_f, and average hysteresis A_s-M_f for the samples can be seen in Figure 6.6 (a, b and c) can be seen respectively. As the transformation temperatures of all the SI samples are above 100ºC we call these SMAs as high-temperature shape memory alloys (HTSMA).

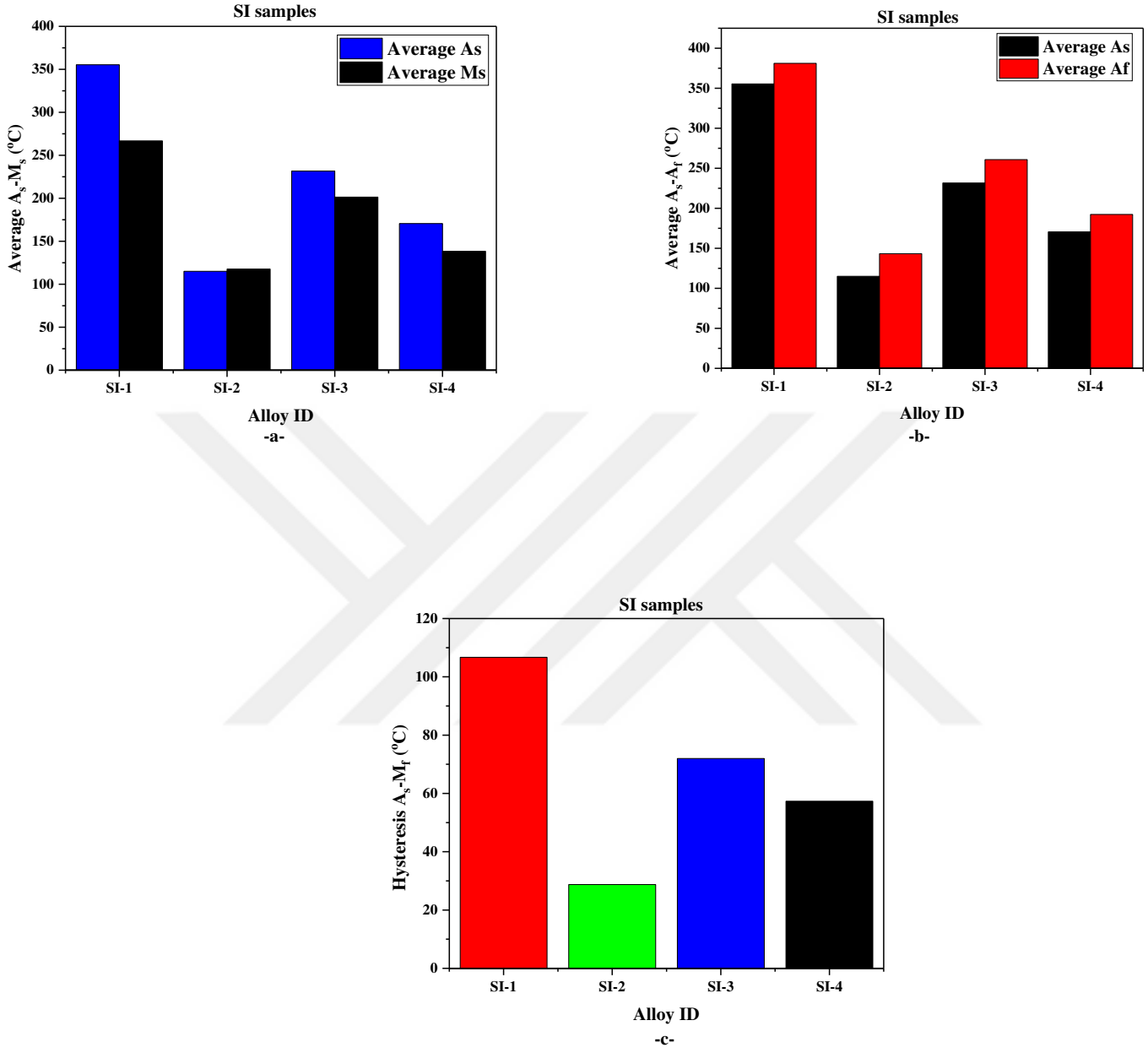

Figure 6.6. (a) The average values of A_s- M_s for SI samples. (**b)** The average values of A_s- A_f for SI samples. (**c)** The average values of hysteresis (A_s- M_f) for SI samples.

As it is seen in the tables the effect of quenching on SI-2 sample increased A_s and A_f values by some degrees on the same time decreased M_s and M_f values and that led to an expansion in hysteresis (A_s- M_f) range. Figure 6.7 (a and b) as columnar graphs shows the changes in A_s, A_f, M_s and M_f average value for each SI-2 sample that quenched in different

media. As we can see from Figure 6.7 (c) the highest value goes to boiling water quenched sample while the lowest value belongs to SI-2 homogenized non quenched sample.

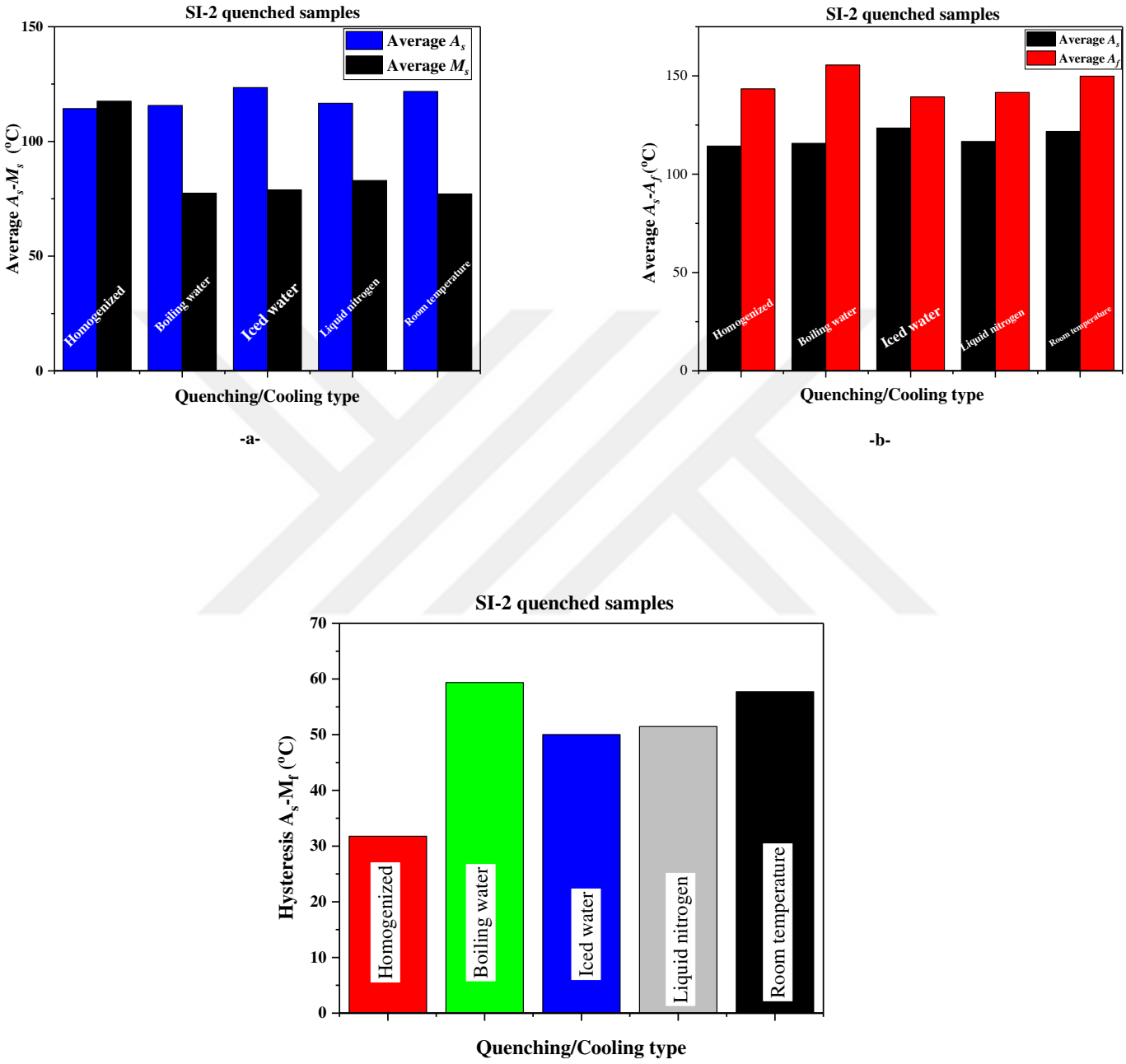

Figure 6.7 (a) The average values of A_s- M_s for SI-2 quenched samples. **(b)** The average values of A_s- A_f for SI-2 quenched samples.**(c)** The average values of hysteresis (A_s- M_f) for SI-2 quenched samples.

The highest A_s value is for SI-4 quenching/cooling sample in boiling water and the highest M_s value is for homogenized non-quenched sample, The lowest A_s value M_s value belong to the homogenized non-quenched and liquid nitrogen samples respectively. The highest value for A_f observed by boiling water quenched sample but the lowest A_f value is for non-quenched homogenized sample while the highest and lowest M_f value is for homogenized and iced water quenched sample, Figure 6.8 (a) and Figure 6.8 (b) shows the average change of these values for the types of quenching/cooling samples. In Figure 6.8 (c) the average hysteresis value for the samples can be seen and as it is obvious that the highest value of hysteresis is for boiling water sample and the lowest is for a homogenized sample.

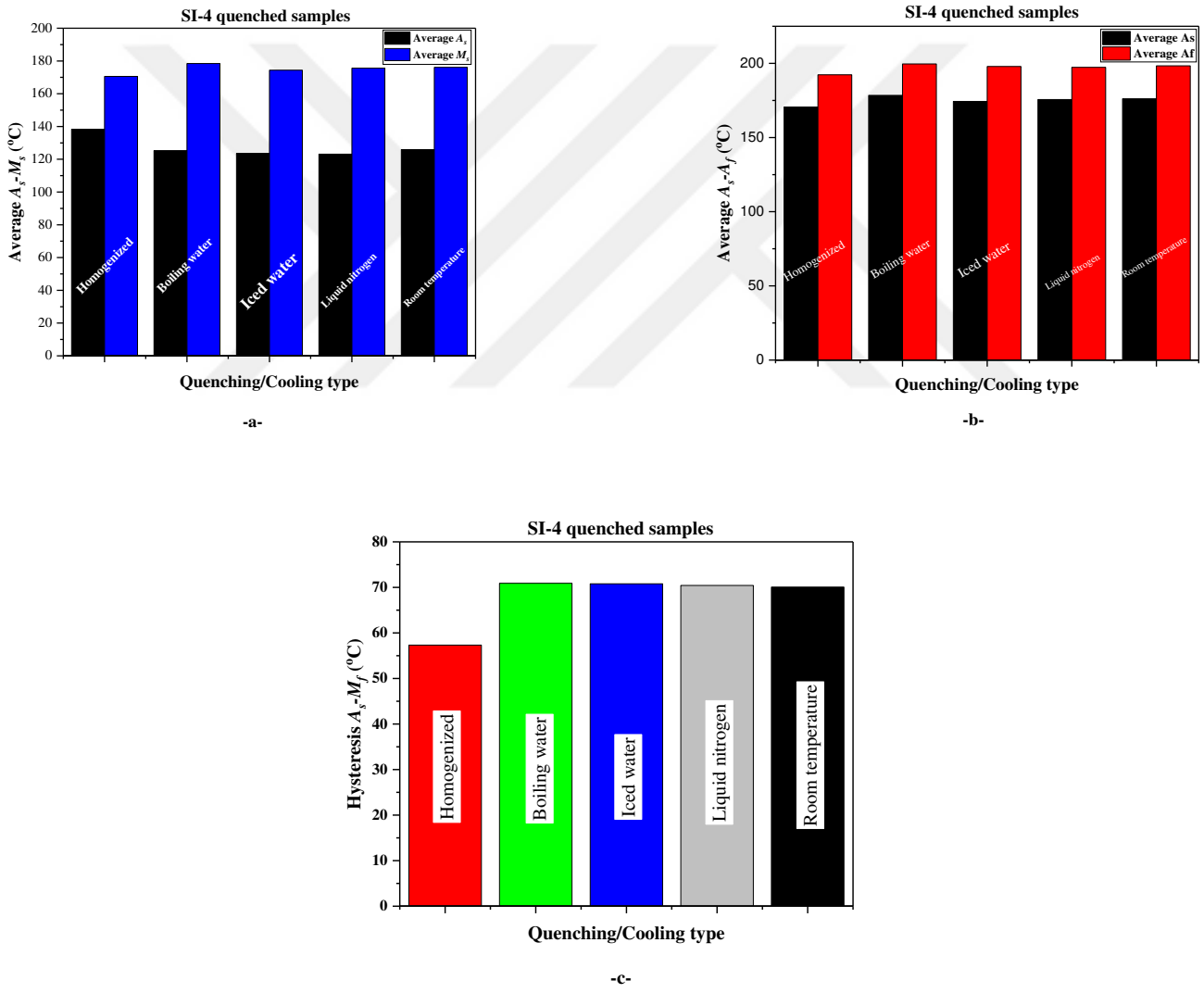

Figure 6.8.(a) The average values of A_s- M_s for SI-4 quenched samples. (**b**) The average values of A_s- A_f for SI-4 quenched samples. (**c**) The average values of hysteresis (A_s- M_f) for SI-4 quenched samples.

Enthalpy which is defined as a thermodynamic quantity equivalent to the total heat content of the system. It is the internal energy of the system plus the product of pressure and volume [29].

$$H = E + PV \tag{6.2}$$

While entropy is a thermodynamic quantity representing the unavailability of a systems thermal energy for conversion into mechanical work, often interpreted as the degree of disorder in the system. Entropy values were found from the enthalpy value divided by equilibrium temperature T_o .

$$\Delta S_{M\rightarrow A} = \frac{\Delta H_{M\rightarrow A}}{T_o} \tag{6.3}$$

The T_o values written in Table 6.2, Table 6.3 and Table 6.4 were calculated for all of the samples by the Tong and Wayman equation [74] as below;

$$T_0 = \frac{A_f + M_s}{2} \tag{6.4}$$

The enthalpy values obtained from the DSC peaks analyses by taking integration of these peak areas between the phase starts and phase finish temperatures. The entropy values are obtained from the below equation;

$$\Delta S_{M\rightarrow A} = \frac{\Delta H_{M\rightarrow A}}{T_o} \tag{6.5}$$

One of the thermodynamic parameters is T0 equilibrium temperature at where the chemical energies (Gibbs free energies) of the austenite and martensite phases become equalized. As shown in the tables, on average, the value of T0 temperature took the highest value by SI-1 323.75°C and the lowest value belongs to SI-2 130.98°C. T_o values for SI-2 quenched samples from Table 6.3 as average can be seen, the highest value is 130.5°C for homogenized SI-2 sample and the lowest is 112.14°C for SI-2 sample quenched in iced water. For SI-4 quenched samples the highest value is 165.305ºC for the homogenized sample and the lowest value is for liquid nitrogen sample 160.23°C.

Enthalpy is a kinetic parameter (heating) transformation for the phases; enthalpy change of $\Delta H_{M\rightarrow A}$ is the martensite (*M*) to austenite (*A*) transformation ability of a sample,

as much as the sample has higher enthalpy value this means that it is more difficult for a sample to transform and the vise verse. The highest average enthalpy value belongs to SI-1 9.95(J/g) while 6.20(J/g), 7.55(J/g) belong to SI-2, SI-3 in turn and the lowest average value is 5.22(J/g) for SI-4 which means that the transformation in this sample is the easiest. As we see in Figure 6.9 (a) that both samples SI-2 and SI-4 have lower values compared to SI-1 and SI-3 and this result is in agreement with the results that we got from the crystallite size that both SI-2 and SI-4 transformation is easier rather than SI-1 and SI-3. This is because of the addition of Mn which is higher in SI-2 and SI-4 while in SI-1 Mn does not exist at all.

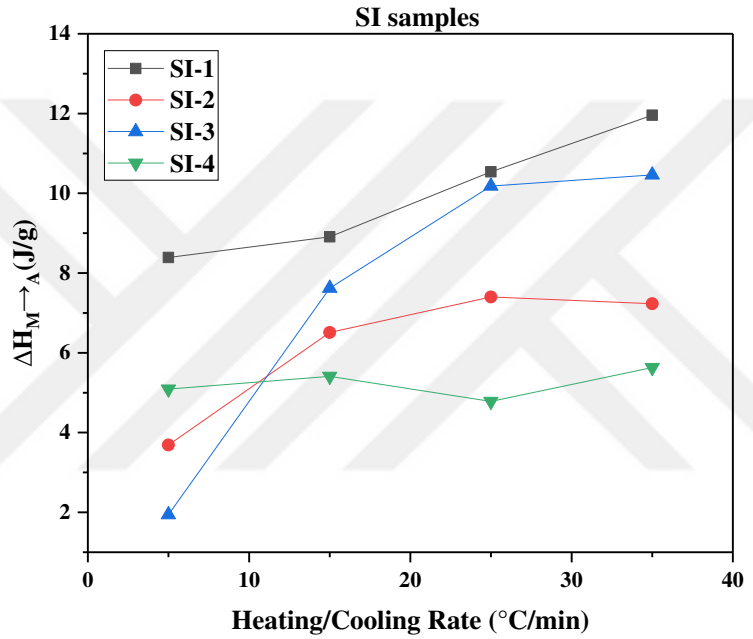

Figure 6.9 (a) The enthalpy $\Delta H_{M\rightarrow A}$ values with the Heating/cooling rates of the SI samples.

The highest average enthalpy value belongs to the homogenized sample with an average of 6.53(J/g), 6.452(J/g), 6.392(J/g), 3.702(J/g) for boiling water, iced water, liquid nitrogen and the lowest value with an average 3.36(J/g) for the sample quenched or cooled at room temperature. From Figure 6.9 (b) we can see that rate 35°C/min for the sample have higher values except for boiling water and liquid nitrogen this rate is minimum. The highest value among all the rates for all the samples is 7.5(J/g) homogenized sample rate 35°C/min and the lowest value which is at rate 5°C/min belongs to quenched sample at room temperature 2.37(J/g).

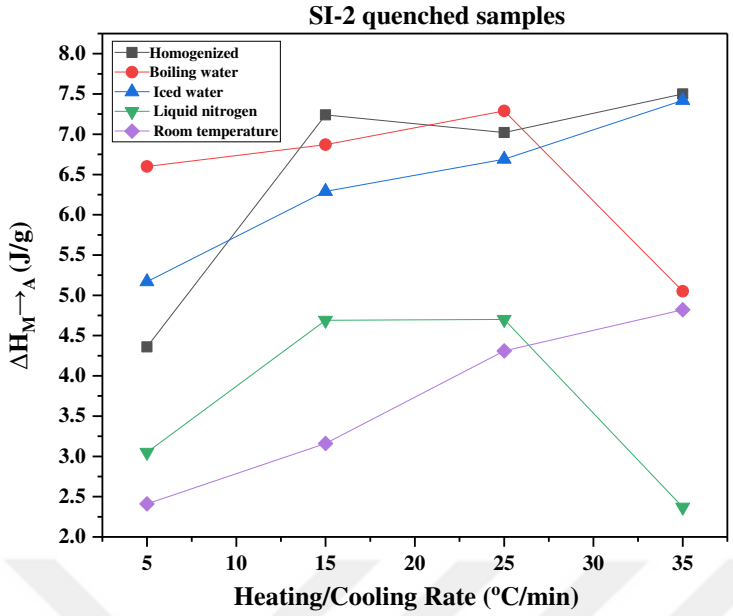

Figure 6.9 (b) The enthalpy $\Delta H_{M\rightarrow A}$ values with the Heating/cooling rates of the SI-2 quenched and non-quenched samples.

Enthalpy average values for SI-4 quenched samples of *M* to *A* transformation ($\Delta H_{M\rightarrow A}$) from the highest to lower for SI-4 samples was found to be 7.072(J/g), 6.507(J/g), 5.59(J/g), 5.52(J/g) and 5.22(J/g) for quenching/cooling sample at room temperature, iced water, boiling water, liquid nitrogen and only homogenized non quenched sample to have the lowest value of martensite to austenite transformation enthalpy value. This shows that the homogenized non quenched sample transformation from *M* to *A* is the easiest compared to the others and the quenching/cooling sample in room temperature is the most difficult to transform from *M* to *A*. In Figure 6.9 (c), we can see that almost all the samples at rate 35°C/min have higher values compared to other rates except for boiling water sample which shows the highest value at rate 25°C/min among all other rates for the same sample. All the samples show the lower value in rate 5°C/min for liquid nitrogen.

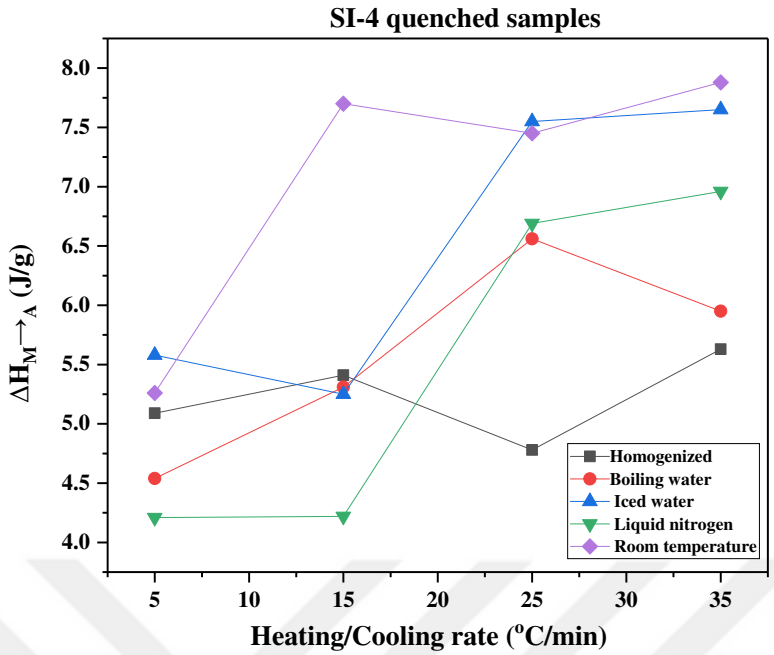

Figure 6.9 (c) The enthalpy $\Delta H_{M\rightarrow A}$ values with the Heating/cooling rates of the SI-4 quenched samples.

The entropy values from highest to lowest for SI samples are 0.05(J/g˚C), 0.0335(J/g˚C), 0.031(J/g˚C), and 0.0302(J/g˚C) for the samples SI-2, SI-3, SI-4, and SI-1 and in series and this can be seen in Figure 6.10 (a).

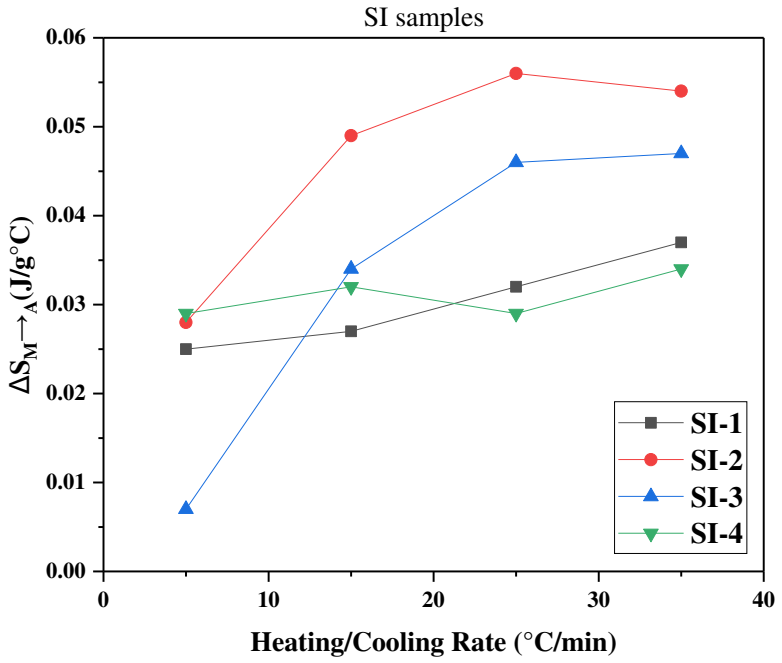

Figure 6.10 (a) The entropy $\Delta S_{M\rightarrow A}$ values with the Heating/cooling rates of the SI samples.

Entropy transformation for SI-2 *M* to *A* (*ΔSM→A*) average shows the highest value for quenching/cooling type iced water 0.0569(J/g°C), 0.0558(J/g°C), 0.05(J/g°C), 0.0325(J/g°C) for boiling water, homogenized non quenched , liquid nitrogen and the lowest value 0.0292(J/g°C) belong to quenching/cooling at room temperature. Figure 6.10 (b) is for all the rates of quenching/cooling types with the homogenized samples and we can see that generally with increasing the rates the entropy values increase except for liquid nitrogen and boiling water samples their values does not increase at the rate 35°C/min and their maximum value is at rate 25 °C/min, Iced water at rate 35 is the highest entropy value from the graph above while rate 5°C/min for room temperature sample is the lowest. Because of high temperature (above 100ºC) transition of all SI-2 quenched samples, we call these SMAs as high-temperature shape memory alloys (HTSMA).

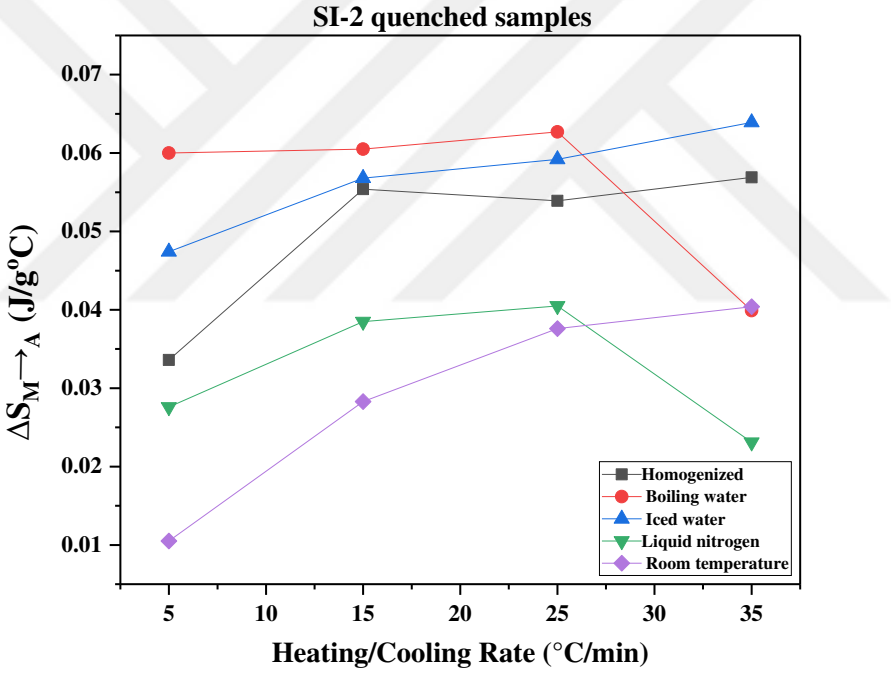

Figure 6.10 (b) The entropy $\Delta S_{M\rightarrow A}$ values with the Heating/cooling rates of the SI-2 quenched samples.

The average entropy values for SI-4 quenched samples of *M* to *A* transformation (Δ*SM→A*) as we can see from the table that the quenching/ cooling sample at room temperature has the highest value with an average of 0.0435(J/g°C), 0.0405(J/g°C) iced water sample,0.03435(J/g°C) liquid nitrogen , 0.0344 (J/g°C) boiling water and the lowest value for homogenized sample with an average of 0.0316(J/g°C). From the above graph we see that all quenching/cooling type of the samples with their rates are shown and as we see

in Figure 6.10 (c), that for almost all the samples at a rate 35°C/min shows the higher entropy value compared with other rates except for boiling water which has it is highest at a rate 25 °C/min. The graph also shows a lower value for rate 5°C/min for most of the samples, the lowest value belongs to liquid nitrogen at a rate of 5°C/min.

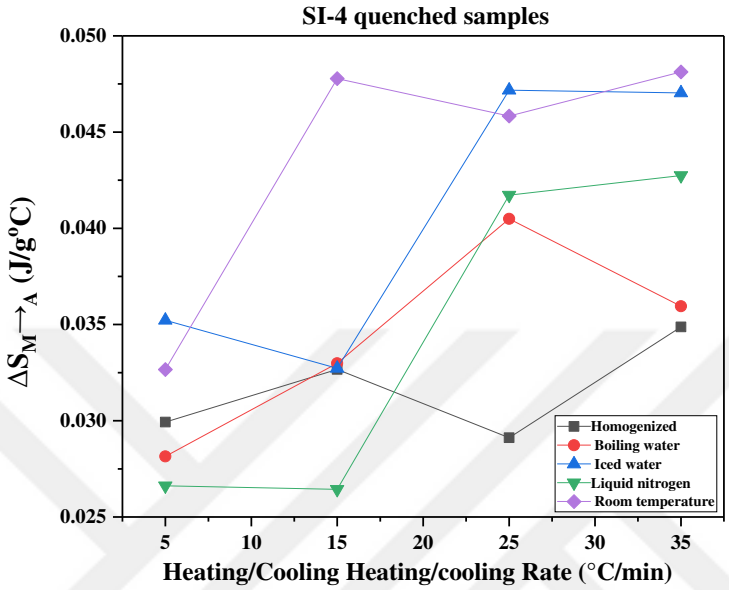

Figure 6.10 (c) The entropy $\Delta S_{M\rightarrow A}$ values with the Heating/cooling rates of the SI-4 quenched samples.

Electron concentration (e/a) in any alloy is an effective parameter for the characteristics of transformation temperature because both e/a and transformation temperature depend on the composition and the percentages of the element in the composition. For a thermoelastic martensite transformation to occur in Cu-based SMA, the e/a ratio should be between 1.45-1.51. The e/a values of SI samples can be seen in Table 6.1, and the relation between e/a ratio with both average entropy values and average hysteresis values can be seen in Figure 6.11. and Figure 6.12. respectively. From these figures, we understand more about the relation of electron concentration with order and disorder and the transformation temperature of the alloys [57]. If the value of e/a ratio of an alloy is between (1.45- 1.51) then both martensite forms types of 2H and 18R exist in the alloy. If e/a is higher than 1.51 then the dominant phase form is 2H martensite structures while if e/a is less than 1.45 then the highest dominant phase form is 18R [73]. To calculate the value of e/a rate of the alloy, a formula [74] is given as below:

$$\frac{e}{a} = \sum f_i v_i \qquad (6.1)$$

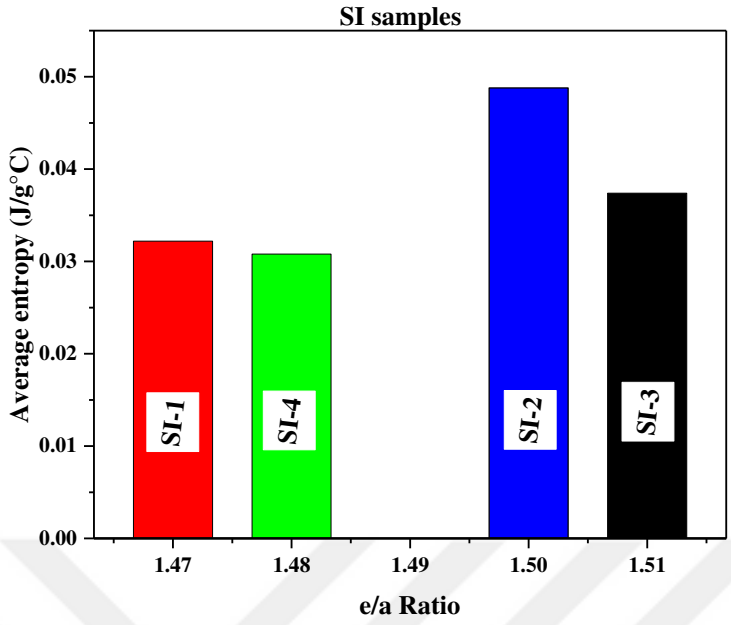

Figure 6.11 The average entropy $\Delta S_{M \rightarrow A}$ values with e/a ratio of SI samples.

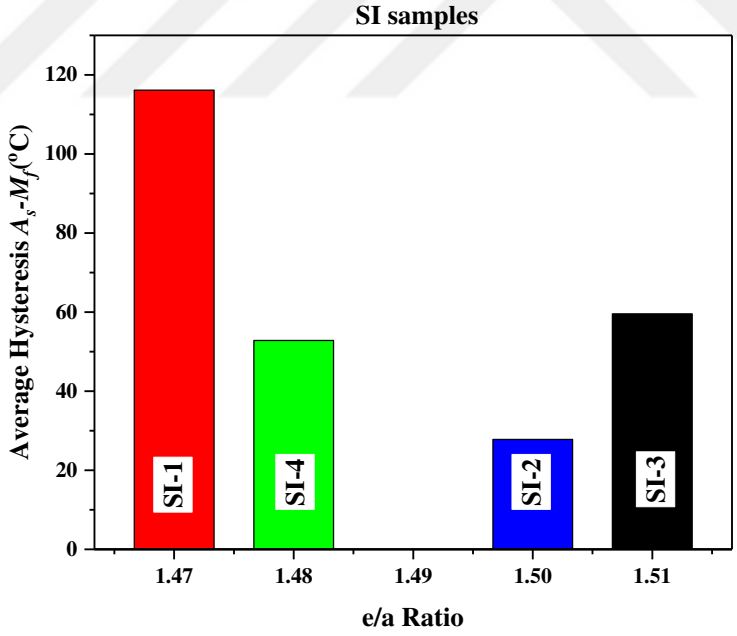

Figure 6.12 The average hysteresis values with e/a ratio of SI samples.

6.3.1. Activation Energy Calculations

The activation energy is essential to define the crystallization behavior and also to calculate the required energy during the transformations. Activation energy or as it called sometimes Gibbs free energy, the energy needed for a chemical reaction to happen or in shape memory better to say the amount of energy which is calculated to transfer an alloy from one phase to another $M \leftrightarrow A$ and that really needed especially in industry to make a shape memory alloy to understand the amount of energy needed for this alloy to change its phase. Two equations are mainly used in this field of research and they are both used for the same aim which is activation energy, the equations are Kissinger and Ozawa methods. The activation energy can be acquired from the peak shift in the DSC curves as shown in Figure 6.3.(a, b and c), which were conducted at different heating rates [75].

6.3.1.1. Kissinger Method for Activation Energy

One of the methods is Kissinger activation energy, the following method developed by the Kissinger [76]:

$$\frac{E_a}{R} - = \frac{d\left[\ln\left(\phi / T_m^{\,2}\right)\right]}{d\left(1/T_m^{\,2}\right)} \tag{6.6}$$

Where E_a is the activation energy, R is the gas constant which is equal to (8.314 J/mol. K.) and $\frac{d\left[\ln\left(\phi / T_m^{\,2}\right)\right]}{d\left(1/T_m^{\,2}\right)}$ is the slope of the graph between $\left[\ln\left(\phi / T_m^{\,2}\right)\right]$ on y-axis and $\left(1/T_m^{\,2}\right)$ on x-axis, where ϕ is the heating rate, T_m is the temperature of the maximum peak in the DSC curve during the heating process. Figure 6.13 (a) show the graphed activation energy for SI-1, SI-2, SI-3, and SI-4 samples. We can see that order of the activation energy values for these samples from high to low is 666.36, 495.33, 216.87 and 82.94kJ/mol for SI-1, SI-2, SI-4, and SI-3 respectively. See Table 6.5.

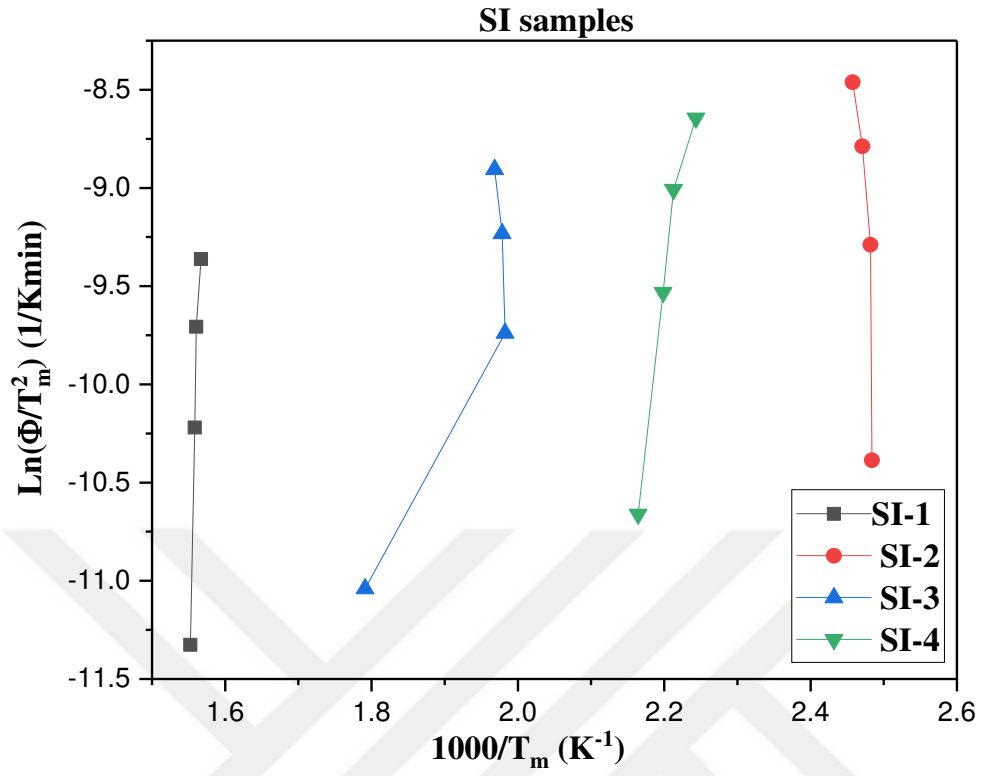

Figure 6.13 (a) Activation energy curves of SI-1, SI-2, SI-3, and SI-4 samples.

Table 6.5. Activation energy values of SI samples using the Kissinger method.

SI samples activation energy (kJ/mol)	
SI-1	666.36
SI-2	495.33
SI-3	82.94
SI-4	216.87

The Kissinger activation energy for SI-2 quenched samples as it can be seen in Figure 6.13 (b) are also obtained. The highest activation energy value is for the homogenized sample and the lowest value belong to sample quenched at room temperature; all the values can be seen in Table 6.6.

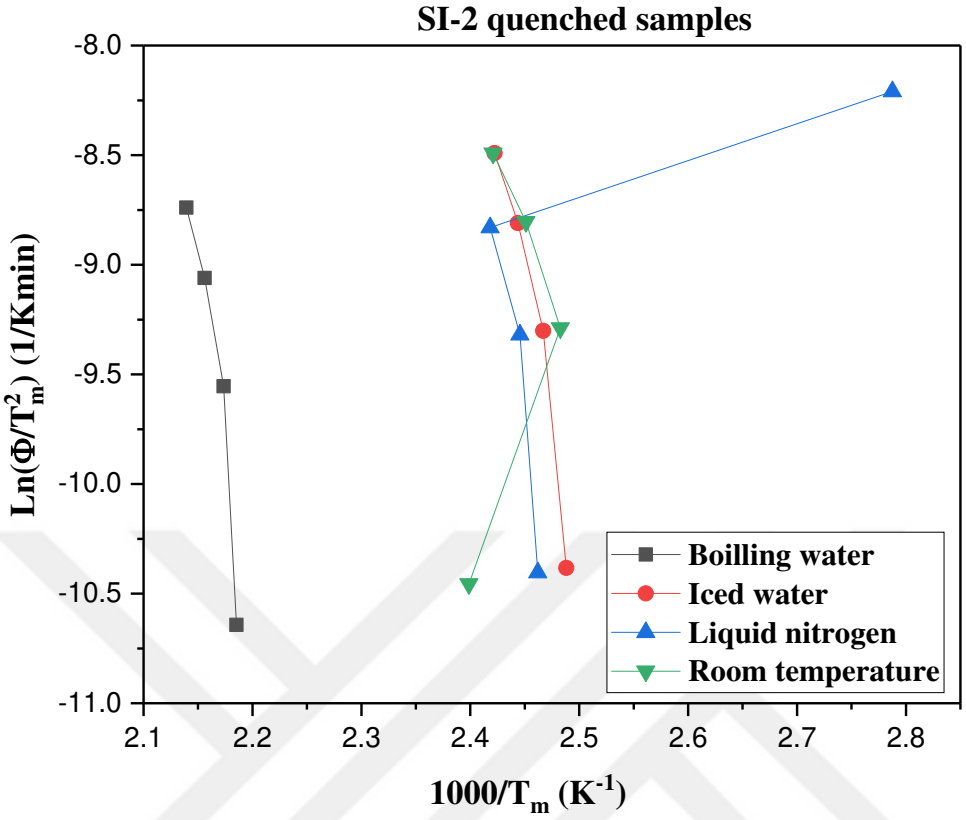

Figure 6.13 (b) Activation energy curves of SI-2 quenched samples.

Table 6.6 Activation energy values of SI-2 quenched samples using the Kissinger method.

SI-2 quenched samples activation energy (kJ/mol)	
Boiling water	72.75
Iced water	231.495016
Liquid nitrogen	28.068064
Room temperature	79.964052

SI-4 quenched samples activation energy is shown in Table 6.7 and we can see that the highest value and the lowest value is for sample quenched in room temperature and homogenized sample correspondingly. The activation energy value with the quenching/cooling type of the sample can be seen in Figure 6.13 (c).

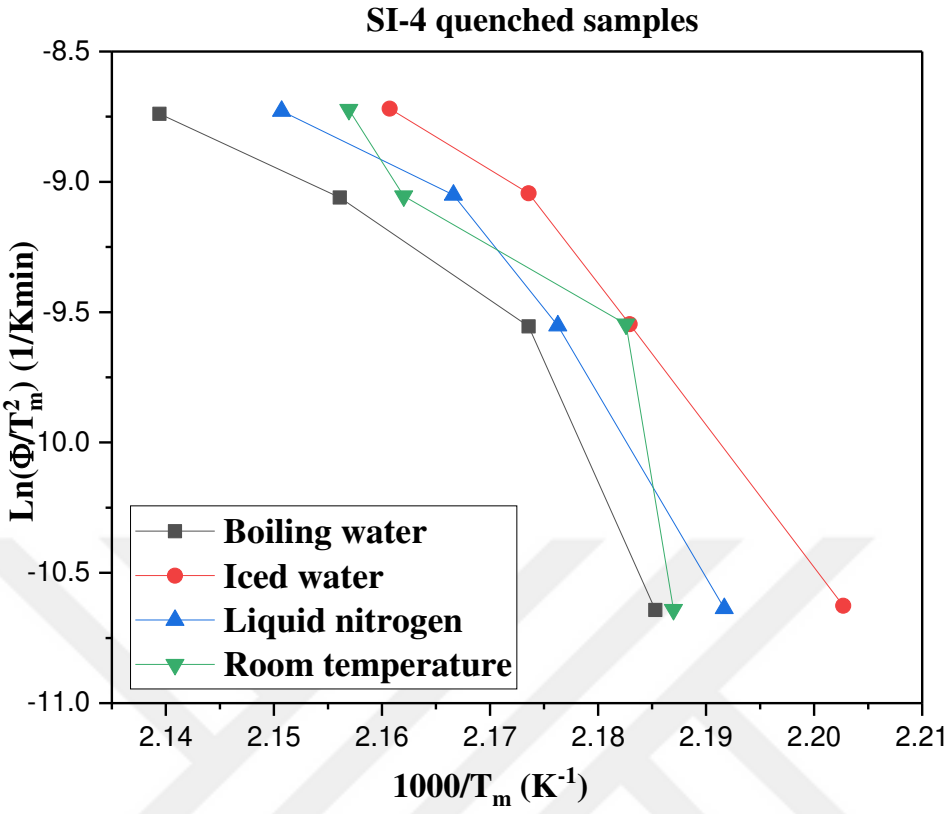

Figure 6.13 (c) Activation energy curves of SI-4 quenched samples.

Table 6.7 Activation energy values of SI-4 quenched samples using the Kissinger method.

SI-4 quenched samples activation energy (kJ/mol)	
Boiling water	322.42
Iced water	387.76496
Liquid nitrogen	388.746012
Room temperature	423.05789

6.4. Thermogravimetric/ Differential Thermal Analysis (TG/DTA) Measurement Results

Differential thermal analyses (DTA) measurements with a heating rate of 25 °C/min were taken for SI samples, to determine the order-disorder phase transitions at high temperatures as it can be seen in Figure 6.14 (a). Generally, β (A2) $\rightarrow\beta_2$ (B2) $\rightarrow\beta_1$($L2_1$) phase transitions can be observed in Cu-based SMAs. From far left, the transformations can be described as; A2→B2, B2→$L2_1$, and $L2_1$→9R or 18R transition, respectively. Liquefaction point of the samples is placed above A2→B2 transition at high temperature.

The endothermic peak which is slightly above 200ºC is the $L2_1$ (DO_3) →9R, 18R and above 500ºC the eutectoid point can be observed while above 600ºC is for A2→B2 transition.

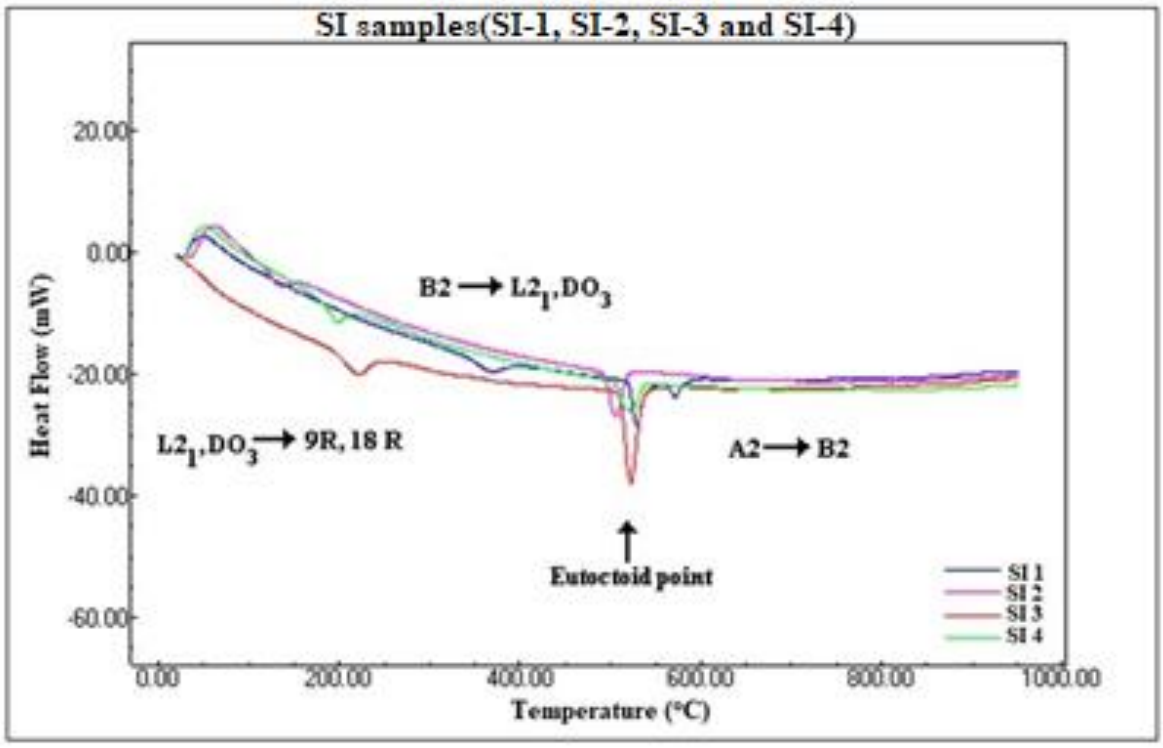

Figure 6.14 (a) DTA curves of SI-1, SI-2, SI-3 and SI-4 samples with a heating/cooling rate of 25 ˚C/min.

For SI-2 quenched samples also DTA measurements at a rate of 25°C/min were made as it is shown in Figure 6.14 (b), starting from left with the first endothermic peak of β1′(9R, 18R)→β1(L21) forward transitions which lay between 100-150°C, then metastable (β2)phase forms from β1 phase after that to the mixture of α and γ2 precipitation phases at 450-500°C. The eutectoid points as a deepest endothermic peak at around 500-550°C, then A2→B2 transitions observed at around 600°C and these characteristic transitions are common for Cu-Al based SMAs as mentioned in many literature reports [57, 74]. The deepest endothermic peak belongs to boiling water sample as we could observe this from the average enthalpy values that boiling water sample had the second-highest average enthalpy value.

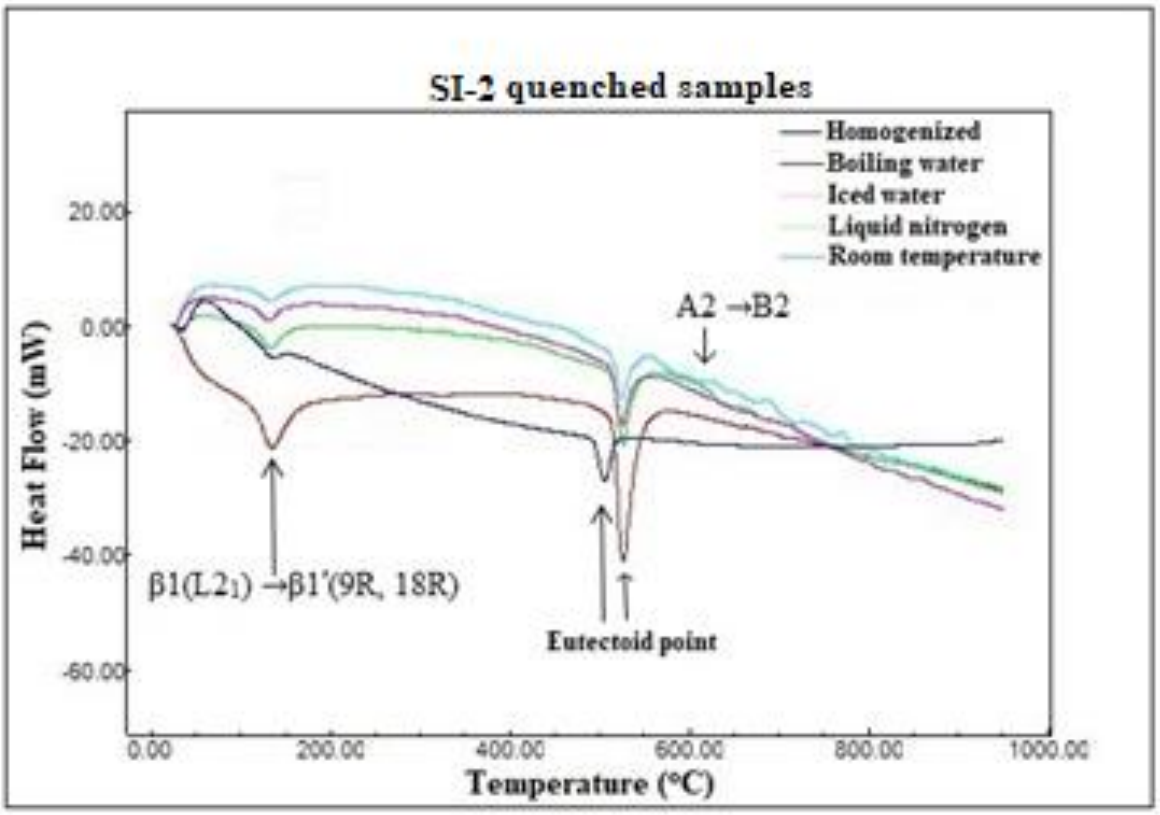

Figure 6.14 (b) DTA curves of SI-2 quenched sample with a heating/cooling rate of 25 ˚C/min.

The result of DTA measurements for all the SI-4 quenched samples at rate of 25°C/min shows that on the left side of the graph (Figure 6.14 (c)) nearly at between 170 and 200°C the first downward endothermic peaks of direct M(β1′; 9R, 18R)→A(β1; L21) transformations occurred in all samples. At around 450°C we can see the decomposition of β1 phase transfer at first into a metastable B2 (β2) then into the mixture of γ2and α precipitation phases. The eutectoid reaction that lays between 500 to 550ºC can be seen also. As it is obvious from Figure 6.14 (c) that the effect of quenching on the sample is very clear, were homogenized sample curve is on one side compared to the sample's curves.

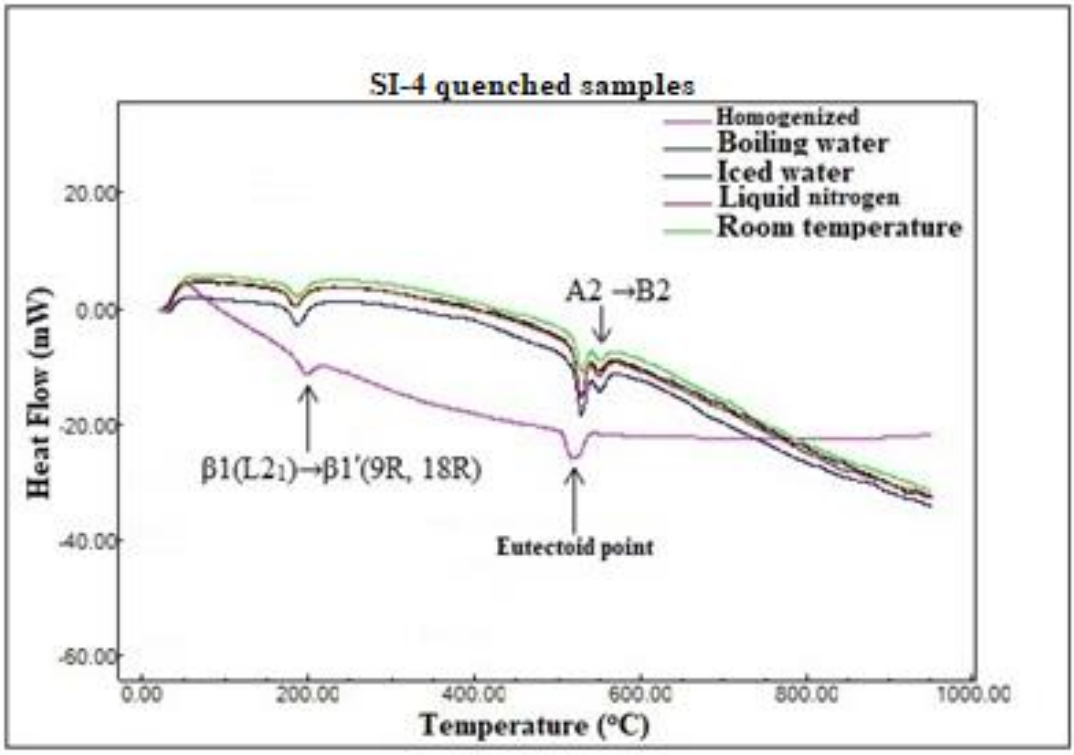

Figure 6.14 (c) DTA curves of SI-4 quenched samples with a heating/cooling rate of 25 ˚C/min.

7. CONCLUSIONS

In this study CuAlFeMn HTSMA samples of various compositions were prepared with arc-melting, four new SMA compositions were prepared and the thermal and structural properties were investigated. Two of these four samples were heat treated (SI-2 at 200˚C and SI-4 at 250˚C) and then quenched in four different cooling media, the mediums are boiling water, liquid nitrogen, iced water, room temperature and a reference sample (non-quenched) were kept as well. Thermal and structural analyses for quenched samples were also made. From the XRD results, we found that all the peaks are β1′(122) β1′(1210), β1′(2012) and β1′(0022) for all the samples can be seen, except in SI-1, the β1′(0022) can't be seen. The highest intensity peak belongs to 1210 plane for SI-2 among all the SI samples. The calculation for the structural analyzes of the SI samples on crystallite size shows that SI-2 has the largest crystallite size among other samples and that's in an agreement with the results of the XRD analyses. The differential scanning calorimetry for SI samples at a rate of 25°C/min showing martensite (M) to austenite (A) phase transitions and vice versa transition in the samples. martensite and austenite start and finish temperature, endothermic (martensite to austenite) and exothermic (austenite to martensite) temperatures and other thermodynamic characters were investigated. The analyzing results of this measurements are in an agreement with the previous measurements as the SI-2 sample shows the lowest endothermic transition and SI-1 the highest endothermic transition and that's, of course, related to the different percentages of elements wherein SI-2 the Mn percentage is higher compared to other SI samples. As well as the highest hysteresis value is for SI-1 and the lowest belong to SI-2 sample. The average enthalpy values that were calculated which we can see it as a rate of how easy a transformation may happen is the highest in SI-1 and lower in SI-2 but lowest in SI-4, so SI-1 is the hardest to transform and SI-4 easiest. The degree of order and disorder of samples from the average entropy values shown that SI-2 is the most ordered and least ordered is SI-4 , this result is also in agreement with the values that we got from the entropy values where the easiest sample to transform is SI-4 sample that has the lowest degree of order and SI-2 is the most ordered sample and it is harder compared to transform compared to SI-4. The highest electron concentration to average entropy value belongs to SI-2 and highest electron concentration value with average hysteresis value is for SI-1. All the SI sample electron concentration values fall in the acceptable range that shows the SME in samples.

The SI-2 sample quenched in four different media is also investigated thermally and structurally. The XRD measurements were made for these quenched samples also and monoclinic β1′(0022) of long order martensite (M18R) plane could be seen. The main diffracted planes for SI-2 both quenched samples and the non-quenched sample could be seen in SI-2 homogenized sample as the highest intensity peak and the lowest intensity peak is for SI-2 quenched in boiling water. The calculation of the crystallite size of all the aged/quenched and non-aged/non-quenched SI-2 samples was made and the same as the intensity peaks that we got from XRD measurements, the largest crystallite size (D) is for SI-2 quenched at room temperature sample and the smallest crystallite size is for SI-2 non-quenched homogenized sample. The analyzed results of average enthalpy values gives the same results as the crystallite size of the samples were the highest enthalpy value belong to SI-2 homogenized non-quenched sample and that shows that the sample with smallest crystallite size is more difficult to transform and that's how we see, that this sample has highest enthalpy values compared to other samples while the lowest average enthalpy values are for SI-2 quenched in liquid nitrogen and room temperature samples compared to other SI-2 quenched samples. The average entropy value is a degree of order of a sample, the sample that has higher opportunity to transform with higher enthalpy average also has higher entropy value which belongs to SI-2 homogenized non-quenched sample and the lowest entropy value is for SI-2 sample quenched at room temperature. The activation energy analyzed values of SI-2 samples also approved that SI-2 homogenized non-quenched sample has the highest activation energy value and that shows that in agreement with enthalpy and crystallite size calculations, SI-2 homogenized non-quenched sample needs more energy to transform. The lower activation energy can be seen for SI-2 sample quenched in boiling water and the lowest value is for SI-2 sample quenched in room temperature which shows that it is easier to transform, and this result could be seen in enthalpy and entropy average values.

SI-4 samples were structurally investigated and the highest intensity peak diffracted is for SI-4 quenched in liquid nitrogen and the lowest value is SI-4 homogenized non-quenched sample in agreement with these results, the calculation of crystallite size for SI-4 samples showed that the largest crystallite size is for SI-4 quenched in liquid nitrogen and smallest is for SI-4 quenched in boiling water and SI-4 homogenized non-quenched samples. The thermal analyzes for SI-4 samples show that the highest hysteresis value is for SI-4 quenched in boiling water and SI-4 quenched in liquid nitrogen samples while the

lowest hysteresis value belongs to SI-4 non-quenched homogenized sample. The average enthalpy values show that SI-4 homogenized non-quenched sample is the easiest to transform among the other SI-4 samples having the lowest average enthalpy value. The lowest entropy value is for SI-4 homogenized non-quenched sample as well, showing it as the least order sample between all the SI-4 samples. SI-4 quenched sample at room temperature and liquid nitrogen has the higher activation energy value showing them as more difficult sample between the SI-4 sample to transform while SI-4 homogenized non-quenched is the easiest sample among other SI-4 samples to be able to transform.

In conclusion, we found Cu-based shape memory alloys with four new compositions and their kinetic and structural characteristics were all changed by composition and besides these characteristic parameters were modified for two alloys among these alloys by thermal aging and also by the quenching media used after aging as coolant materials. Among the homogenized and non-aged + quenched SI samples, the effects of different amounts of Mn element were observed that different Mn additions decreased all the thermal parameters of the samples and according to this as much as the percentage of Mn is more, the thermal parameters decreases more, also the effects of Mn on the XRD results became also obvious, we know these Mn effects from previous studies in literature [55]. We see that SI-2 had greater crystallite size as the Mn percentage increased. When SI-2 quenched we can see that the effect of quenching on the samples are less compared to the effect that we can see in changing the compositions. The enthalpy entropy values for SI-2 quenched in liquid nitrogen and room temperature decreased to half of the main value that we got for other samples. The changes in SI-4 quenched samples thermal parameter is higher if we compare it with the number of changes that can be seen in SI-2 quenched samples, but in the main while in opposite with SI-2 quenched sample in room temperature the enthalpy value for SI-4 quenched in room temperature is higher compared to other SI-4 quenched samples. The effect of quenching media in SI-2 samples on the crystallite size is quite noticeable and it shows obviously that quenching increased the crystallite size in the samples, but the same thing doesn't apply for all the SI-4 quenched samples because SI-4 quenched in boiling water showed less crystallite size value compared to SI-4 non-quenched sample. The activation energy value decreased for SI-2 when it was quenched but for SI-4 is increased. The DTA values on the DTA graphs for all the samples show that in SI-2 quenched samples the transformation peaks seems to be more rapid especially in the eutectic points. The boiling water effect on thermal and structural parameters for SI-2 samples was the most

noticed among the other quenching medias effect and for SI-4 it gave a good result as well, so we can say that boiling water as a quenching media is one of the most effective media's that can be use for high temperature shape memory alloys (alloys which have A_s values higher than boiling water temperature, too) since the molecules of the boiling water vibrate fast and that makes the number of collusions between the molecules of boiling water and the surface of the any hotter shape memory alloy sample more. So the difference between quenching media's temperature and sample's A_s or aging temperature is important to make the sample cool down fast or slow and this cooling ability of a quenching medium affects the characteristics of SMAs dramatically.

8. REFERENCES

[1]. **Sreekumar, M., T. Nagarajan, and M. Singaperumal**, *Design of a shape memory alloy actuated compliant smart structure: elastica approach.* Journal of Mechanical Design, 2009. **131**(6): p. 061008.

[2.] **Sreekumar, M.**, et al., *Recent advances in nonlinear control technologies for shape memory alloy actuators.* Journal of Zhejiang University-Science A, 2007. **8**(5): p. 818-829.

[3]. **Ölander, A**., *An electrochemical investigation of solid cadmium-gold alloys.* Journal of the American Chemical Society, 1932. **54**(10): p. 3819-3833.

[4]. **Vernon, L.B. and H.M. Vernon,** *Process of manufacturing articles of thermoplastic synthetic resins*. 1941, Google Patents.

[5]. **Kauffman, G.B. and I. Mayo**, *The story of nitinol: the serendipitous discovery of the memory metal and its applications.* The chemical educator, 1997. **2**(2): p. 1-21.

[6]. **Canbay, C.A., A. Aydoğdu, and Y. Aydoğdu**, *The investigation of thermal and magnetic properties and microstructure analysis of Cu–Al–Mn shape memory alloys.* Journal of superconductivity and novel magnetism, 2011. **24**(1-2): p. 871-877.

[7]. **Furuya, Y**., *Design and material evaluation of shape memory composites.* Journal of intelligent material systems and structures, 1996. **7**(3): p. 321-330.

[8]. **Wang, Y. and E. Ma**, *Strain hardening, strain rate sensitivity, and ductility of nanostructured metals.* Materials Science and Engineering: A, 2004. **375**: p. 46-52.

[9]. **He, G., et al**., *Novel Ti-base nanostructure–dendrite composite with enhanced plasticity.* Nature materials, 2003. **2**(1): p. 33.

[10]. **Wang, Y., E. Ma, and M. Chen**, *Enhanced tensile ductility and toughness in nanostructured Cu.* Applied physics letters, 2002. **80**(13): p. 2395-2397.

[11]. **Wycliffe, P., U. Kocks, and J. Embury**, *On dynamic and static strain ageing in substitutional and interstitial alloys.* Scripta Metallurgica, 1980. **14**: p. 1349-1354.

[12]. **Wycliffe, P**., *Dynamic and static strain aging in substitutional and interstitial alloys.* TMS (The Metallurgical Society) Paper Selection;(USA), 1980. **56**(CONF-840909--).

[13]. **Goldschmid, H.J**., *Interstitial alloys*. 2013: Springer.

[14]. **Porter, D.A., K.E. Easterling, and M. Sherif**, *Phase Transformations in Metals and Alloys, (Revised Reprint)*. 2009: CRC press.

[15]. **Meyrick, G. and G.W. Powell**, *Phase transformations in metals and alloys.* Annual Review of Materials Science, 1973. **3**(1): p. 327-362.

[16]. **Christian, J.W**., *The theory of transformations in metals and alloys*. 2002: Newnes.

[17]. **Vodárek, V.**, *"Phase Transformations"*. Ostrava 2013 Technická univerzita Ostrava: Technická univerzita Ostrava. p. page.2.

[18]. **Christensen, A., et al.**, *Phase diagrams for surface alloys.* Physical Review B, 1997. **56**(10): p. 5822.

[19]. URL: www.doitpoms.ac.uk/tlplib/phase-diagrams/phasediags2.php *Phase Transformation Diagrams.20.06.2018*

[20]. **Mehrer, H. and N. Stolica**, *Diffusion in solid metals and alloys.* Landolt-Börnstein numerical data and functional relationships in science and technology, Group III, 1990. **26**.

[21]. **Offerman, S., et al**., *Grain nucleation and growth during phase transformations.* Science, 2002. **298**(5595): p. 1003-1005.

[22]. **Doremus, R.H.**, *Rates of phase transformations.* 1985.

[23]. **Rios, P.R., et al**., *Nucleation and growth during recrystallization.* Materials Research, 2005. **8**(3): p. 225-238.

[24]. URL:http://community.dur.ac.uk/sharon.cooper/lectures/cryskinetics/handoutsalla .html *Nuclei and Growth of Phases.20.06.2018* .

[25]. J**ames, R.D. and K.F. Hane**, *Martensitic transformations and shape-memory materials.* Acta materialia, 2000. **48**(1): p. 197-222.

[26]. **Airoldi, G**., *Shape Memory Alloys: From Microstructure to Macroscopic Properties*. 1997: Trans Tech Publ.

[27]. **Nishiyama, Z**., *Martensitic transformation*. 2012: Elsevier.

[28]. **Johnson, D.F. and E.A. Carter**, *Nonadiabaticity in the iron bcc to hcp phase transformation.* The Journal of chemical physics, 2008. **128**(10): p. 104703.

[29]. **Khachaturyan, A**., *Theory of structural transformations in solids Wiley.* New York. transforms, 1983.

[30.] **Vojtko, M. and S. Longauer.** *Study Of Decomposition Of Thermoelastic And Non-thermoelastic Martensite In Cu-Zn-Al Alloys*. in *European Symposium on Martensitic Transformations*. 2009. EDP Sciences.

[31]. URL: http://www.scielo.br/scielo.php?script=sci_arttext&pid=S1678-77572003000300002 .*Effect of ordering on hypothetical stress-strain curves 20.06.2018.*

[32]. **Greger, M. and L. Kander**, *Development of microstructure and mechanical properties of austenitic stainless steel after ECAP deformation.* Proc. METAL, 2013.

[33]. **Funakubo, H. and J. Kennedy**, *Shape memory alloys.* Gordon and Breach, xii+ 275, 15 x 22 cm, Illustrated, 1987.

[34]. **Law, N., P. Howell, and D. Edmonds**, *Structure of lath martensite and occurrence of retained austenite in as-quenched Fe-VC low-alloy steels.* Metal Science, 1979. **13**(9): p. 507-515.

[35]. **Buehler, W.J. and F.E. Wang,** *A summary of recent research on the nitinol alloys and their potential application in ocean engineering.* Ocean Engineering, 1968. **1**(1): p. 105-120.

[36]. **Liu, Y.,** *Some factors affecting the transformation hysteresis in shape memory alloys.* Chen HR, editor, 2010: p. 361-9.

[37]. **Stöckel, D**., *The shape memory effect-phenomenon, alloys and applications.* California, 1995. **94539**: p. 1-13.

[38]. **Cederström, J. and J. Van Humbeeck**, *Relationship between shape memory material properties and applications.* Le Journal de Physique IV, 1995. **5**(C2): p. C2-335-C2-341.

[39]. **Sun, L. and W. Huang,** *Nature of the multistage transformation in shape memory alloys upon heating*. Metal Science and Heat Treatment, 2009. **51**(11): p. 573-578.

[40]. **Buehler, W.J., J. Gilfrich, and R. Wiley,** *Effect of low-temperature phase changes on the mechanical properties of alloys near composition TiNi.* Journal of applied physics, 1963. **34**(5): p. 1475-1477.

[41]. **Huang, W.,** *On the selection of shape memory alloys for actuators.* Materials & design, 2002. **23**(1): p. 11-19.

[42]. **Hartl, D.J. and D.C. Lagoudas,** *Aerospace applications of shape memory alloys.* Proceedings of the Institution of Mechanical Engineers, Part G: Journal of Aerospace Engineering, 2007. **221**(4): p. 535-552.

[43]. **Song, C.,** *History and current situation of shape memory alloys devices for minimally invasive surgery.* The Open Medical Devices Journal, 2010. **2**(1).

[44]. **Jani, J.M., et al.,** *A review of shape memory alloy research, applications and opportunities.* Materials & Design (1980-2015), 2014. **56**: p. 1078-1113.

[45]. **Langbein,** S. *Development of standardised and integrated shape memory components in "one-module"-design*. in *European Symposium on Martensitic Transformations*. 2009. EDP Sciences.

[46]. **Mahtabi, M.J., N. Shamsaei, and M.H. Elahinia,** *Fatigue of shape memory alloys.* Shape memory alloy actuators. John, New York, 2015: p. 155-190.

[47]. **Pons, C.V.U.,** *Improvement of the one-way and two-way shape memory effects in ti-ni shape memory alloys by thermomechanical treatments*. 2011, Universitat Rovira i Virgili.

[48]. **Laureanda, C.,** *One Way and Two Way–Shape Memory Effect: Thermo–Mechanical Characterization of Ni–Ti wires*. 2008, Ph. D. thesis, Universitá degli Studi di Pavia.

[49]. **Huang, W. and W. Toh,** *Training two-way shape memory alloy by reheat treatment.* Journal of materials science letters, 2000. **19**(17): p. 1549-1550.

[50]. **Brailovski, V., et al.**, *Shape memory alloys: fundamentals, modeling and applications*. 2003: École de technologie supérieure.

[51]. **Otsuka, K. and C.M. Wayman,** *Shape memory materials*. 1999: Cambridge university press.

[52]. **Sarı, U. and T. Kırındı,** *Effects of deformation on microstructure and mechanical properties of a Cu–Al–Ni shape memory alloy.* Materials characterization, 2008. **59**(7): p. 920-929.

[53]. **Canbay, C.A. and A. Aydoğdu,** *Thermal analysis of Cu-14.82 wt% Al-0.4 wt% Be shape memory alloy.* Journal of thermal analysis and calorimetry, 2013. **113**(2): p. 731-737.

[54]. **Kohler, F., et al.,** *Peritectic solidification of Cu–Sn alloys: Microstructural competition at low speed.* Acta Materialia, 2009. **57**(1): p. 56-68.

[55]. **Canbay, C.A. and Z. Karagoz,** *The effect of quaternary element on the thermodynamic parameters and structure of CuAlMn shape memory alloys.* Applied Physics A, 2013. **113**(1): p. 19-25.

[56]. **Canbay, C.A. and A. Keskin,** *Effects of vanadium and cadmium on transformation temperatures of Cu–Al–Mn shape memory alloy.* Journal of Thermal Analysis and Calorimetry, 2014. **118**(3): p. 1407-1412.

[57]. **Canbay, C.A., Z.K. Genc, and M. Sekerci,** *Thermal and structural characterization of Cu–Al–Mn–X (Ti, Ni) shape memory alloys.* Applied Physics A, 2014. **115**(2): p. 371-377.

[58]. **Sutou, Y., R. Kainuma, and K. Ishida,** *Effect of alloying elements on the shape memory properties of ductile Cu–Al–Mn alloys.* Materials Science and Engineering: A, 1999. **273**: p. 375-379.

[59]. **Mallik, U. and V. Sampath,** *Effect of alloying on microstructure and shape memory characteristics of Cu–Al–Mn shape memory alloys.* Materials Science and Engineering: A, 2008. **481**: p. 680-683.

[60]. **Shindo, D. and T. Oikawa,** *Analytical electron microscopy for materials science*. 2013: Springer Science & Business Media.

[61]. URL: www.blog.phenom-world.com/edx-analysis-scanning-electron-micrscope-sem *EDX analysis.* 20.05.2018.

[62]. **Patterson, A.**, *The Scherrer formula for X-ray particle size determination.* Physical review, 1939. **56**(10): p. 978.

[63]. **Degeratu, S., et al.,** *Thermal study of a shape memory alloy (SMA) spring actuator designed to insure the motion of a barrier structure.* Journal of thermal analysis and calorimetry, 2013. **111**(2): p. 1255-1262.

[64]. **O'neill, M.,** *The Analysis of a Temperature-Controlled Scanning Calorimeter.* Analytical chemistry, 1964. **36**(7): p. 1238-1245.

[65]. URL: www.shimadzu.com/an/C160-E013A. *DSC analysis. 20.05.2018.*

[66]. **Pineda, R., A. Robledo, and H. Correa,** *CALORIMETRÍA AC DE ALTA RESOLUCIÓN HIGH RESOLUTION AC CALORIMETRY.*

[67]. **Jonsson, J., et al.,** *Electroluminescence from polyolefins subjected to a homogeneous ac field.* IEEE transactions on dielectrics and electrical insulation, 1995. **2**(1): p. 107-113.

[68]. **Paulik, F.,** *Special trends in thermal analysis*. 1995: John Wiley & Son Ltd.

[69]. **Ozawa, T.,** *Thermal analysis—review and prospect.* Thermochimica Acta, 2000. **355**(1-2): p. 35-42.

[70]. URL: www.shimadzu.com/an/C160-E006H.*Schemadzu DTA. 21.05.2018.*

[71]. **Mallik, U. and V. Sampath,** *Influence of quaternary alloying additions on transformation temperatures and shape memory properties of Cu–Al–Mn shape memory alloy.* Journal of Alloys and Compounds, 2009. **469**(1-2): p. 156-163.

[72]. **Yang, S., et al.,** *Microstructure and properties of Cu–Al–Fe high-temperature shape memory alloys.* Materials Science and Engineering: B, 2014. **185**: p. 67-73.

[73]. **Ahlers, M.,** *Phase stability of martensitic structures.* Le Journal de Physique IV, 1995. **5**(C8): p. C8-71-C8-80.

[74]. **Otsuka, K. and C. Wayman,** *Mechanism of shape memory effect and superelasticity.* Shape memory materials, 1998: p. 27-48.

[75]. **Canbay, C.A., S. Gudeloglu, and Z.K. Genc,** *Investigation of the enthalpy/entropy variation and structure of Cu–Al–Mn–Fe shape memory alloys.* International Journal of Thermophysics, 2015. **36**(4): p. 783-794.

[76]. **Kissinger, H.E.,** *Reaction kinetics in differential thermal analysis.* Analytical chemistry, 1957. **29**(11): p. 1702-1706.

ADDITIONS

DSC Measurements for SI-1, SI-2, SI-3, and SI-4 non-quenched homogenized samples at a heating/cooling rate of 5, 15, 25 and 35 ˚C/min

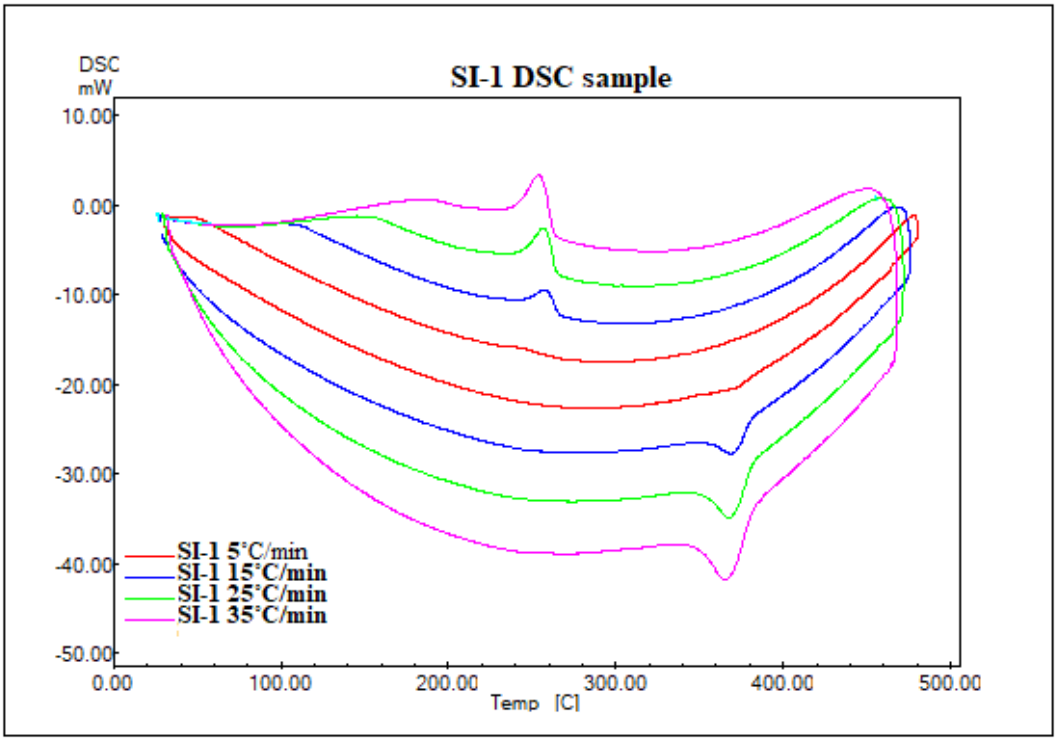

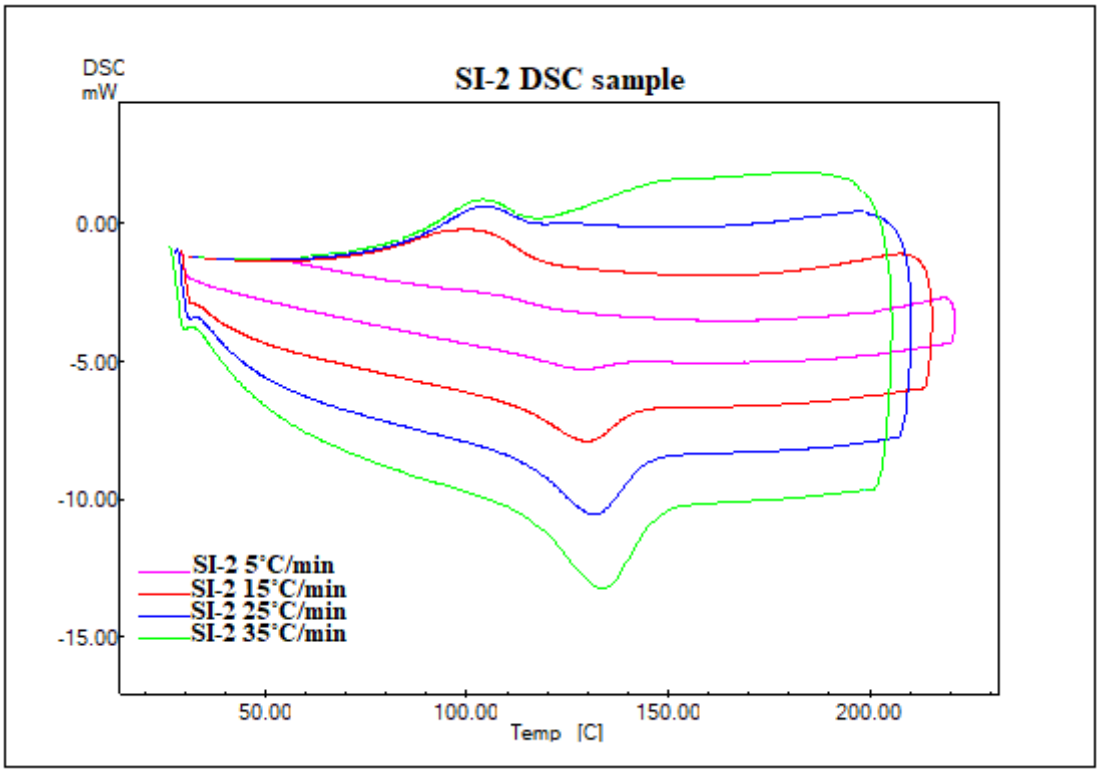

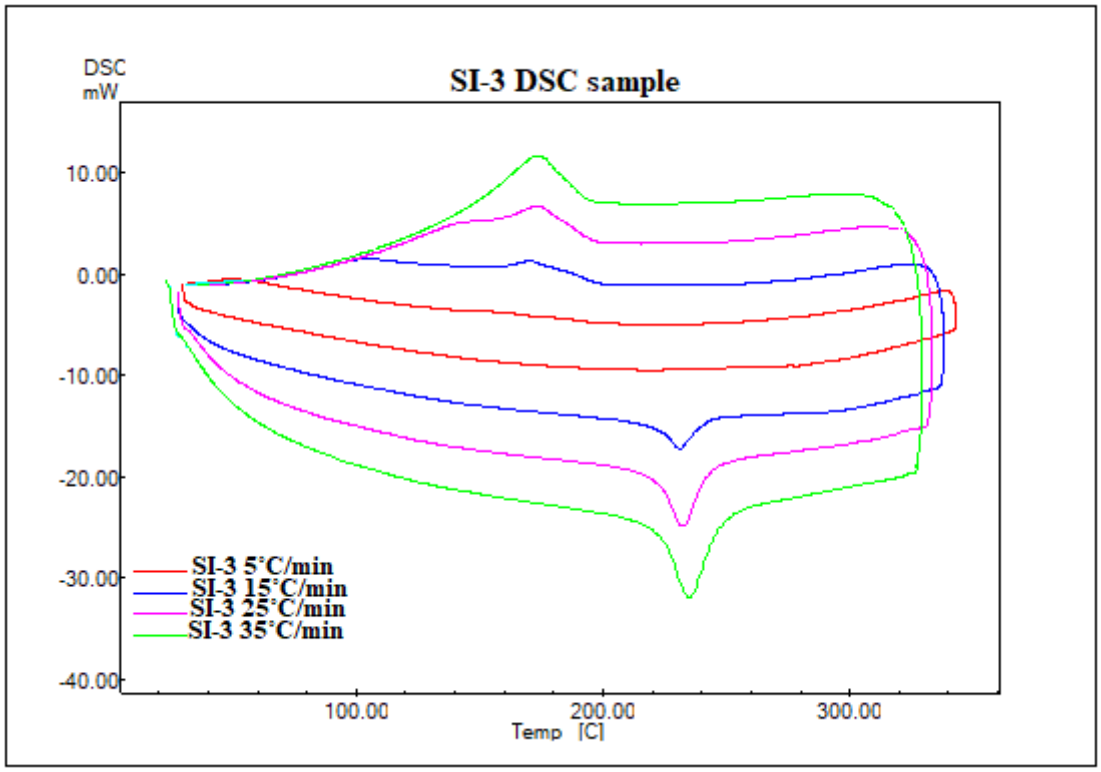
SI-3 DSC sample
DSC
mW
10.00
0.00
-10.00
-20.00
-30.00
-40.00
100.00
200.00
300.00
Temp [C]
SI-3 5°C/min
SI-3 15°C/min
SI-3 25°C/min
SI-3 35°C/min

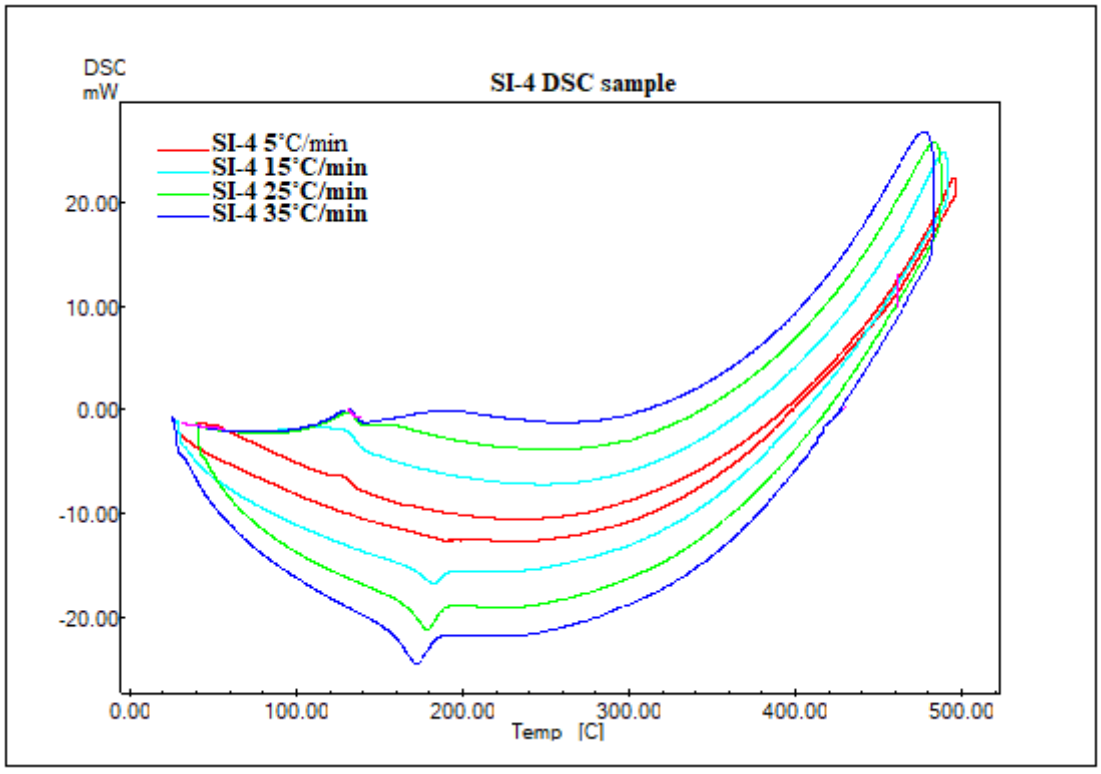
SI-4 DSC sample
DSC
mW
20.00
10.00
0.00
-10.00
-20.00
0.00
100.00
200.00
300.00
400.00
500.00
Temp [C]
SI-4 5°C/min
SI-4 15°C/min
SI-4 25°C/min
SI-4 35°C/min

DSC for SI(1, 2, 3, and 4) homogenized non-quenched samples at a heating/cooling rate of 5, 15, 25 and 35 ˚C/min.

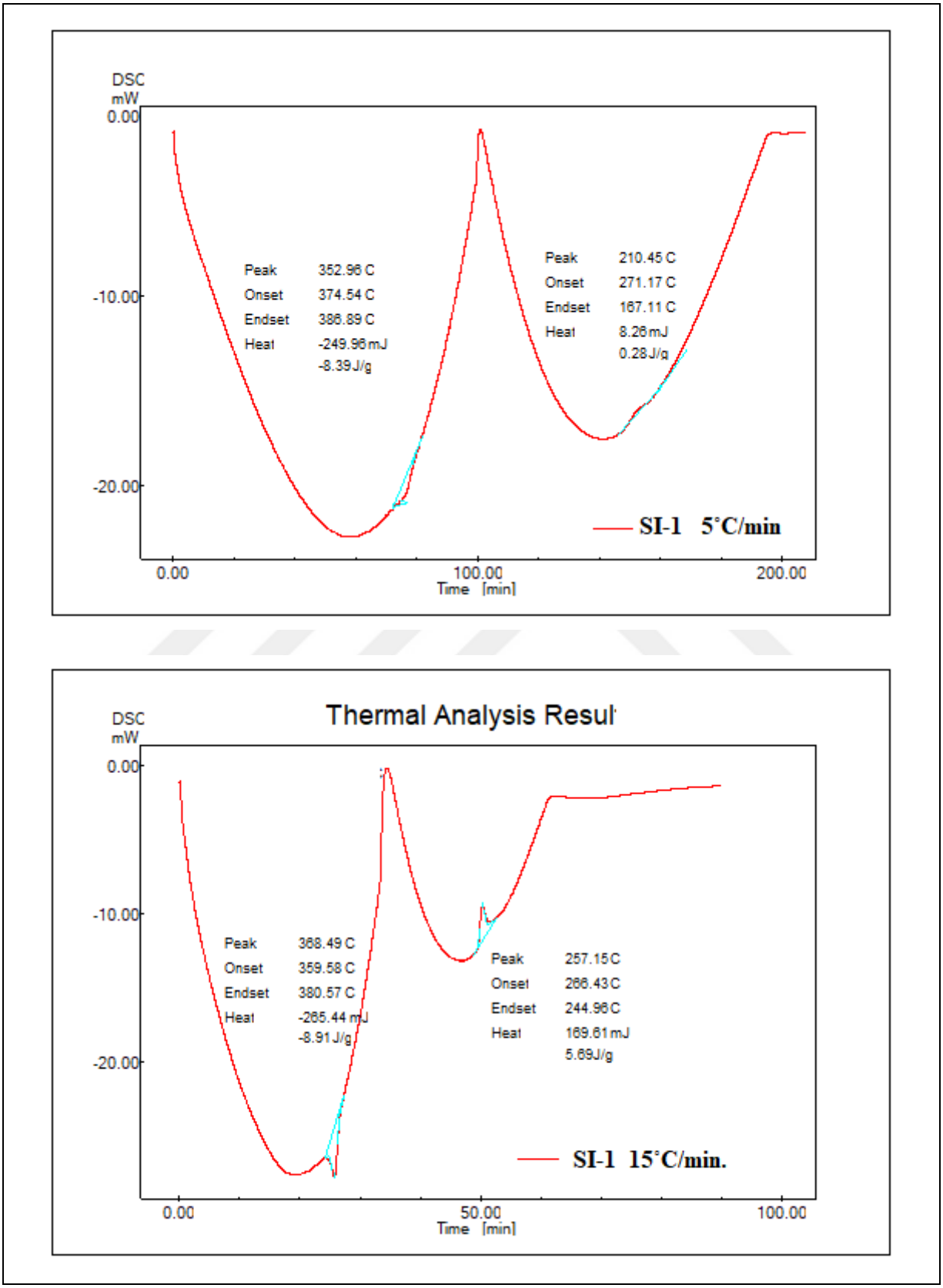

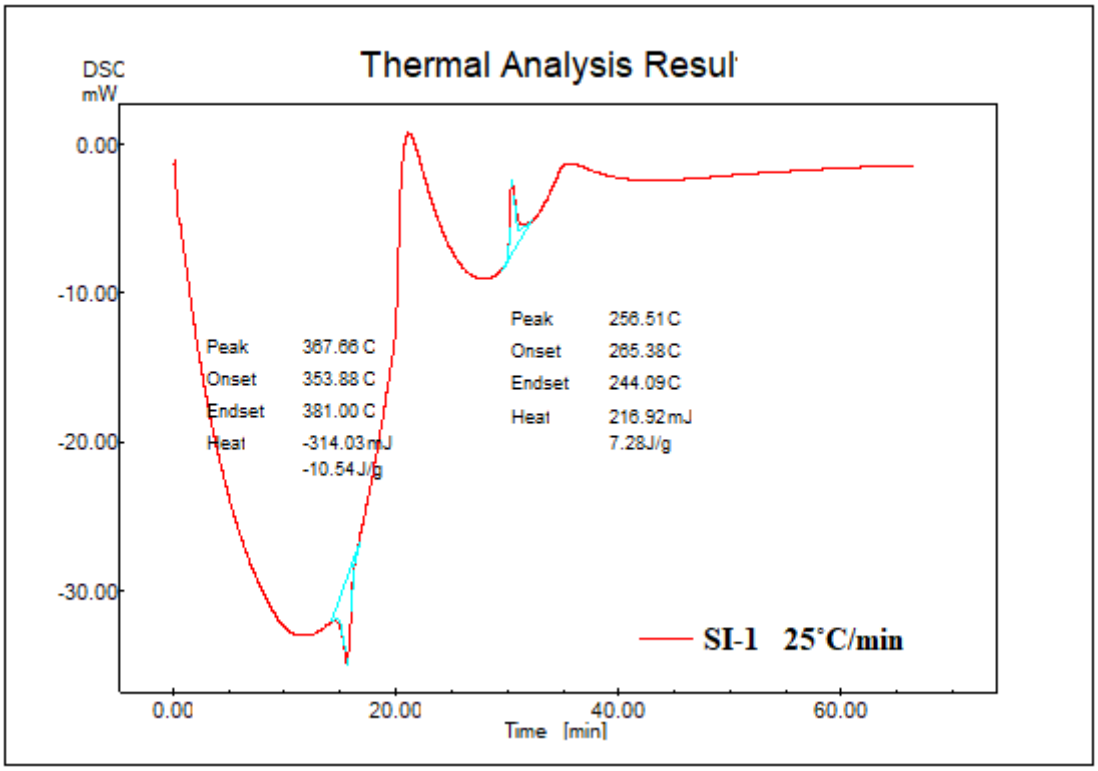

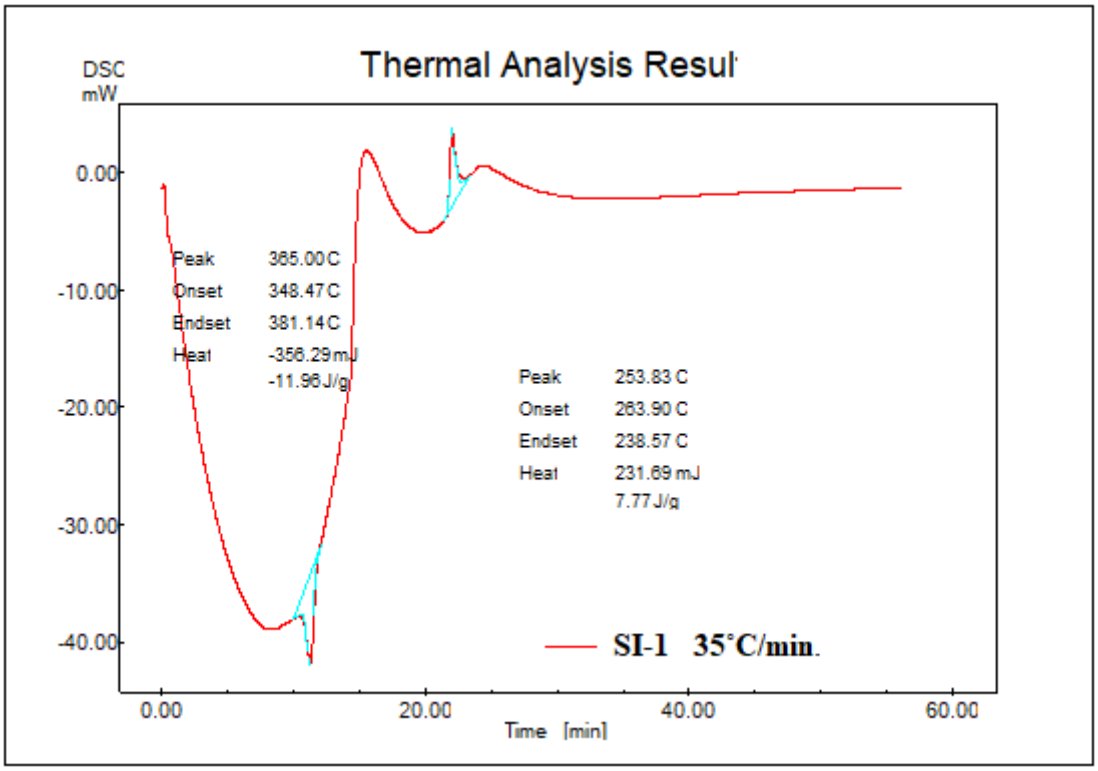

DSC for SI-1 homogenized non-quenched at a heating/cooling rate of 5, 15, 25 and 35 ˚C/min.

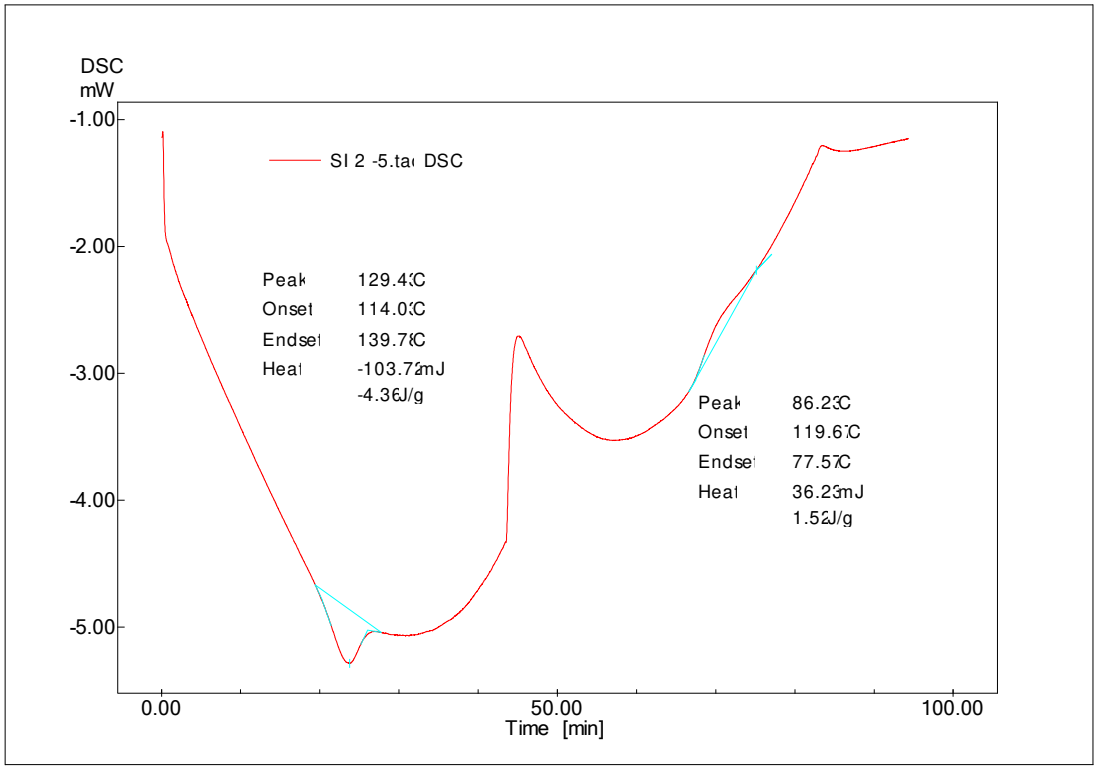
DSC
mW
-1.00
-2.00
-3.00
-4.00
-5.00
SI 2 -5.ta DSC
Peak 129.4
Onset 114.0
Endset 139.7
Heat -103.7 mJ
-4.36 J/g
Peak 86.2
Onset 119.6
Endset 77.5
Heat 36.2 mJ
1.52 J/g
0.00
50.00
100.00
Time [min]

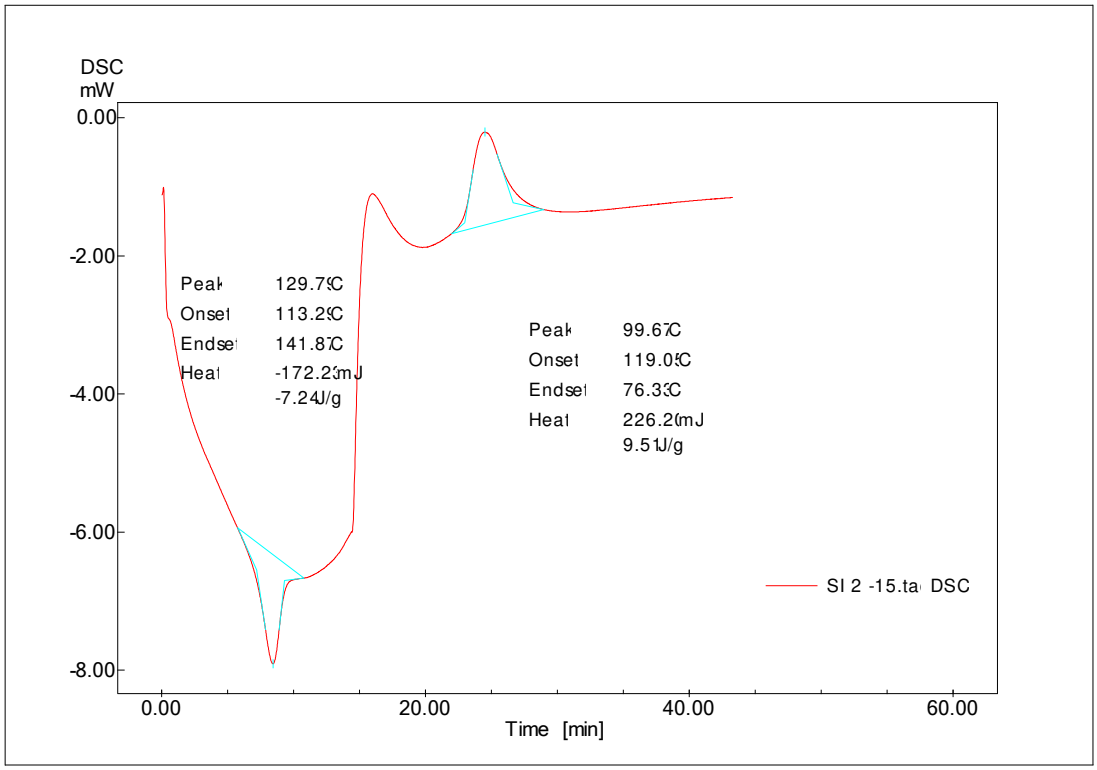
DSC
mW
0.00
-2.00
-4.00
-6.00
-8.00
Peak 129.7
Onset 113.2
Endset 141.8
Heat -172.2 mJ
-7.24 J/g
Peak 99.6
Onset 119.0
Endset 76.3
Heat 226.2 mJ
9.51 J/g
SI 2 -15.ta DSC
0.00
20.00
40.00
60.00
Time [min]

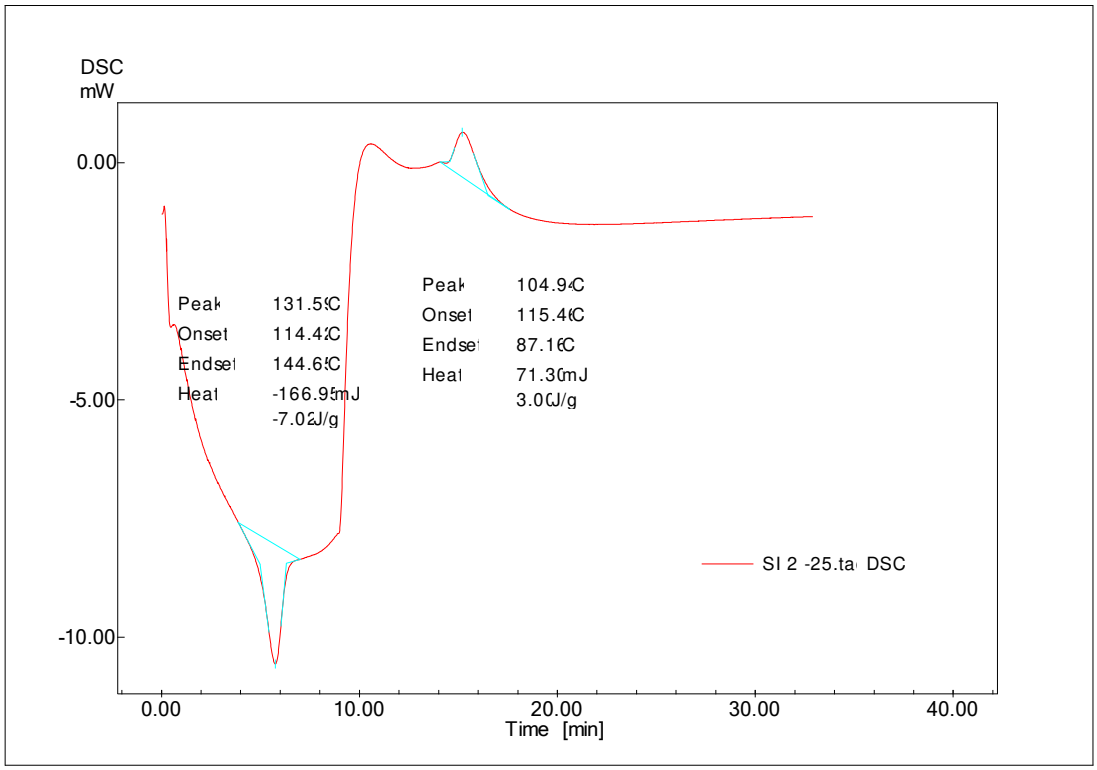

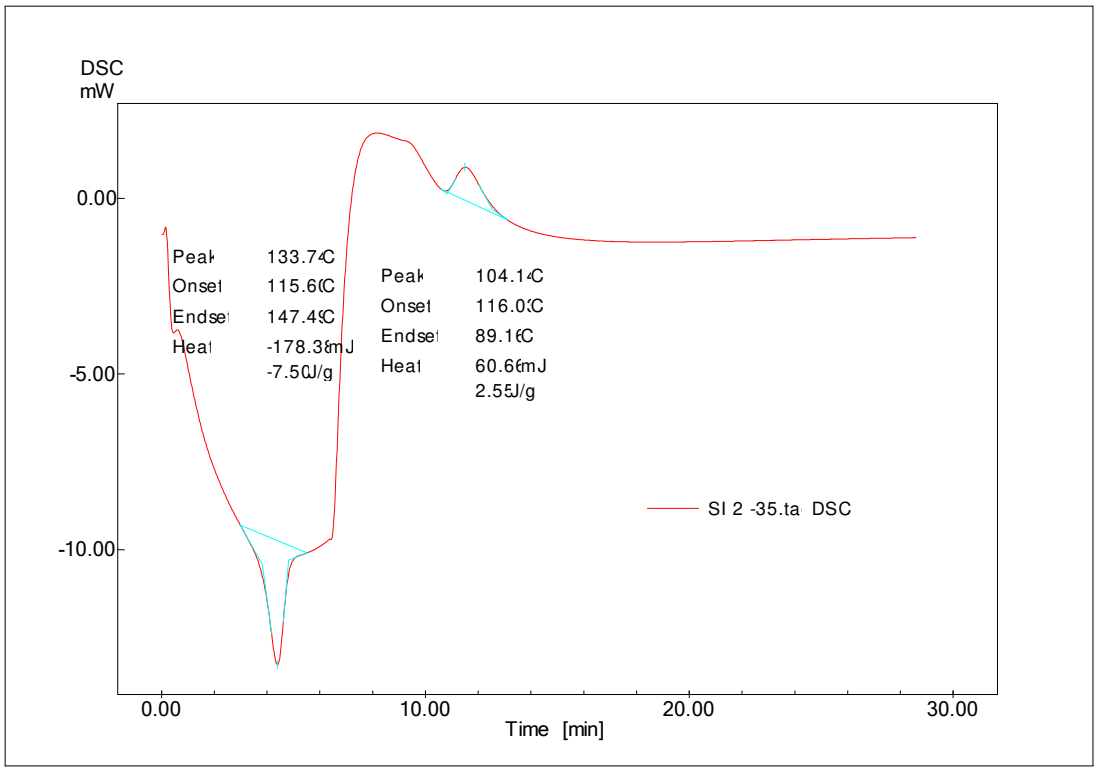

DSC for SI-2 homogenized non-quenched at a heating/cooling rate of 5, 15, 25 and 35 ˚C/min.

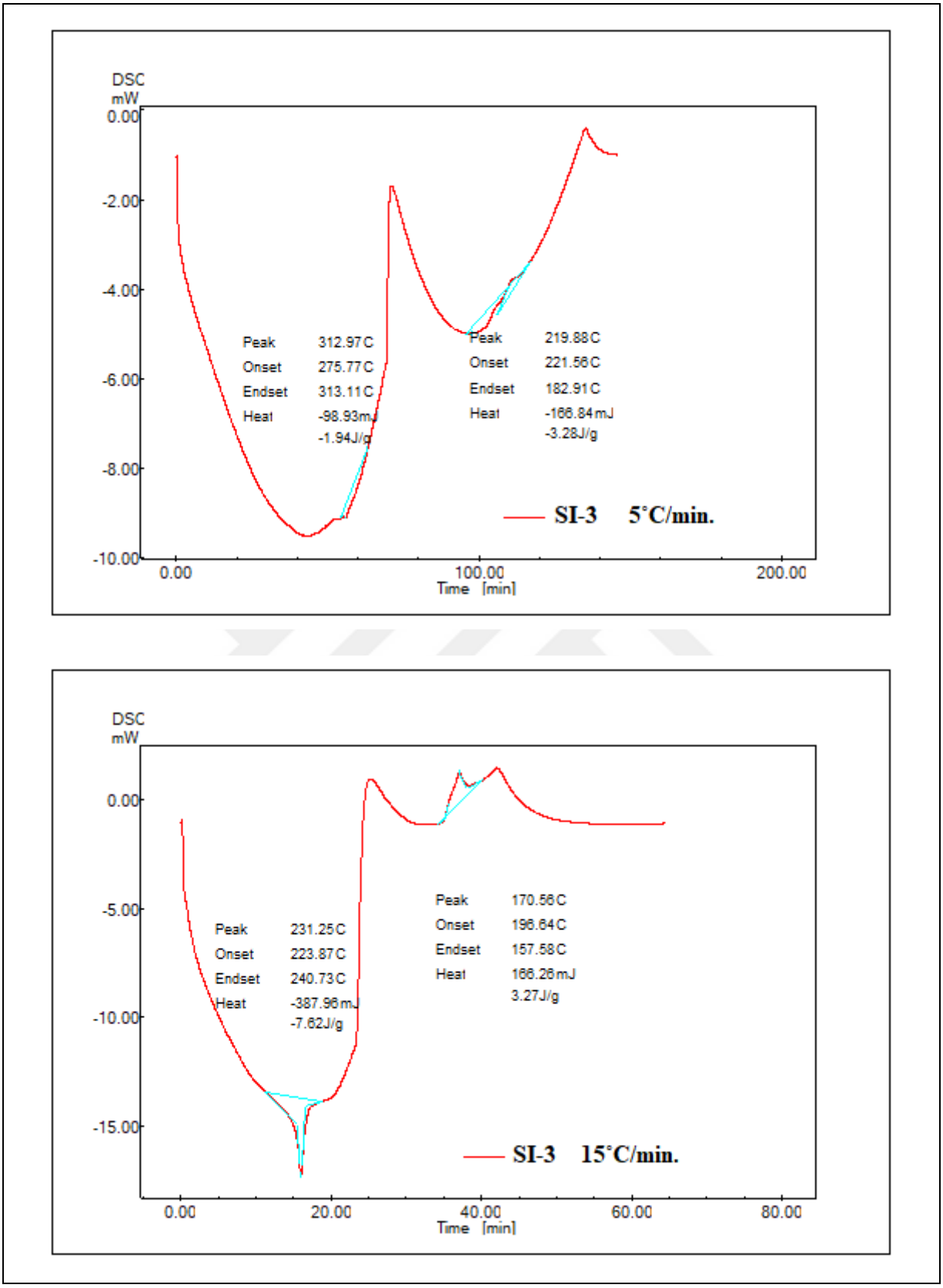
DSC
mW
0.00
-2.00
-4.00
-6.00
-8.00
-10.00
0.00
100.00
200.00
Time [min]
Peak 312.97C
Onset 275.77C
Endset 313.11C
Heat -98.93mJ
-1.94J/g
Peak 219.88C
Onset 221.56C
Endset 182.91C
Heat -166.84mJ
-3.28J/g
SI-3 5°C/min.
DSC
mW
0.00
-5.00
-10.00
-15.00
0.00
20.00
40.00
60.00
80.00
Time [min]
Peak 231.25C
Onset 223.87C
Endset 240.73C
Heat -387.96mJ
-7.62J/g
Peak 170.56C
Onset 196.64C
Endset 157.58C
Heat 166.26mJ
3.27J/g
SI-3 15°C/min.

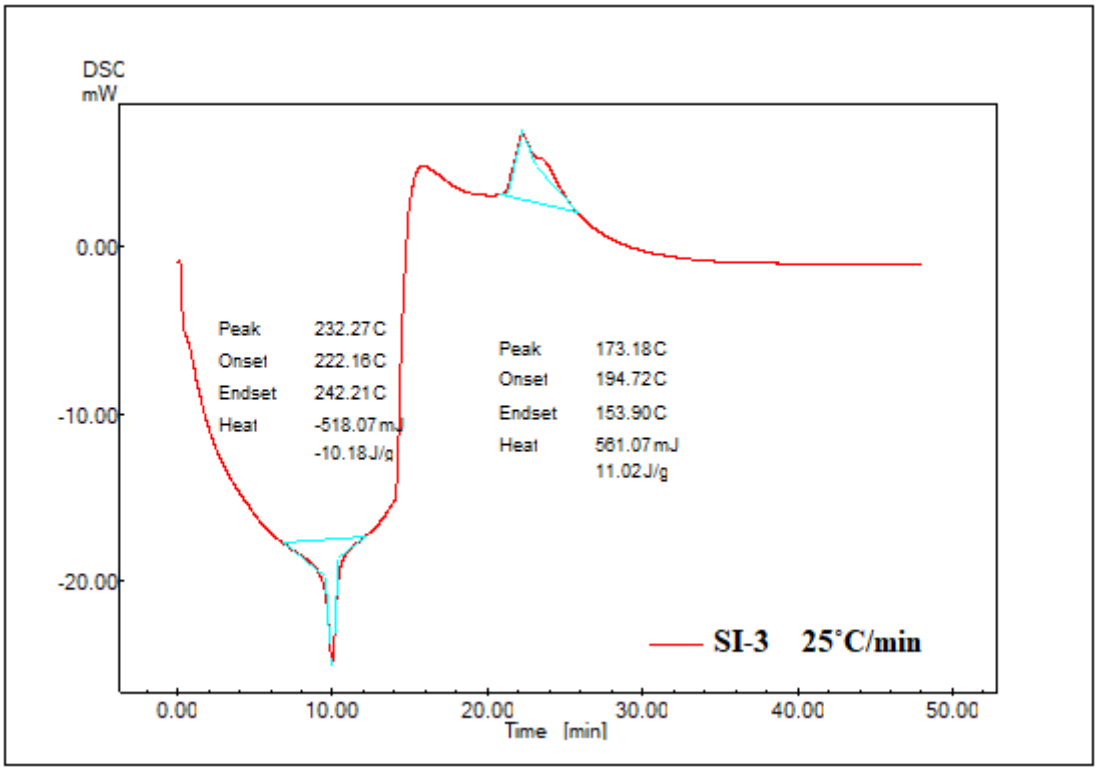

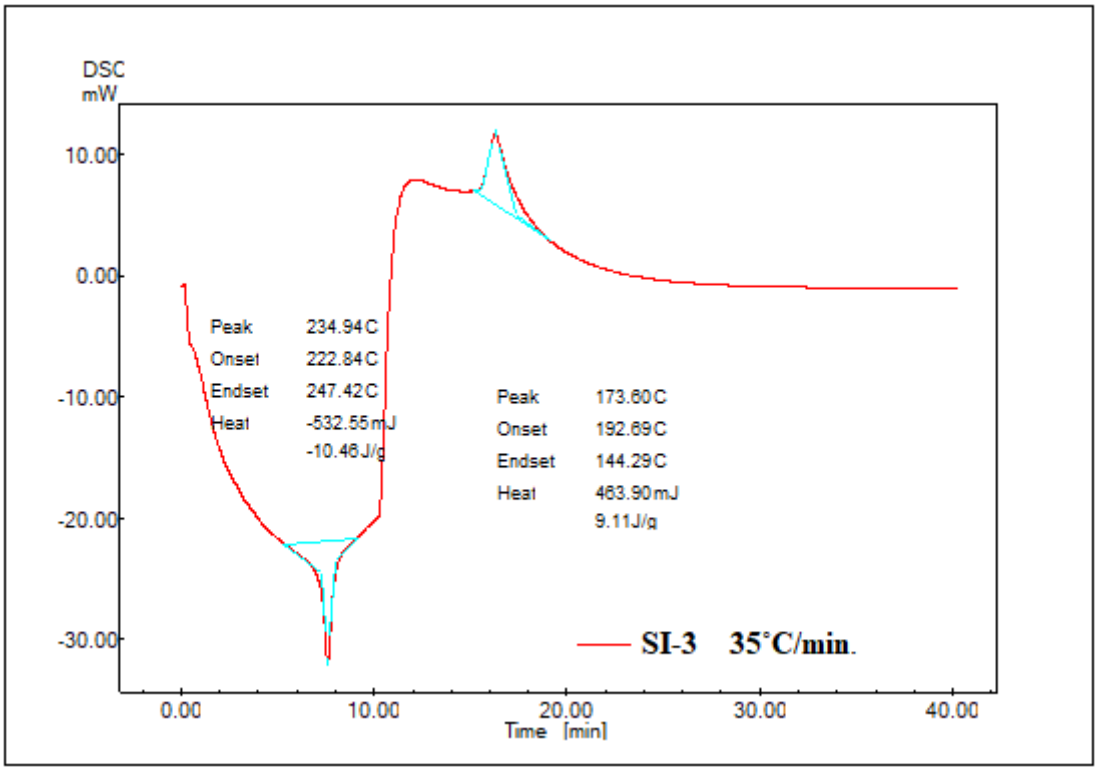

DSC for SI-3 homogenized non-quenched at a heating/cooling rate of 5, 15, 25 and 35 ˚C/min.

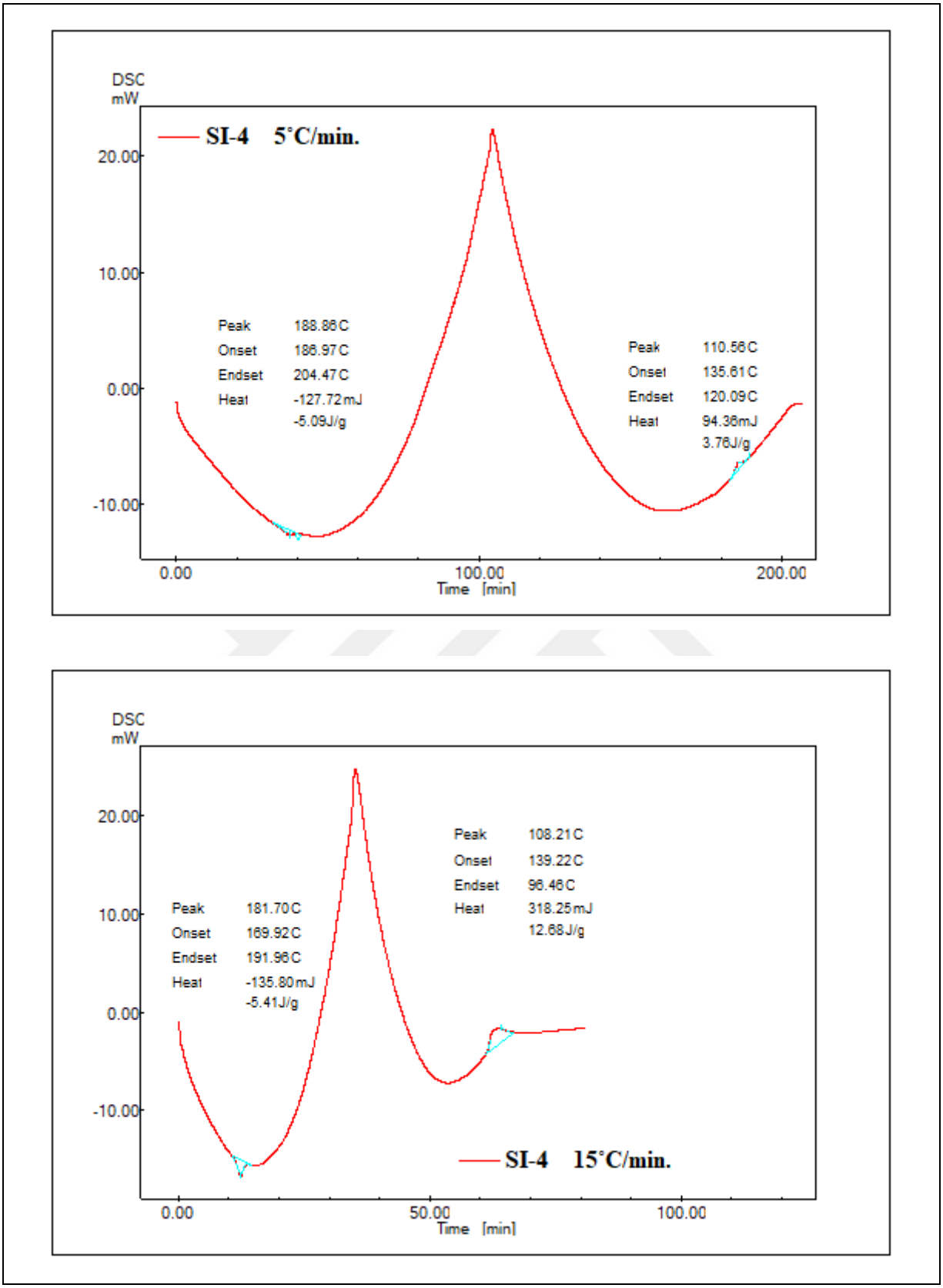
DSC
mW
SI-4 5°C/min.
20.00
10.00
0.00
-10.00
Peak 188.86C
Onset 186.97C
Endset 204.47C
Heat -127.72mJ
-5.09J/g
Peak 110.56C
Onset 135.61C
Endset 120.09C
Heat 94.36mJ
3.76J/g
0.00
100.00
200.00
Time [min]
DSC
mW
20.00
10.00
0.00
-10.00
Peak 108.21C
Onset 139.22C
Endset 96.46C
Heat 318.25mJ
12.68J/g
Peak 181.70C
Onset 169.92C
Endset 191.96C
Heat -135.80mJ
-5.41J/g
SI-4 15°C/min.
0.00
50.00
100.00
Time [min]

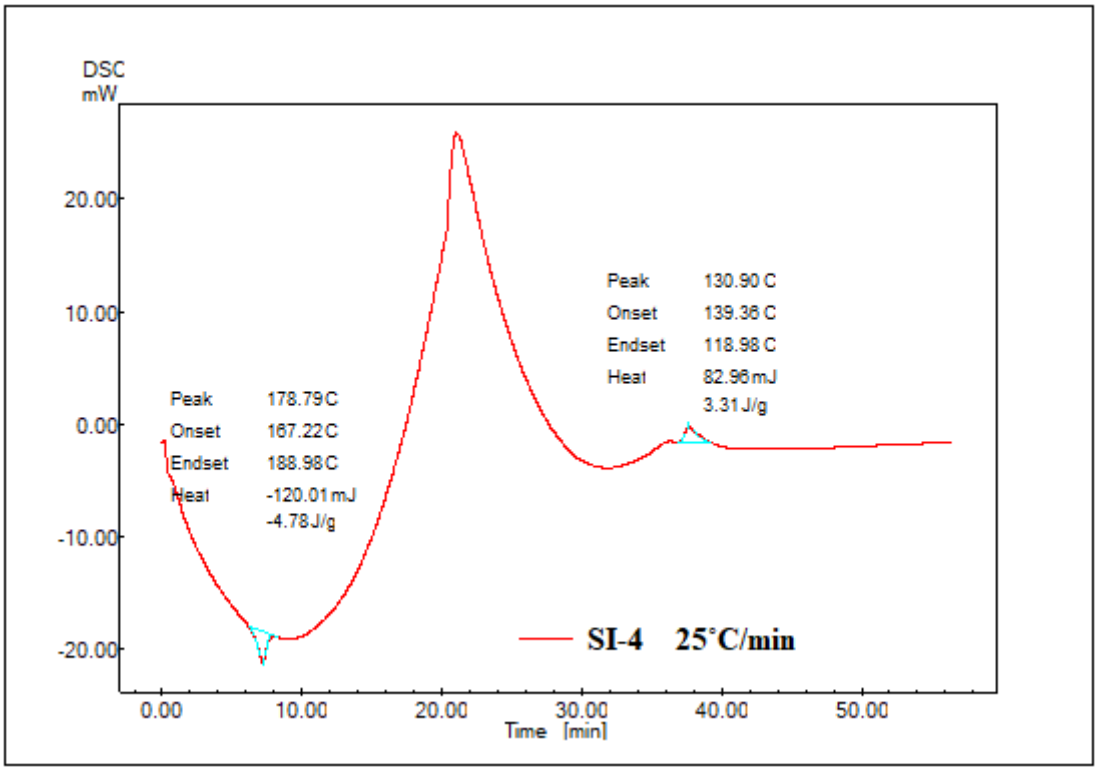

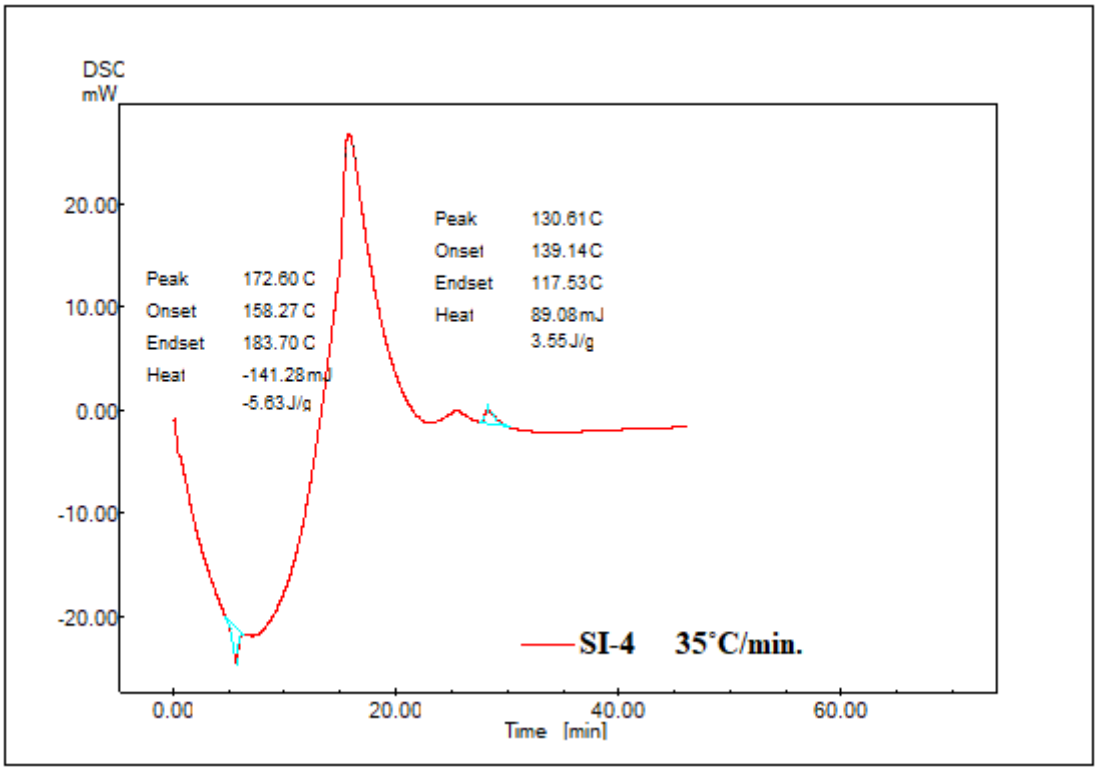

DSC for SI-3 homogenized non-quenched at a heating/cooling rate of 5, 15, 25 and 35 ˚C/min.

The XRD measurements for SI-2 quenched and non-quenched samples

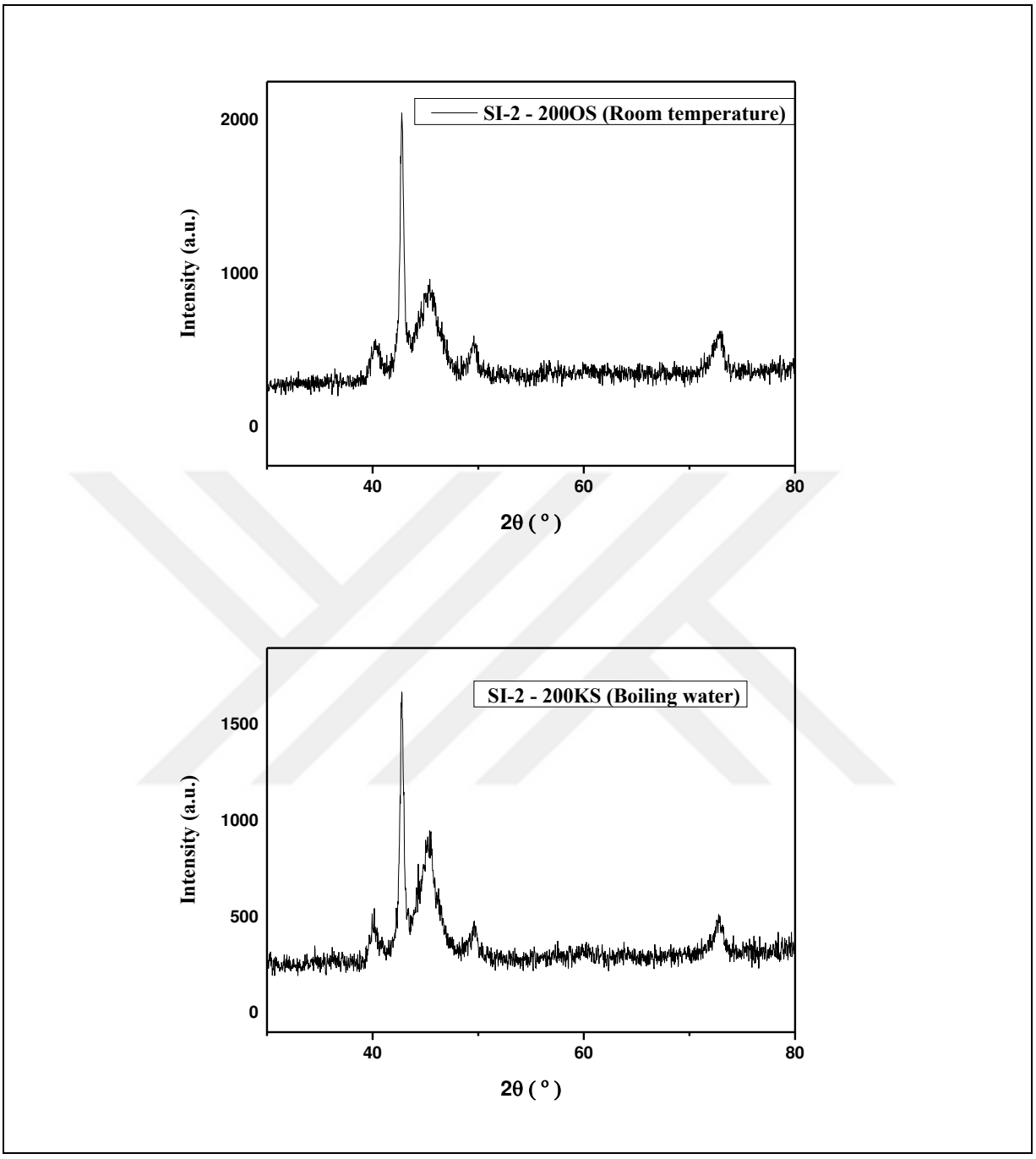

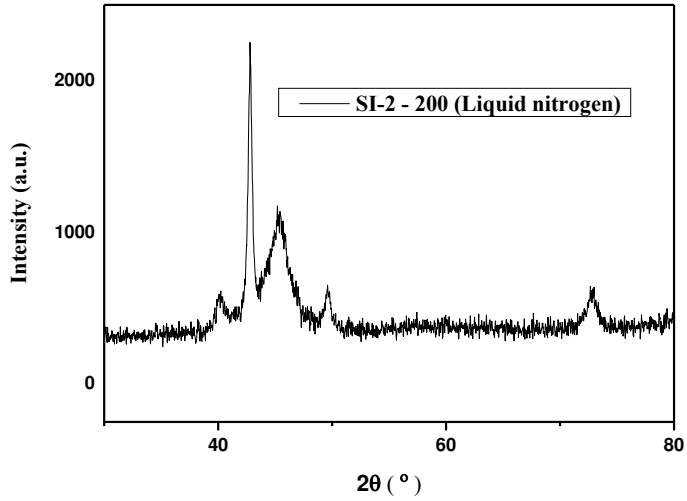
SI-2 - 200 (Liquid nitrogen)
Intensity (a.u.)
2000
1000
0
40
60
80
2θ (°)

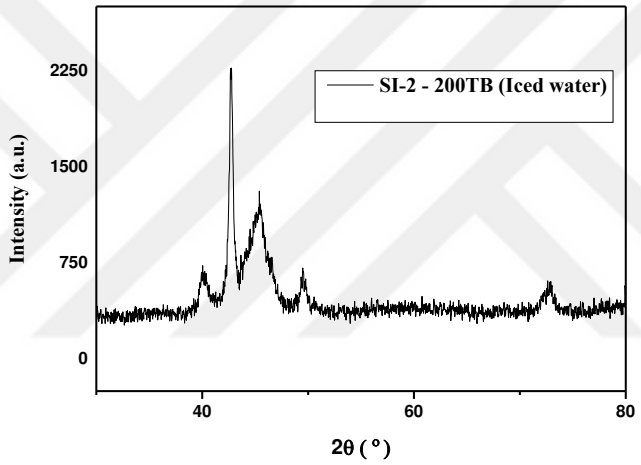
SI-2 - 200TB (Iced water)
Intensity (a.u.)
2250
1500
750
0
40
60
80
2θ (°)

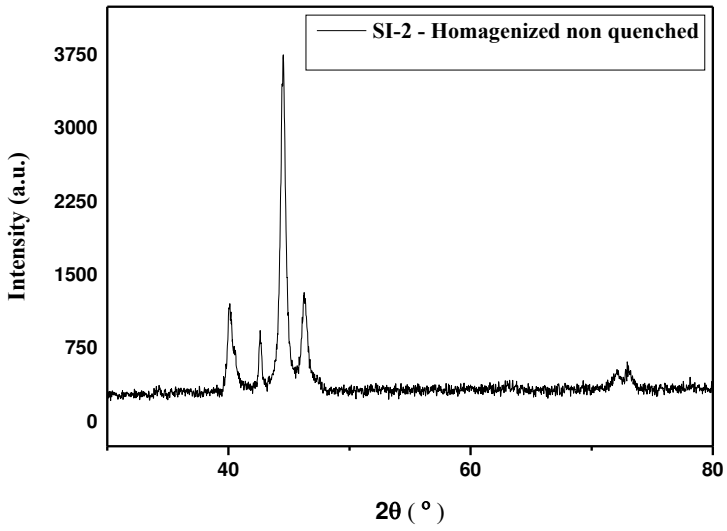
SI-2 - Homagenized non quenched
Intensity (a.u.)
3750
3000
2250
1500
750
0
40
60
80
2θ (°)

DSC Measurements for SI-2 quenched and non-quenched samples at a heating/cooling rate of 5, 15, 25 and 35 ˚C/min

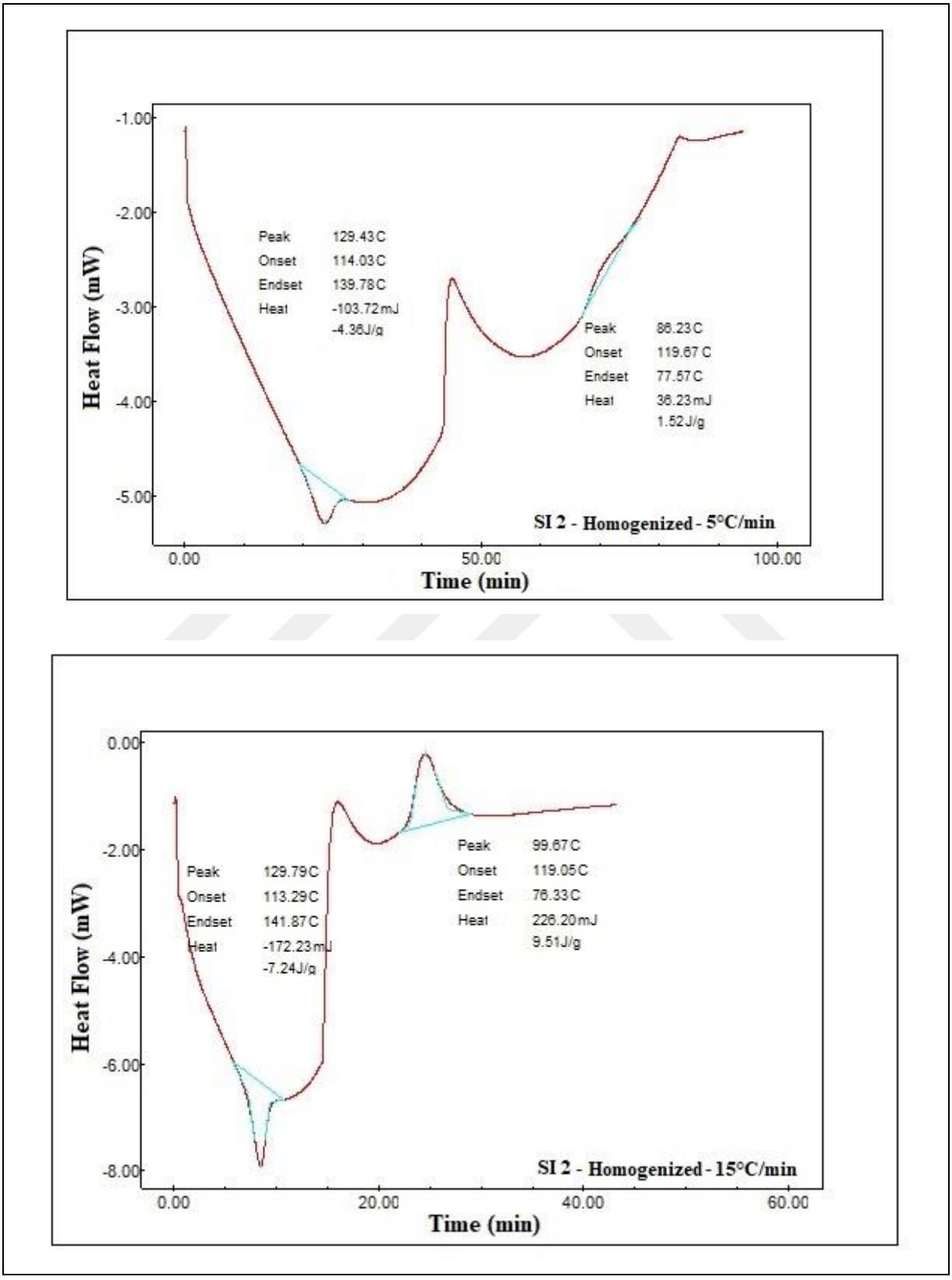

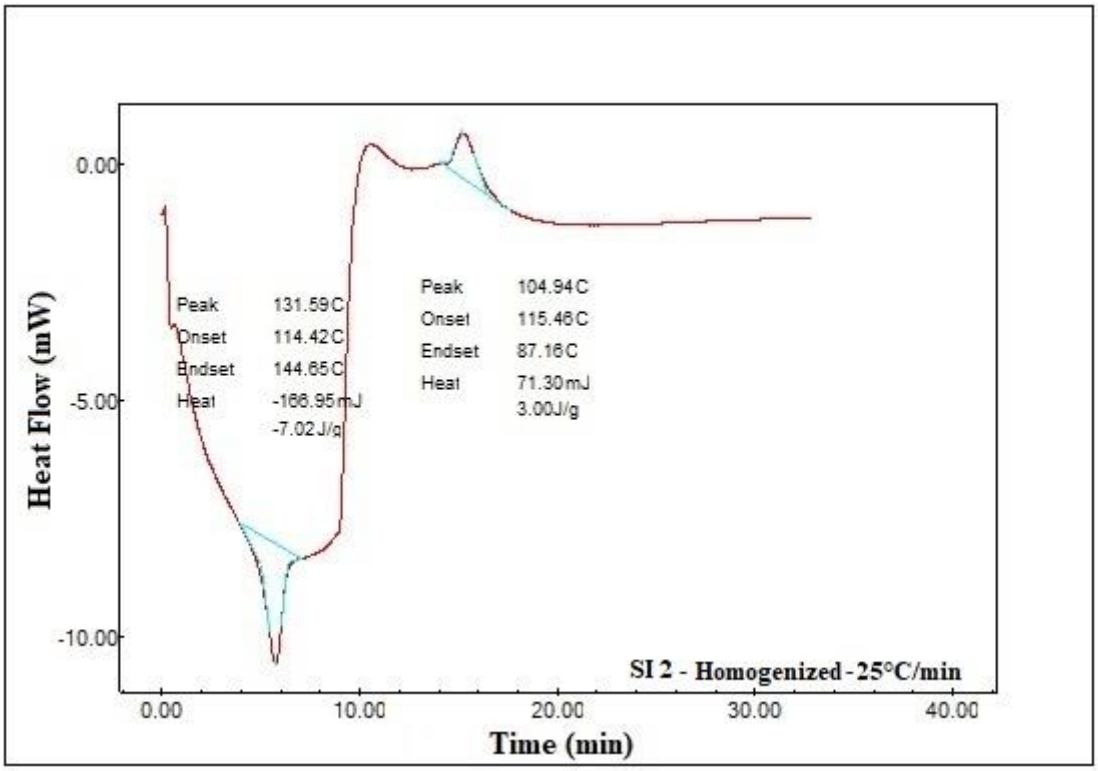

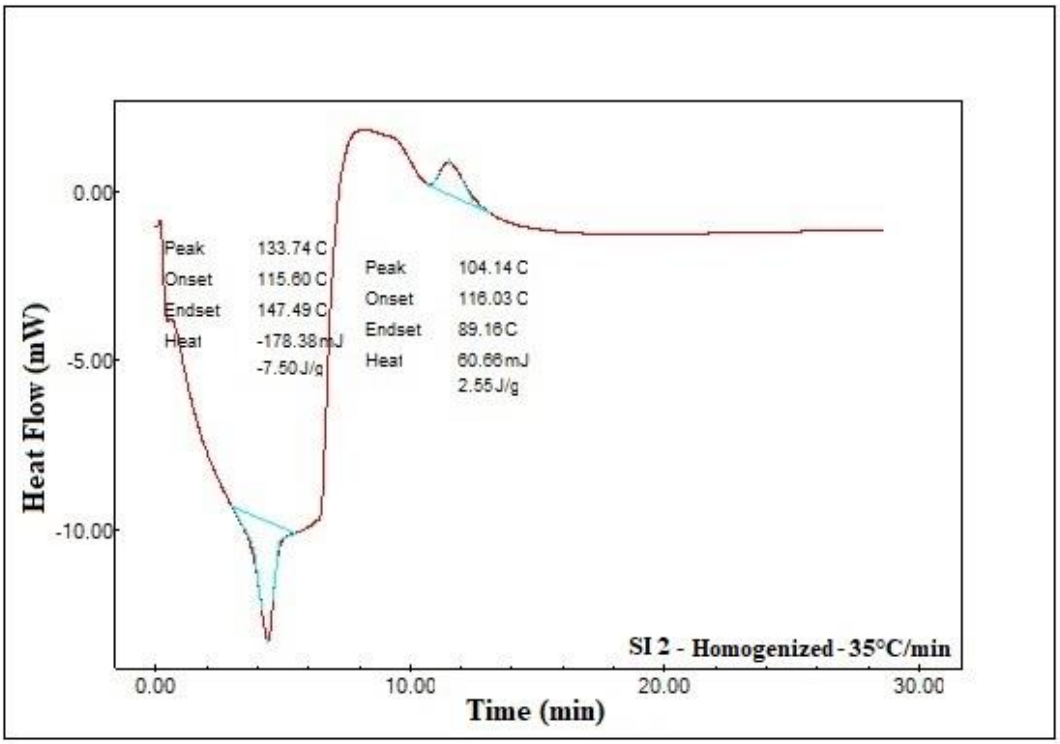

DSC of SI-2 homogenized non-quenched sample at a heating/cooling rate of 5, 15, 25 and 35 ˚C/min.

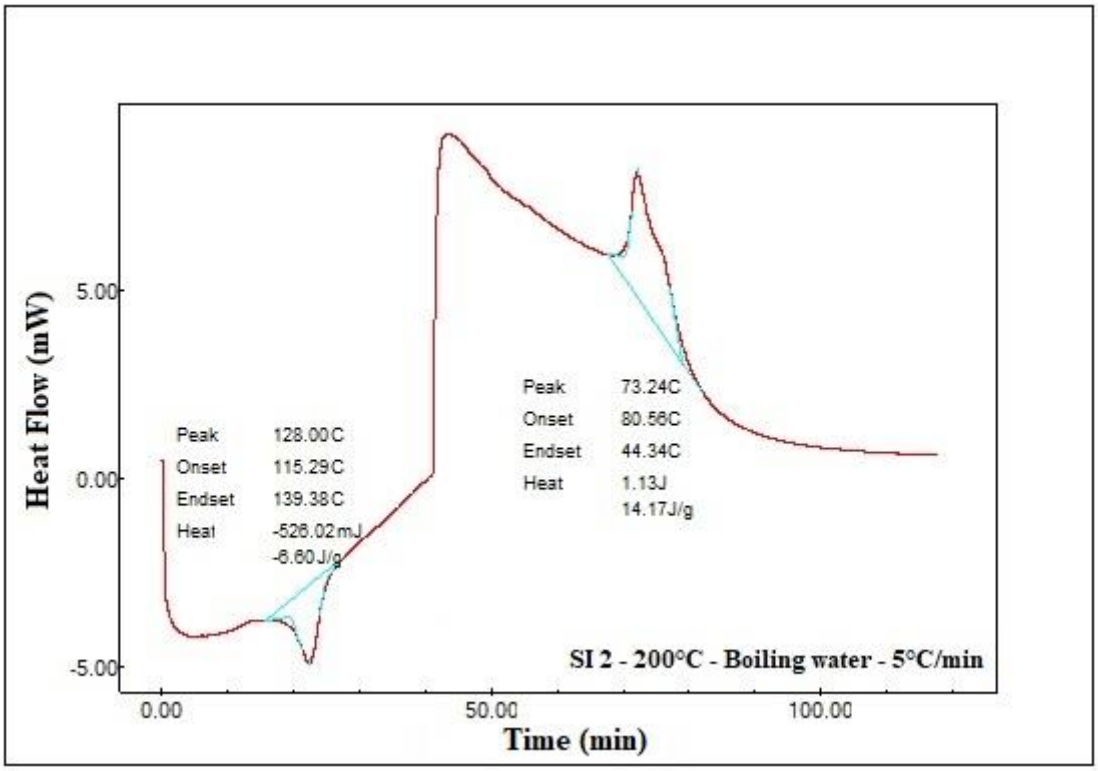
Heat Flow (mW)
5.00
0.00
-5.00
0.00
50.00
100.00
Time (min)
Peak 128.00C
Onset 115.29C
Endset 139.38C
Heat -526.02mJ
-6.60J/g
Peak 73.24C
Onset 80.56C
Endset 44.34C
Heat 1.13J
14.17J/g
SI 2 - 200°C - Boiling water - 5°C/min

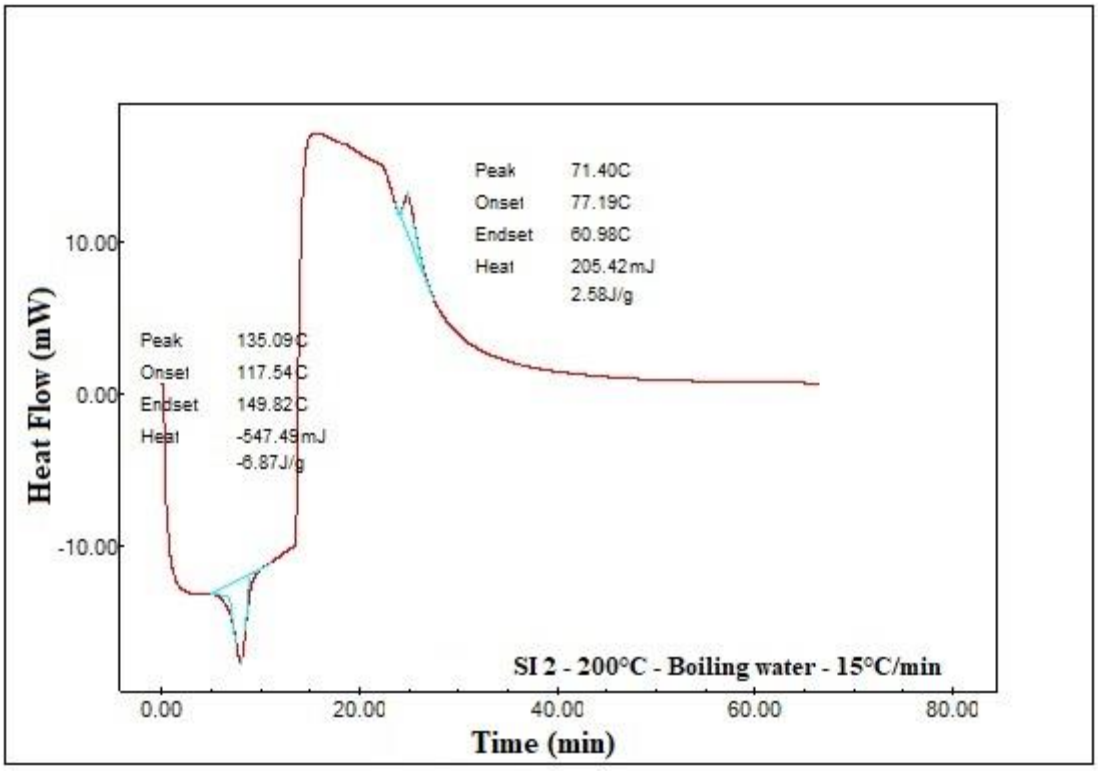
Heat Flow (mW)
10.00
0.00
-10.00
0.00
20.00
40.00
60.00
80.00
Time (min)
Peak 71.40C
Onset 77.19C
Endset 60.98C
Heat 205.42mJ
2.58J/g
Peak 135.09C
Onset 117.54C
Endset 149.82C
Heat -547.49mJ
-6.87J/g
SI 2 - 200°C - Boiling water - 15°C/min

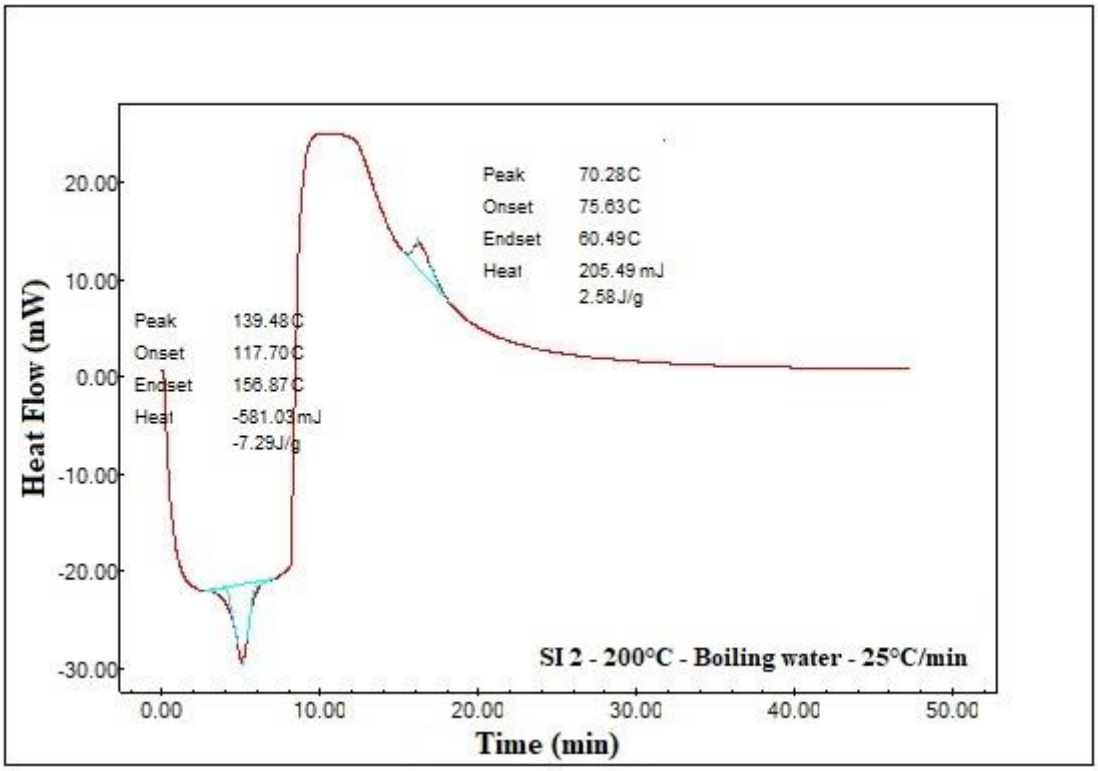

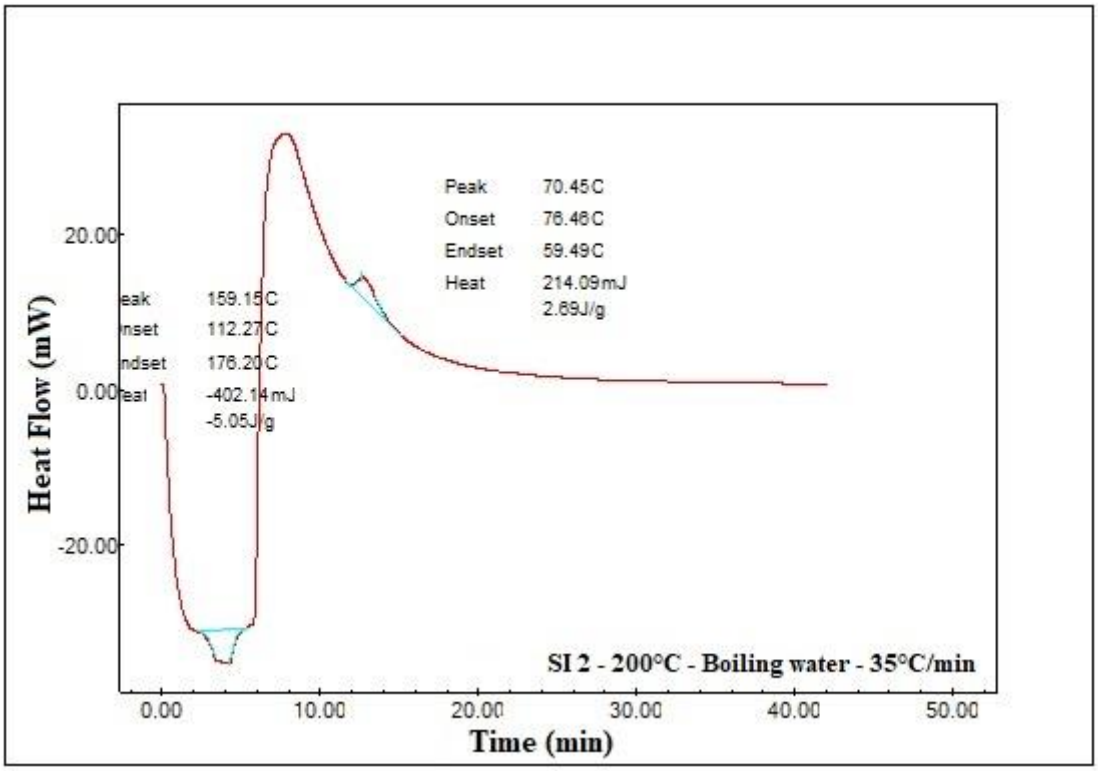

DSC of SI-2 quenched in boiling water at a heating/cooling rate of 5, 15, 25 and 35 ˚C/min.

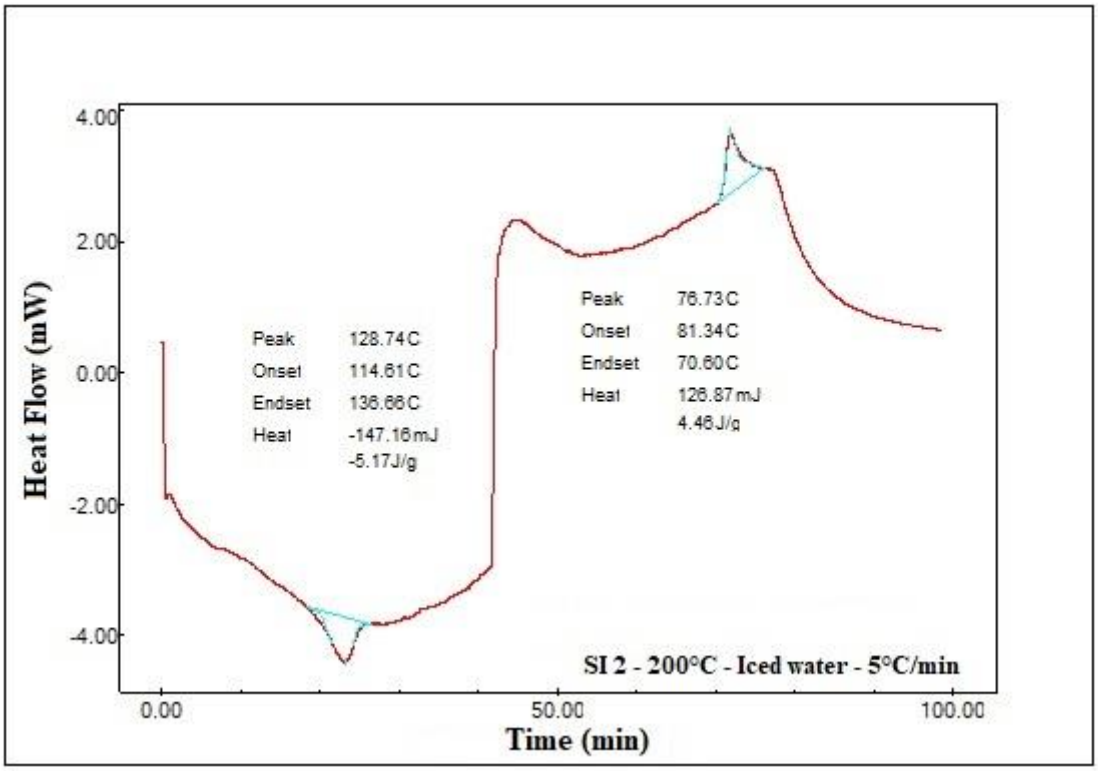
4.00
2.00
0.00
-2.00
-4.00
Heat Flow (mW)
Peak 128.74 C
Onset 114.61 C
Endset 136.66 C
Heat -147.16 mJ
-5.17 J/g
Peak 76.73 C
Onset 81.34 C
Endset 70.60 C
Heat 126.87 mJ
4.46 J/g
SI 2 - 200°C - Iced water - 5°C/min
0.00
50.00
100.00
Time (min)

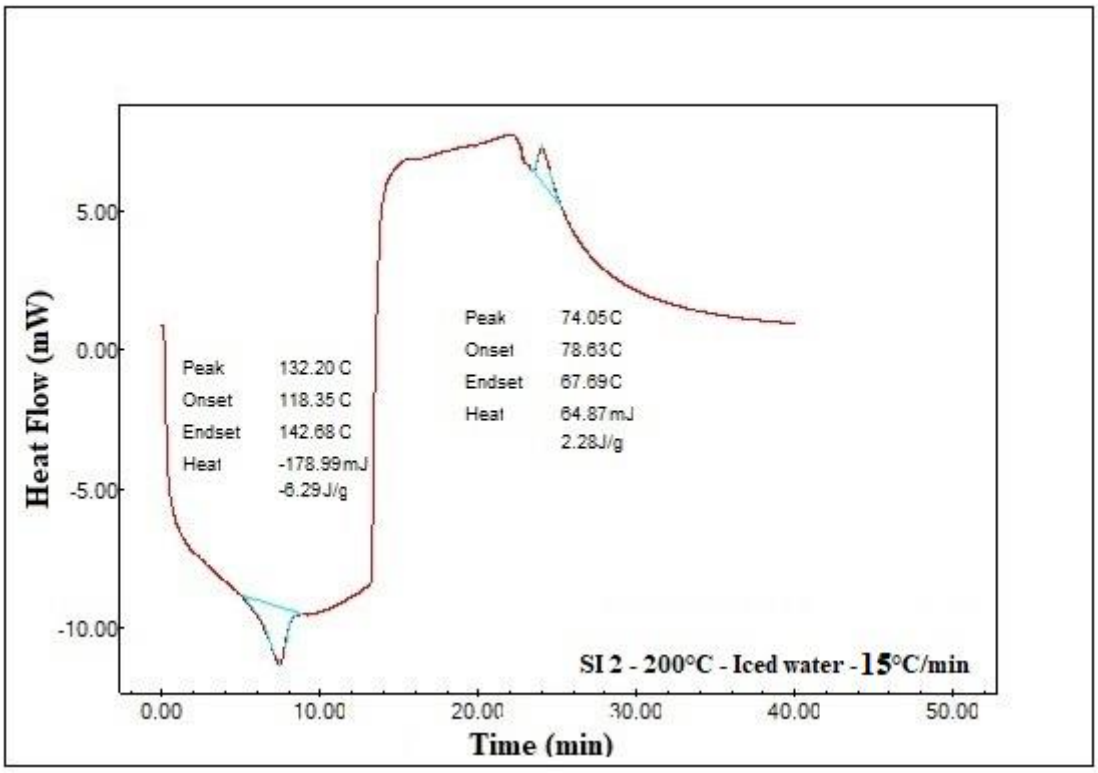
5.00
0.00
-5.00
-10.00
Heat Flow (mW)
Peak 132.20 C
Onset 118.35 C
Endset 142.68 C
Heat -178.99 mJ
-6.29 J/g
Peak 74.05 C
Onset 78.63 C
Endset 67.69 C
Heat 64.87 mJ
2.28 J/g
SI 2 - 200°C - Iced water - 15°C/min
0.00
10.00
20.00
30.00
40.00
50.00
Time (min)

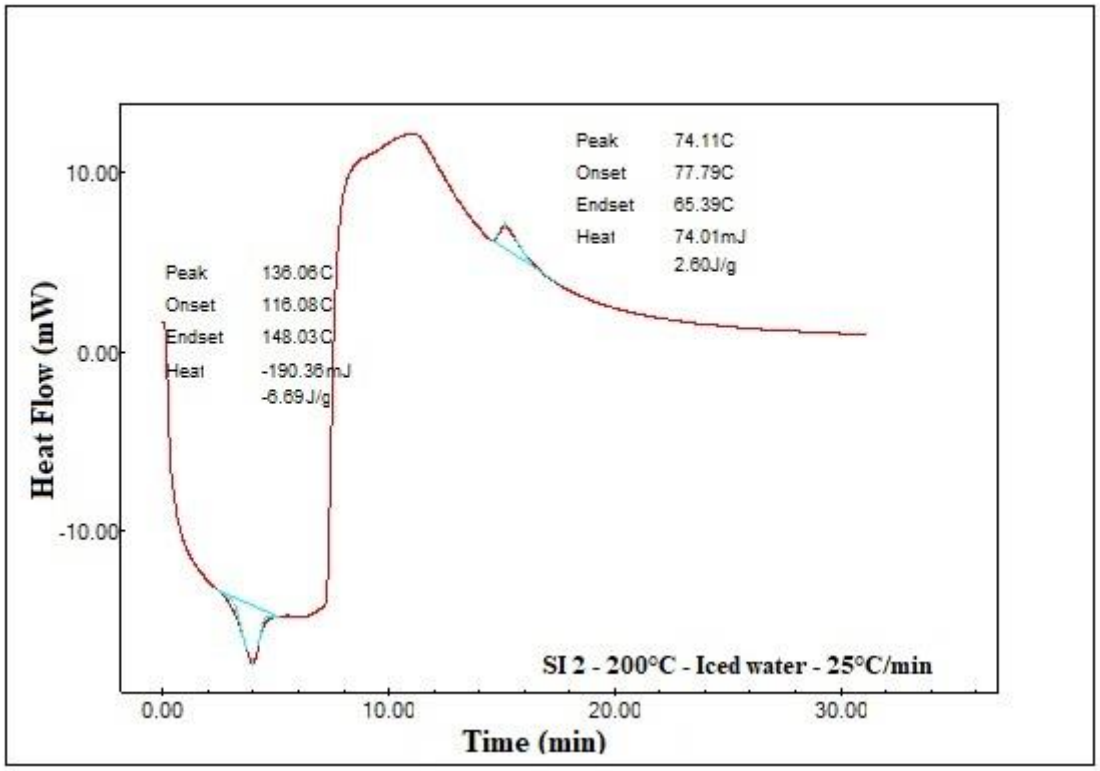

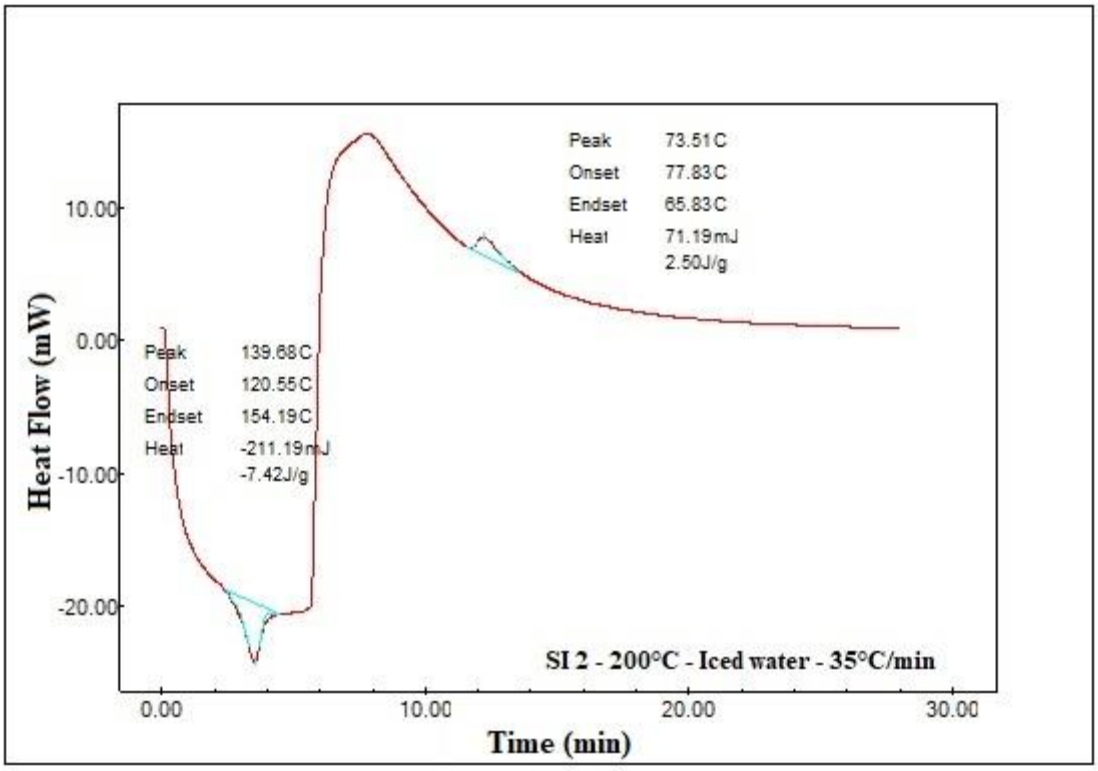

DSC of SI-2 quenched in iced water at a heating/cooling rate of 5, 15, 25 and 35 ˚C/min

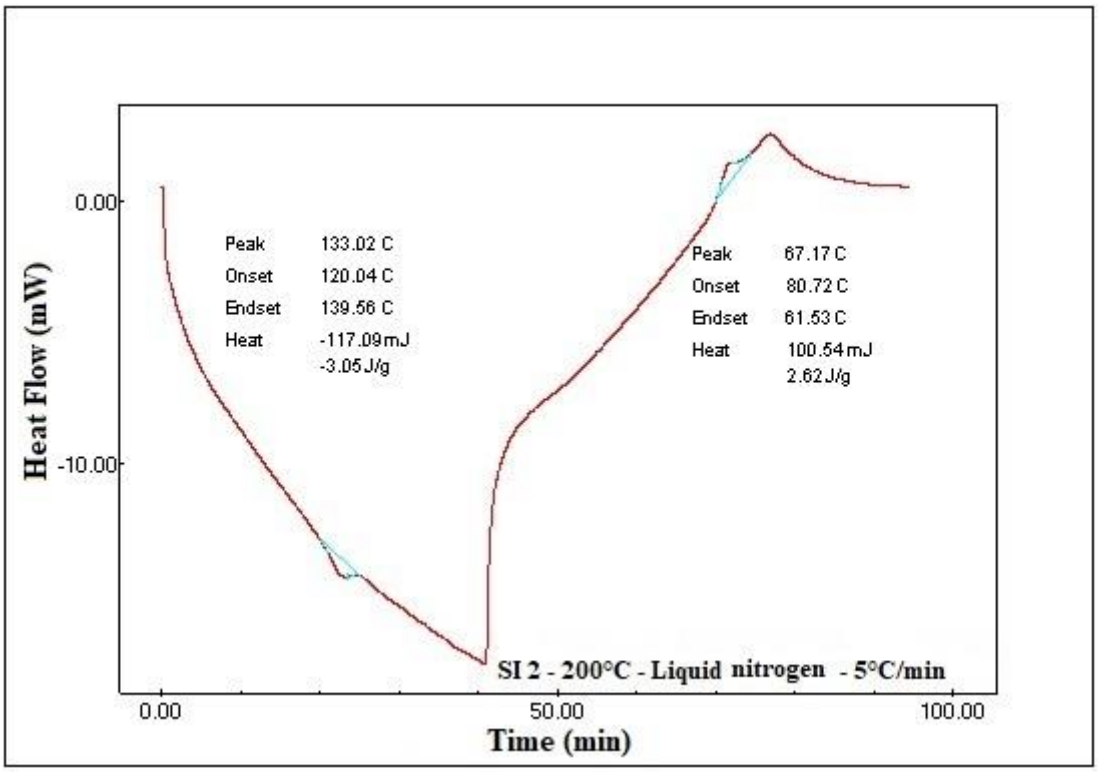
Peak 133.02 C
Onset 120.04 C
Endset 139.56 C
Heat -117.09 mJ
-3.05 J/g
Peak 67.17 C
Onset 80.72 C
Endset 61.53 C
Heat 100.54 mJ
2.62 J/g
SI 2 - 200°C - Liquid nitrogen - 5°C/min
Heat Flow (mW)
0.00
-10.00
0.00
50.00
100.00
Time (min)

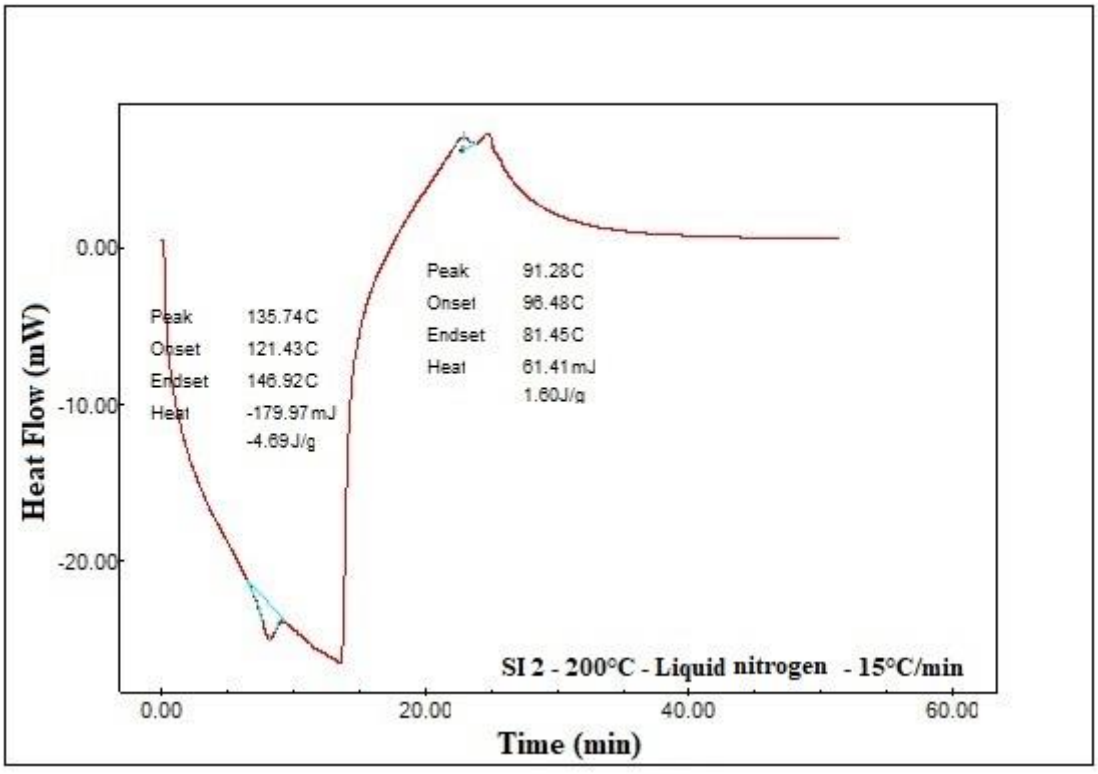
Peak 135.74 C
Onset 121.43 C
Endset 146.92 C
Heat -179.97 mJ
-4.69 J/g
Peak 91.28 C
Onset 96.48 C
Endset 81.45 C
Heat 61.41 mJ
1.60 J/g
SI 2 - 200°C - Liquid nitrogen - 15°C/min
Heat Flow (mW)
0.00
-10.00
-20.00
0.00
20.00
40.00
60.00
Time (min)

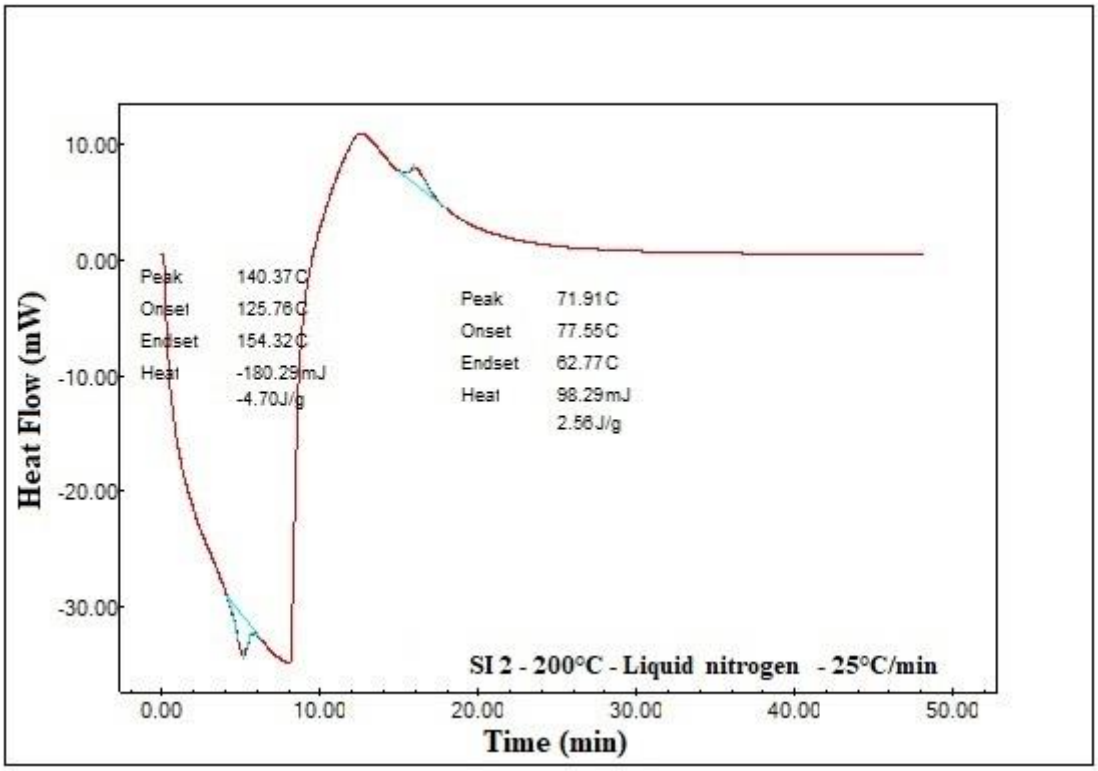

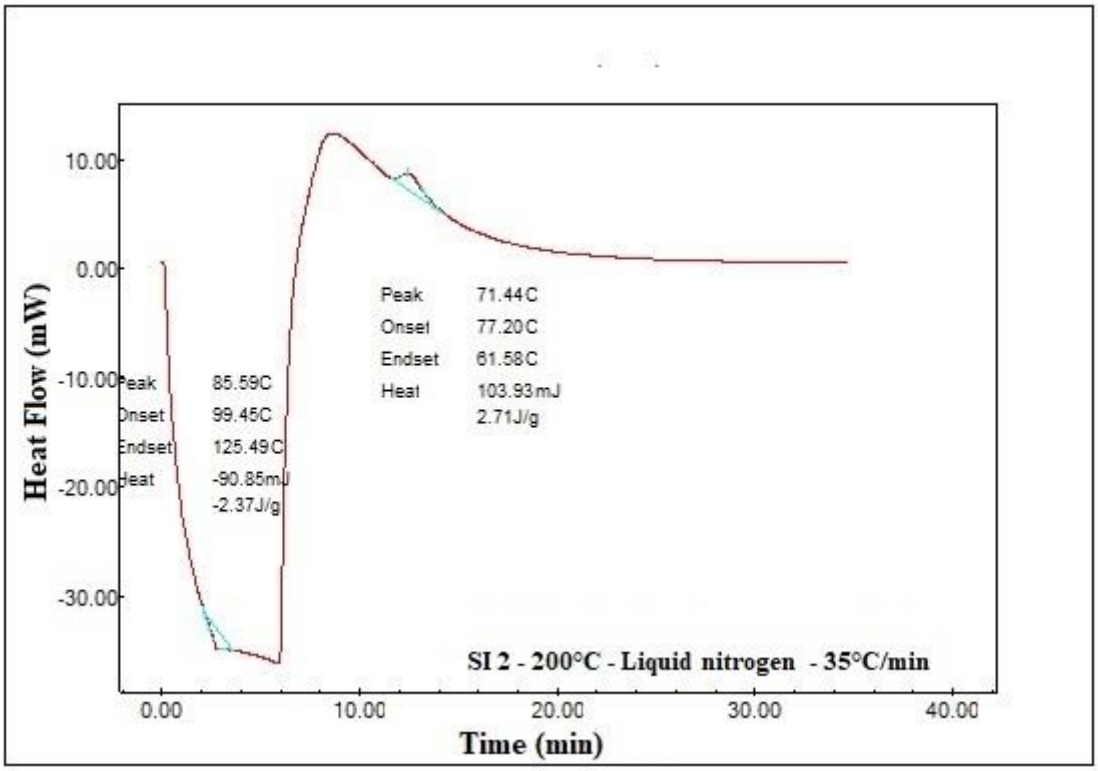

DSC of SI-2 quenched in liquid nitrogen at a heating/cooling rate of 5, 15, 25 and 35 ˚C/min

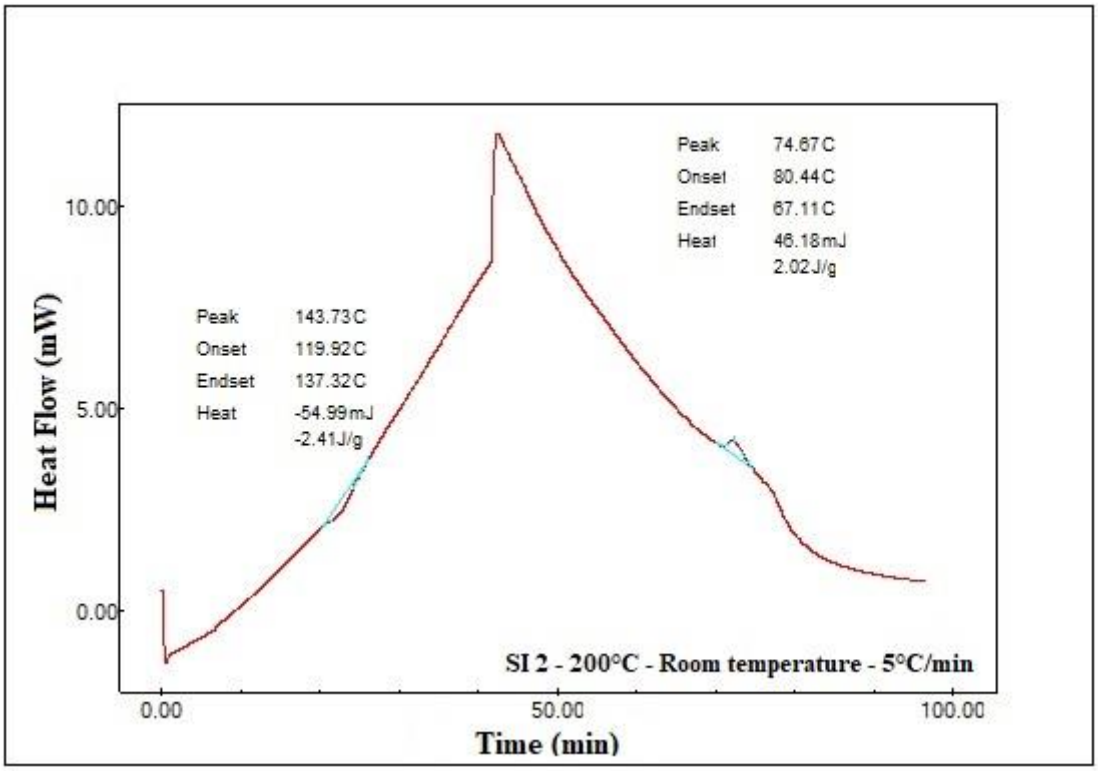
Peak 74.67 C
Onset 80.44 C
Endset 67.11 C
Heat 46.18 mJ
2.02 J/g
Peak 143.73 C
Onset 119.92 C
Endset 137.32 C
Heat -54.99 mJ
-2.41 J/g
10.00
5.00
0.00
Heat Flow (mW)
SI 2 - 200°C - Room temperature - 5°C/min
0.00
50.00
100.00
Time (min)

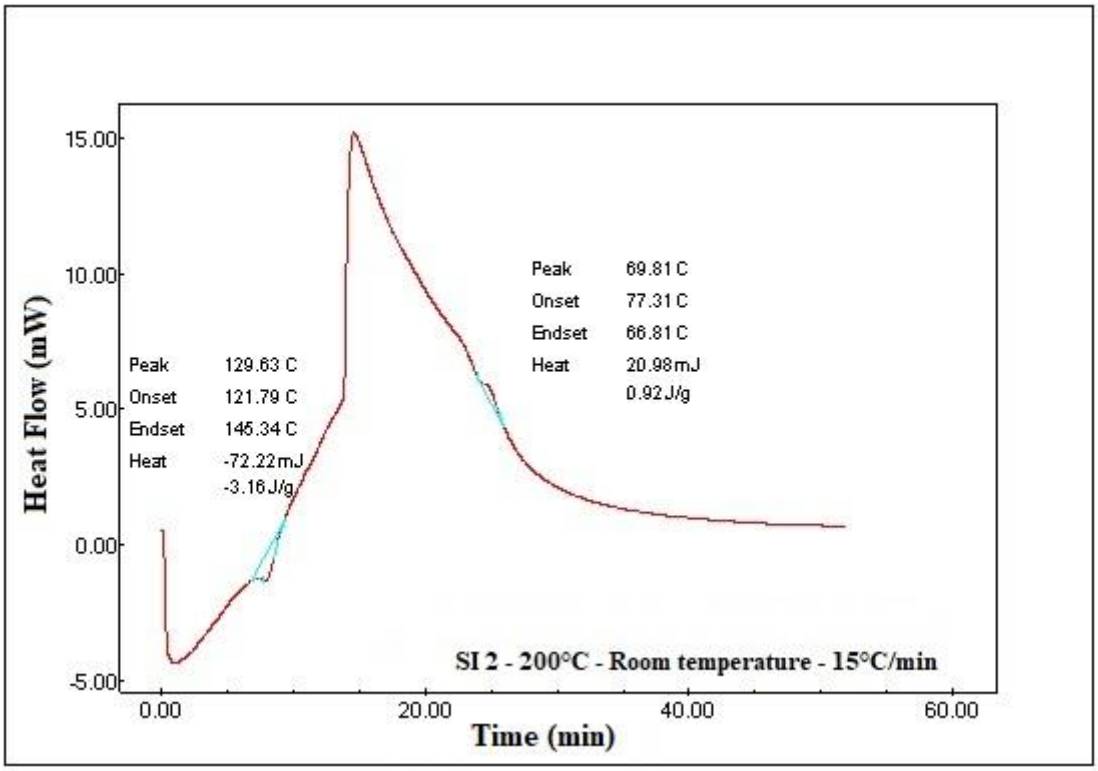
Peak 69.81 C
Onset 77.31 C
Endset 66.81 C
Heat 20.98 mJ
0.92 J/g
Peak 129.63 C
Onset 121.79 C
Endset 145.34 C
Heat -72.22 mJ
-3.16 J/g
15.00
10.00
5.00
0.00
-5.00
Heat Flow (mW)
SI 2 - 200°C - Room temperature - 15°C/min
0.00
20.00
40.00
60.00
Time (min)

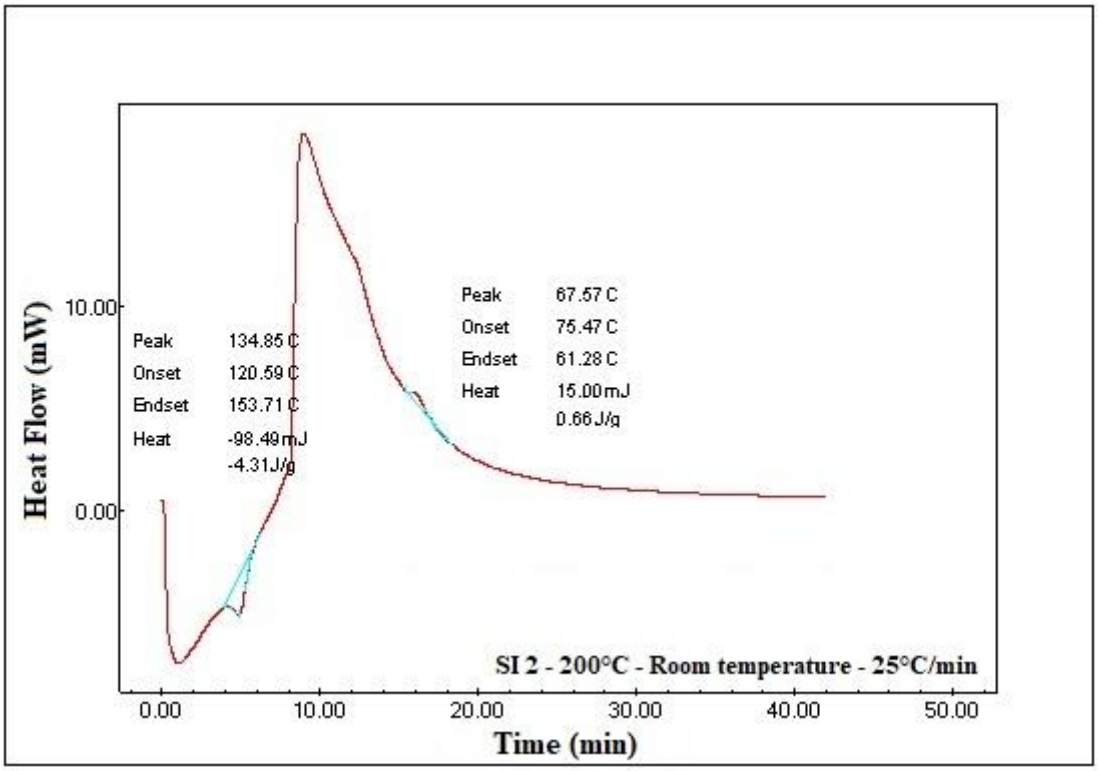

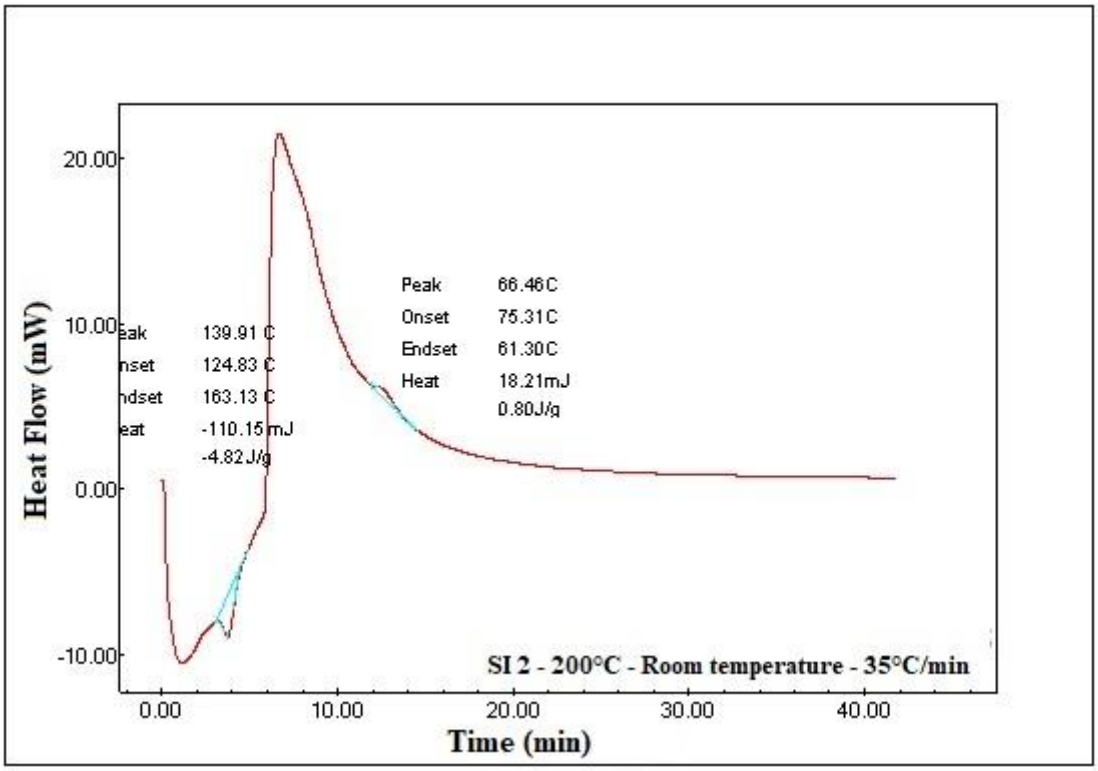

DSC of SI-2 quenched in room temperature at a heating/cooling rate of 5, 15, 25 and 35 ˚C/min

The XRD measurements for SI-4 quenched and non-quenched samples

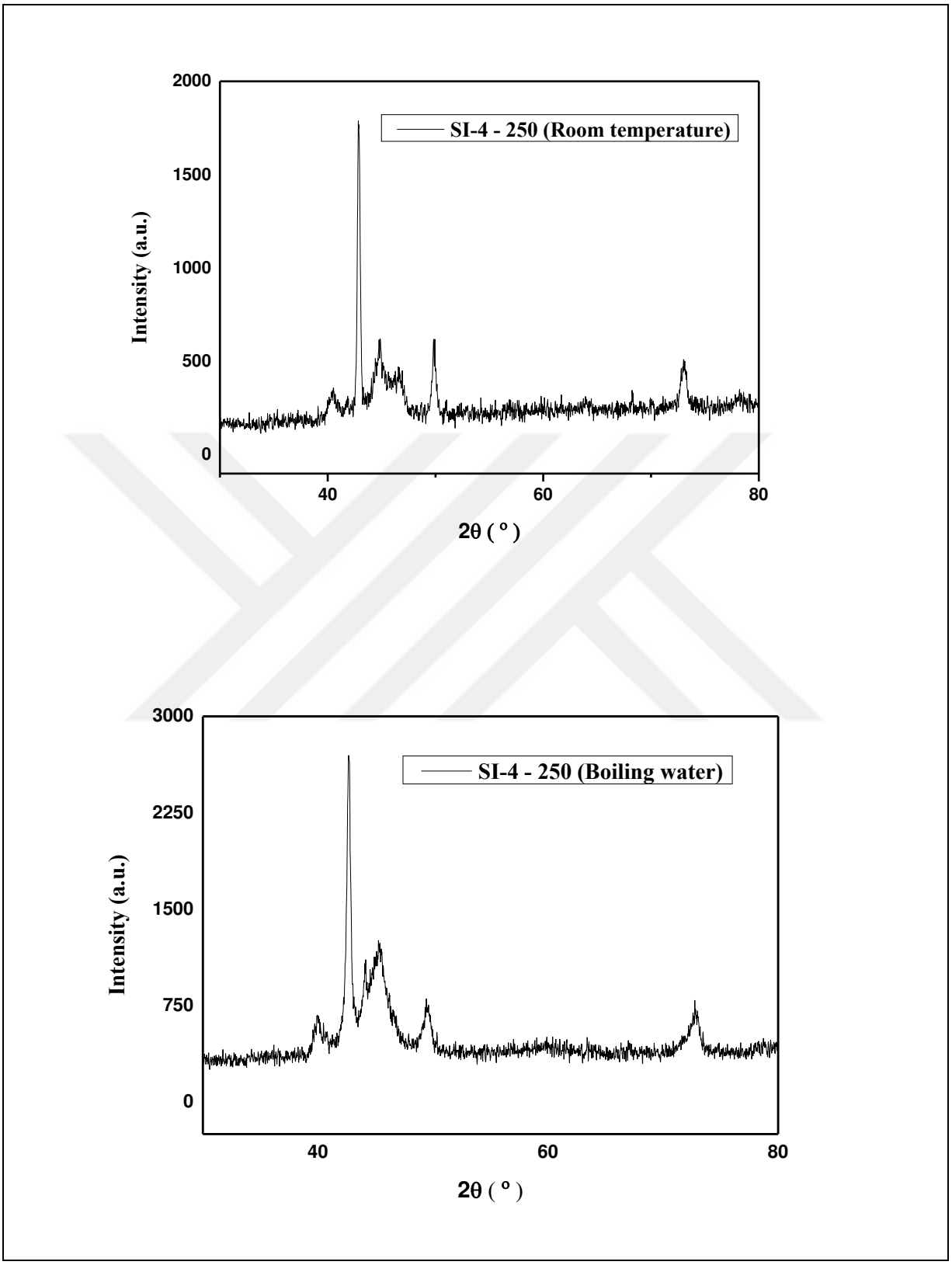

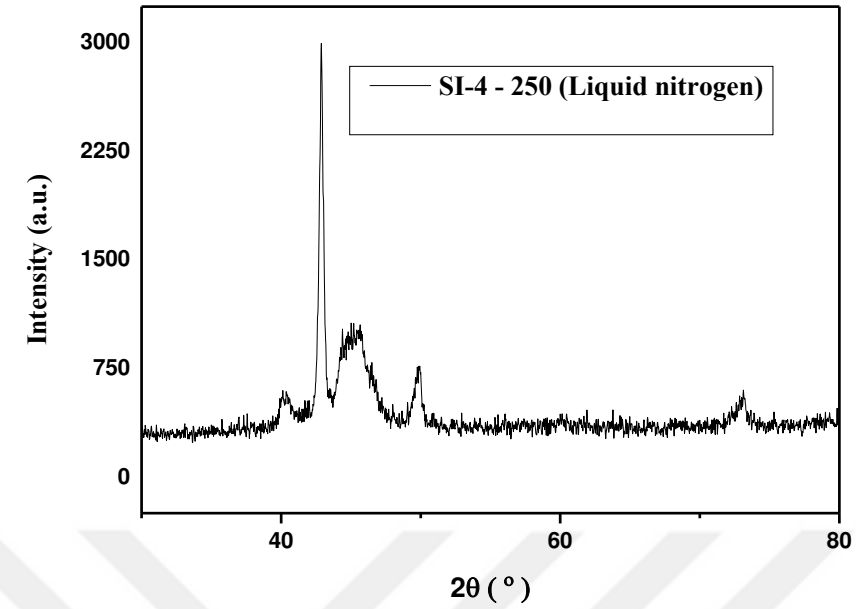
SI-4 - 250 (Liquid nitrogen)
Intensity (a.u.)
3000
2250
1500
750
0
40
60
80
2θ (°)

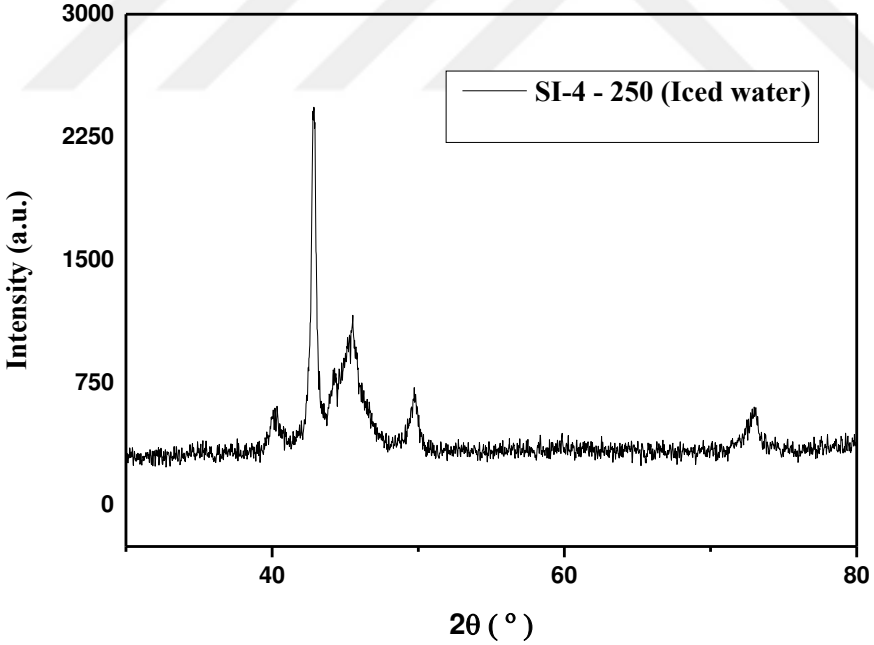
SI-4 - 250 (Iced water)
Intensity (a.u.)
3000
2250
1500
750
0
40
60
80
2θ (°)

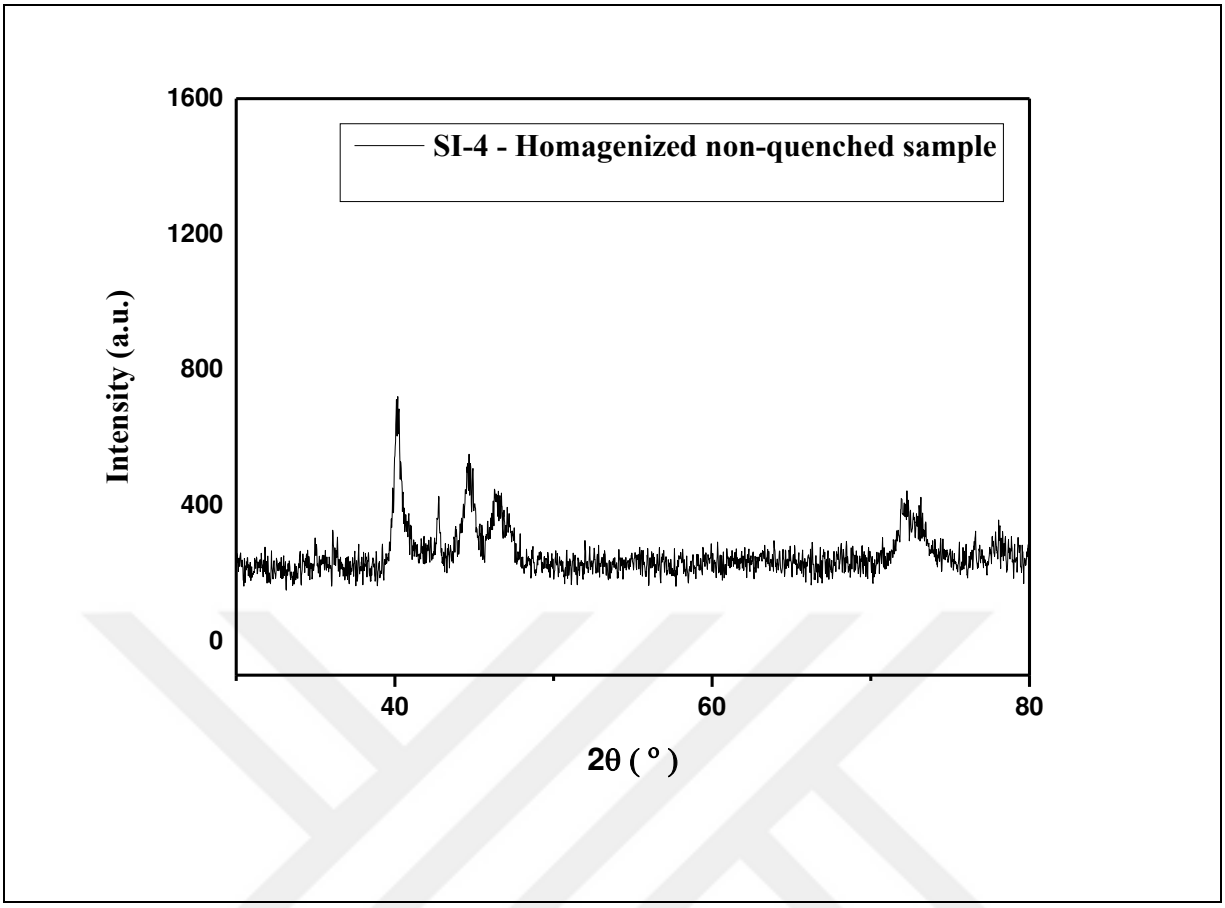
SI-4 - Homagenized non-quenched sample
Intensity (a.u.)
1600
1200
800
400
0
40
60
80
2θ (°)

DSC of SI-4 quenched and non-quenched at a heating/cooling rate of 5, 15, 25 and 35 ˚C/min

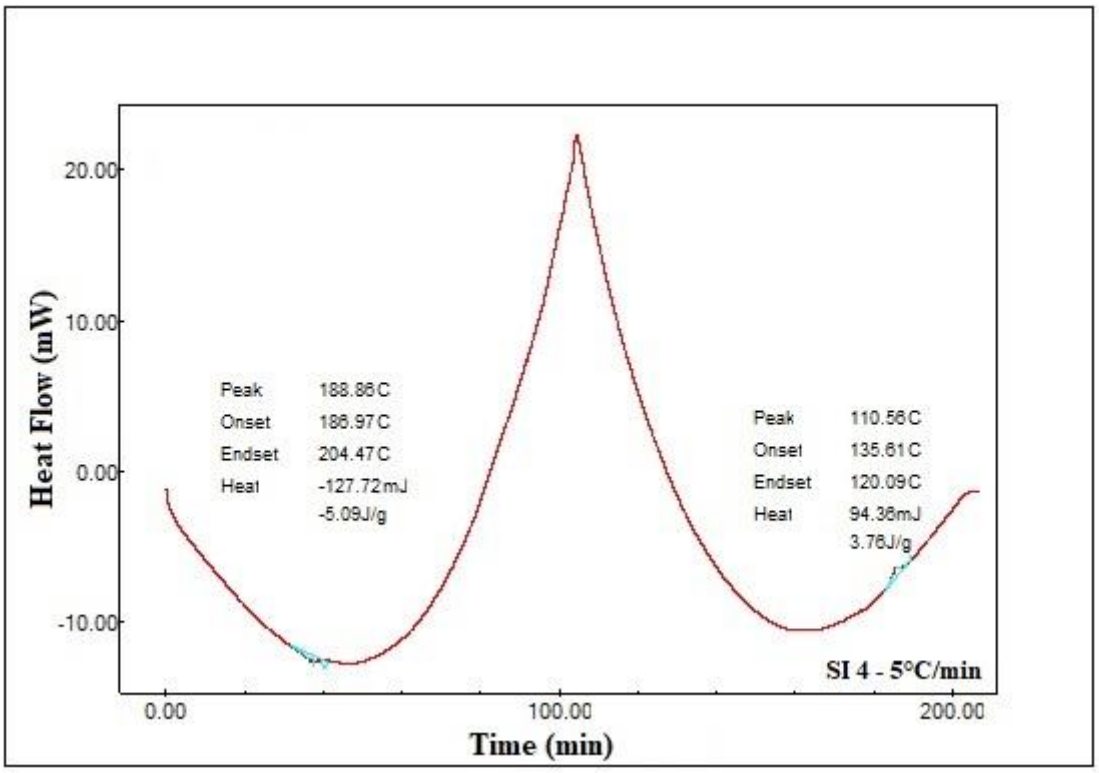

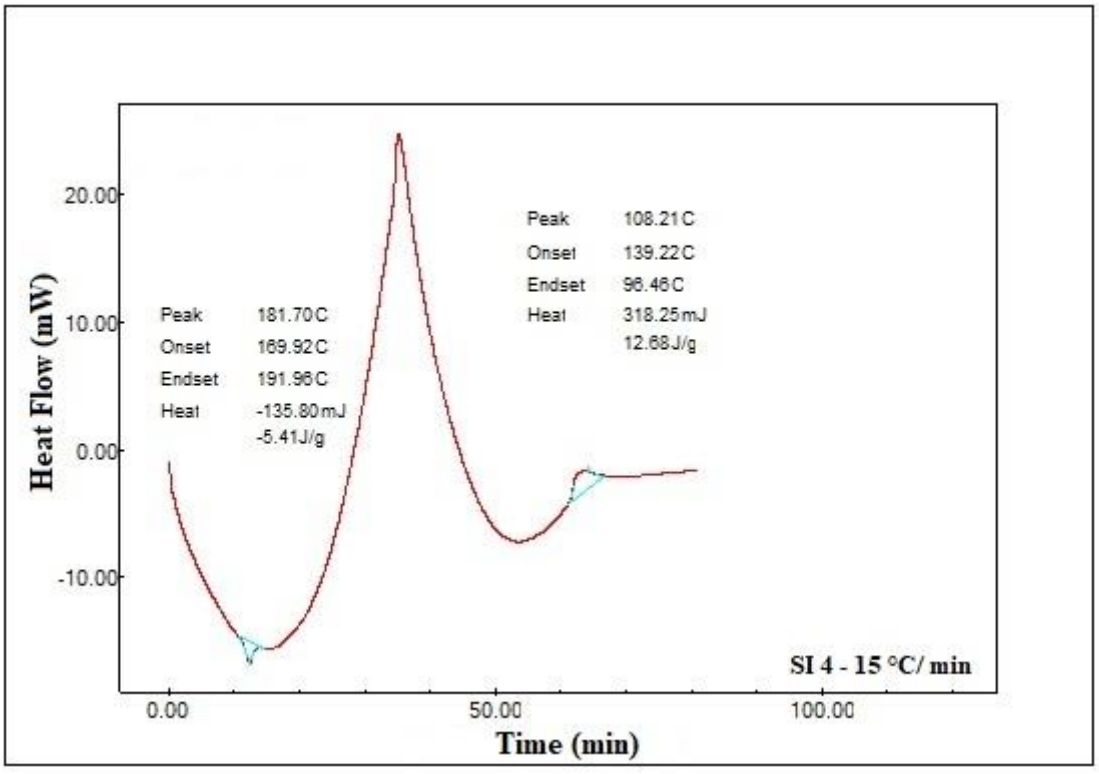

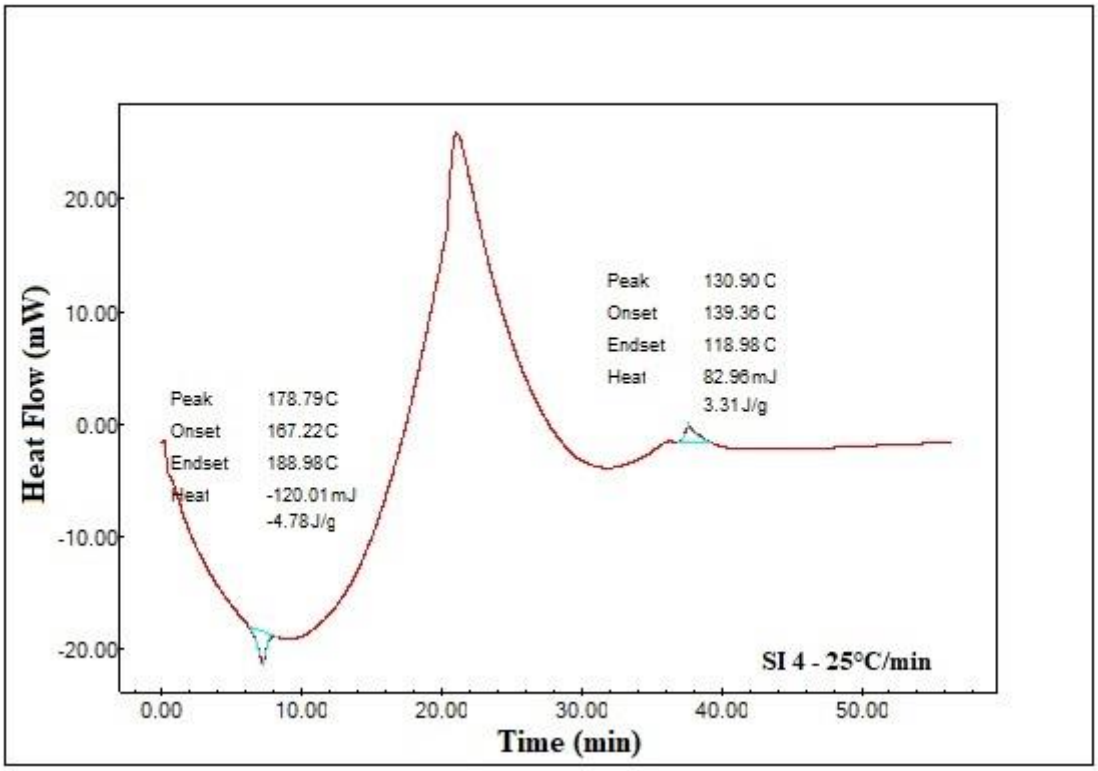

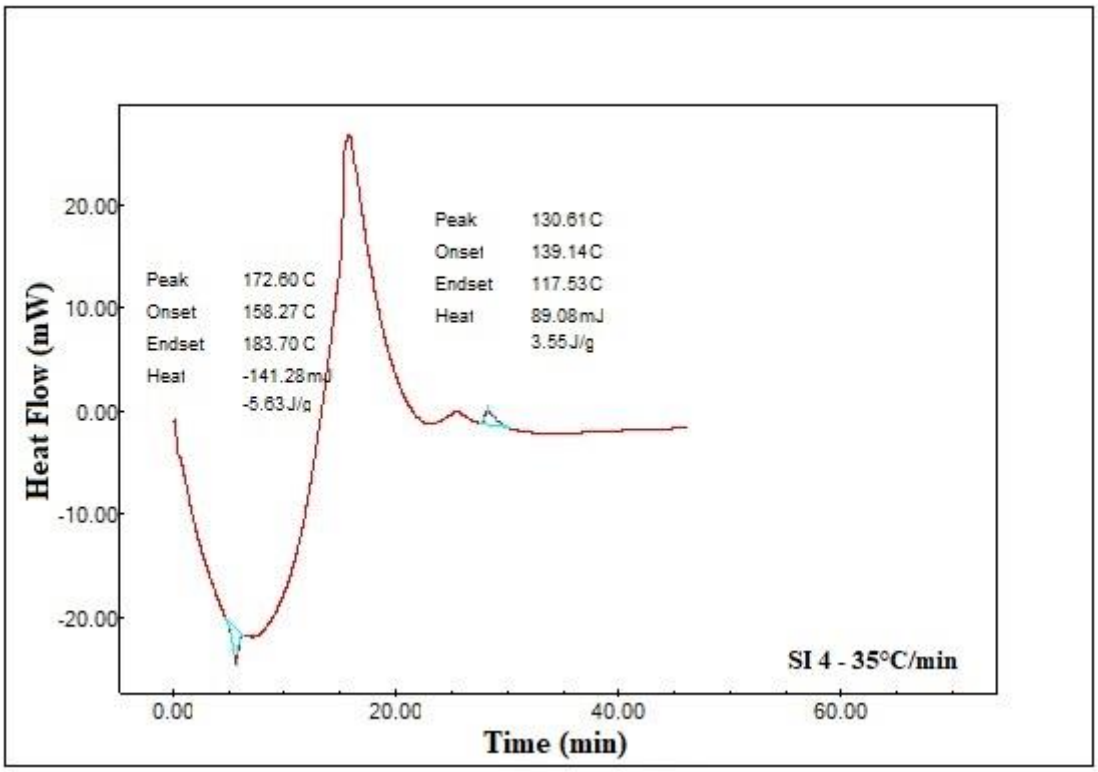

DSC of SI-4 homogenized non-quenched at a heating/cooling rate of 5, 15, 25 and 35 ˚C/min

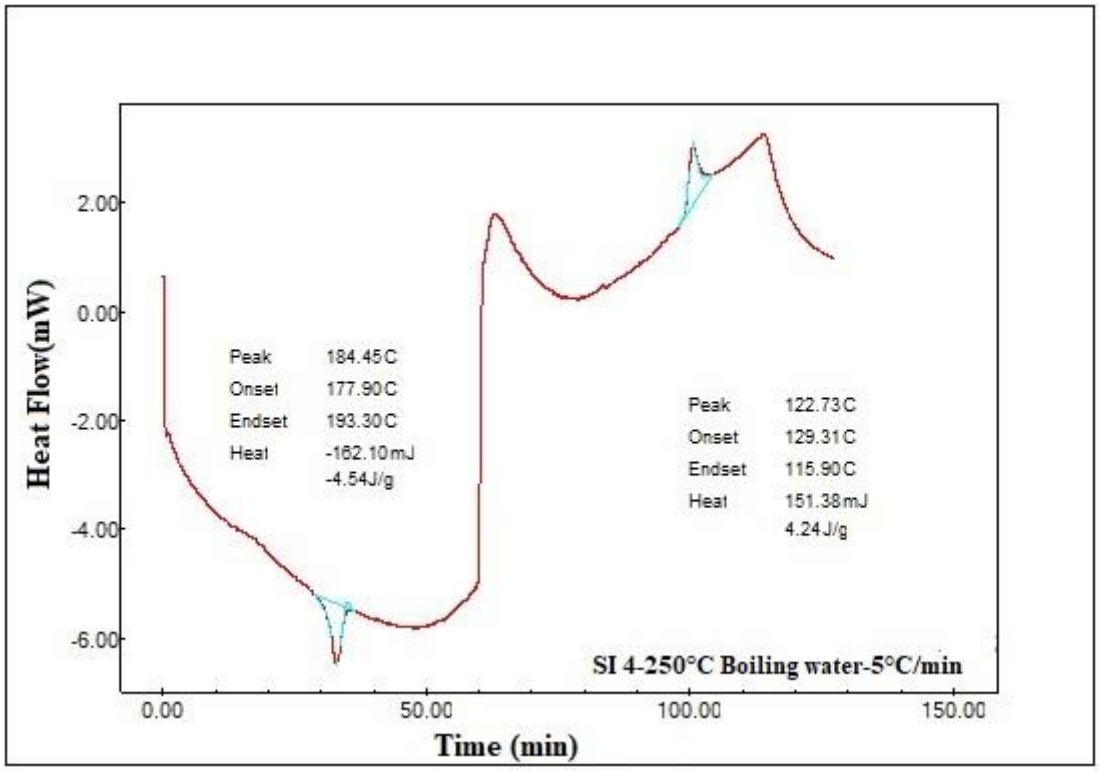
Heat Flow(mW)
2.00
0.00
-2.00
-4.00
-6.00
Peak 184.45C
Onset 177.90C
Endset 193.30C
Heat -162.10mJ
-4.54J/g
Peak 122.73C
Onset 129.31C
Endset 115.90C
Heat 151.38mJ
4.24J/g
SI 4-250°C Boiling water-5°C/min
0.00
50.00
100.00
150.00
Time (min)

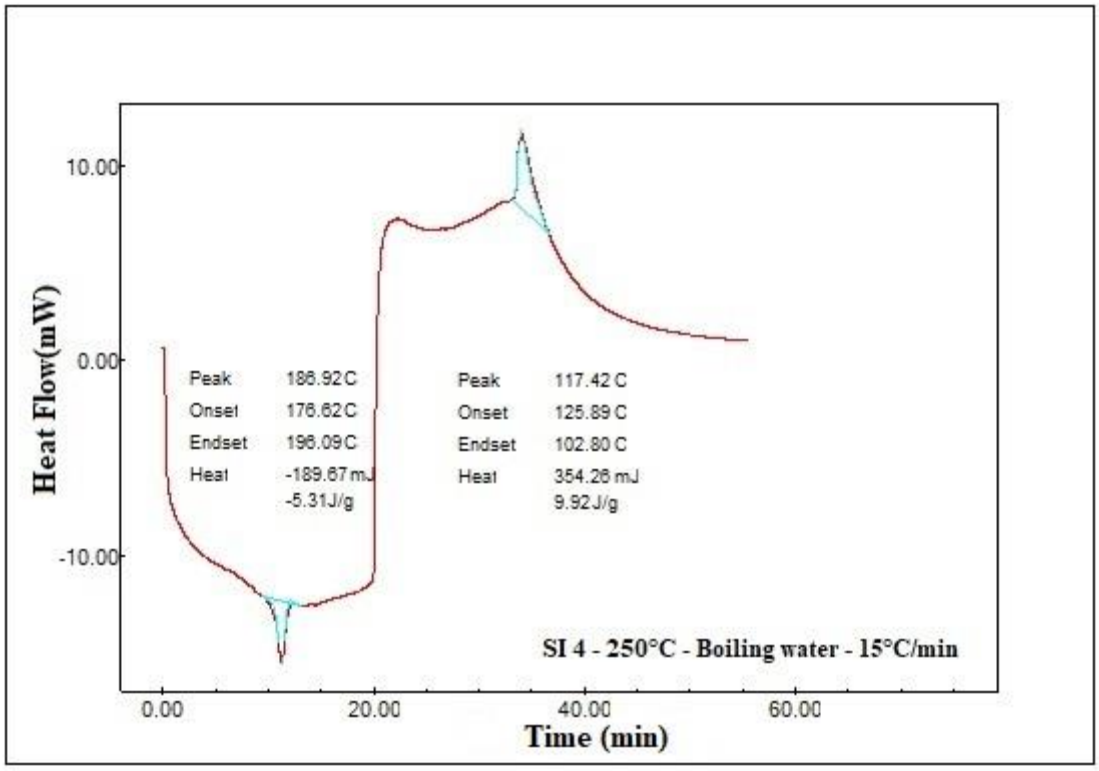
Heat Flow(mW)
10.00
0.00
-10.00
Peak 186.92C
Onset 176.62C
Endset 196.09C
Heat -189.67mJ
-5.31J/g
Peak 117.42C
Onset 125.89C
Endset 102.80C
Heat 354.26mJ
9.92J/g
SI 4 - 250°C - Boiling water - 15°C/min
0.00
20.00
40.00
60.00
Time (min)

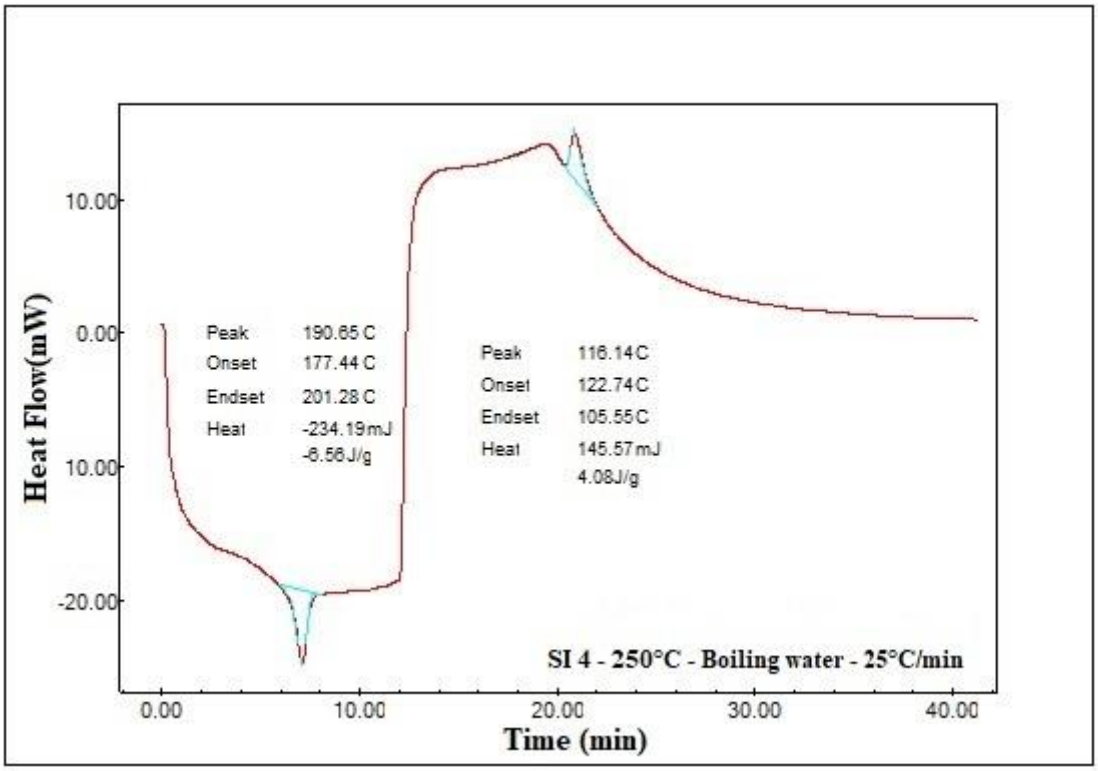

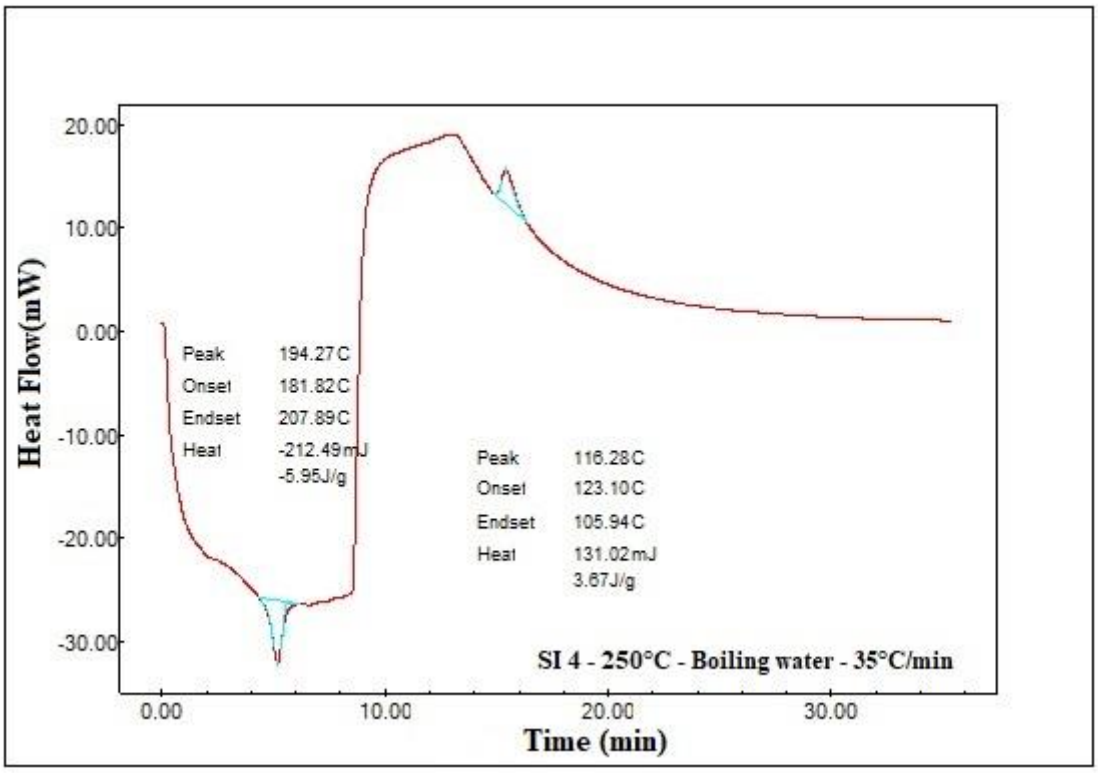

DSC of SI-4 quenched in boiling water at a heating/cooling rate of 5, 15, 25 and 35 ˚C/min

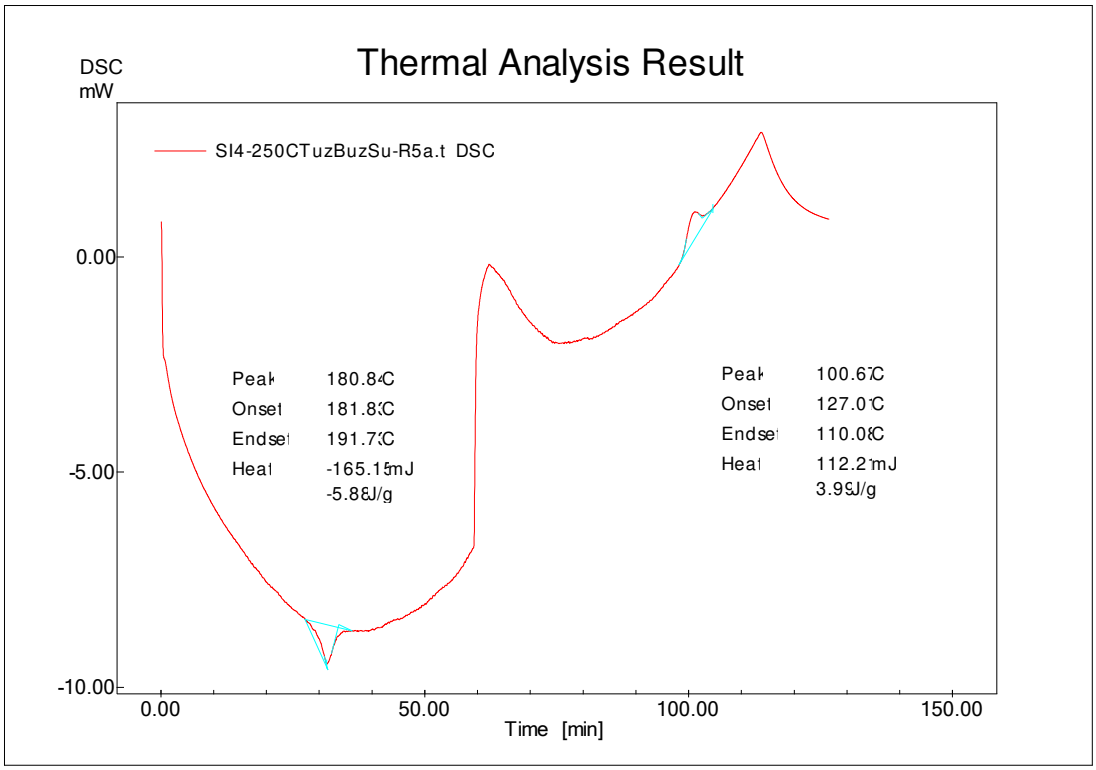
Thermal Analysis Result
DSC
mW
SI4-250CTuzBuzSu-R5a.t DSC
0.00
-5.00
-10.00
Peak 180.84°C
Onset 181.83°C
Endset 191.73°C
Heat -165.15mJ
-5.86J/g
Peak 100.67°C
Onset 127.01°C
Endset 110.08°C
Heat 112.21mJ
3.99J/g
0.00
50.00
100.00
150.00
Time [min]

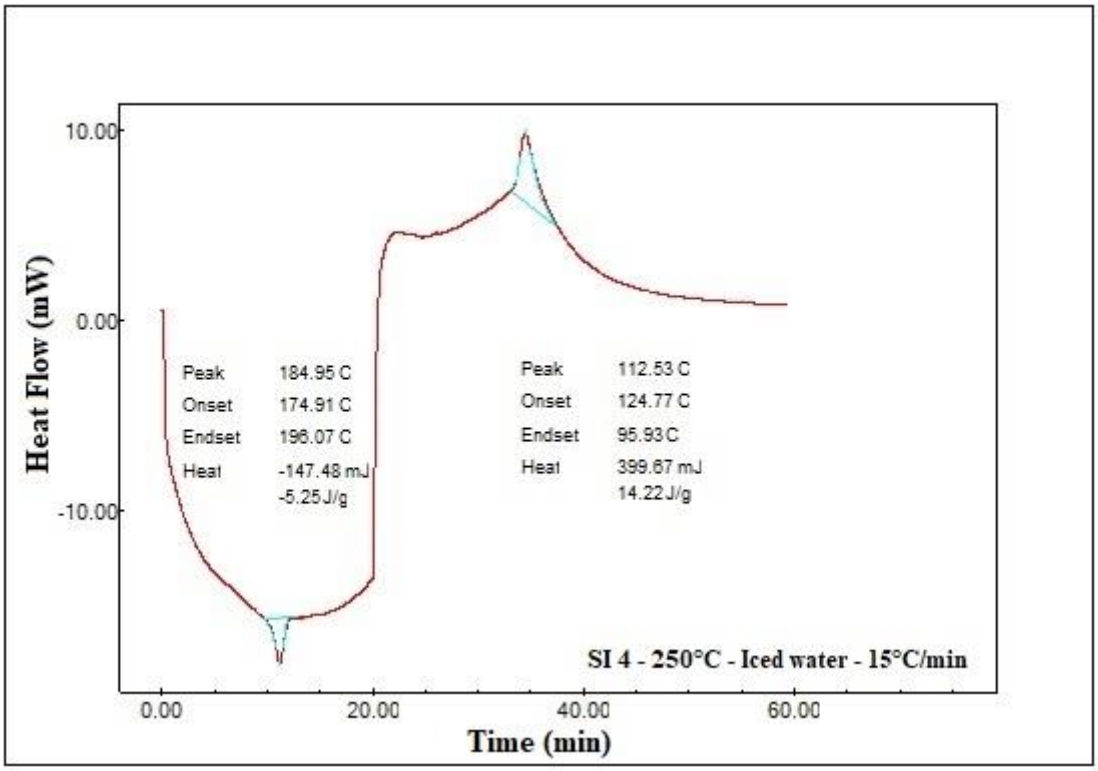
10.00
0.00
-10.00
Heat Flow (mW)
Peak 184.95 C
Onset 174.91 C
Endset 196.07 C
Heat -147.48 mJ
-5.25 J/g
Peak 112.53 C
Onset 124.77 C
Endset 95.93 C
Heat 399.67 mJ
14.22 J/g
SI 4 - 250°C - Iced water - 15°C/min
0.00
20.00
40.00
60.00
Time (min)

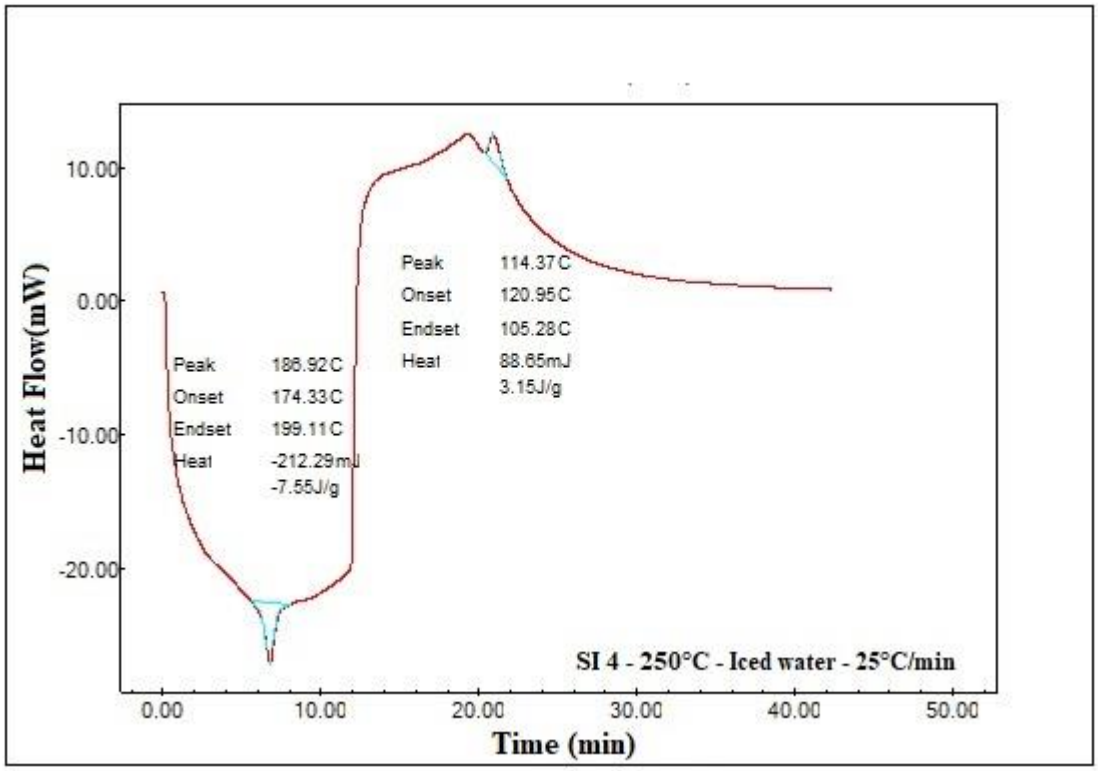

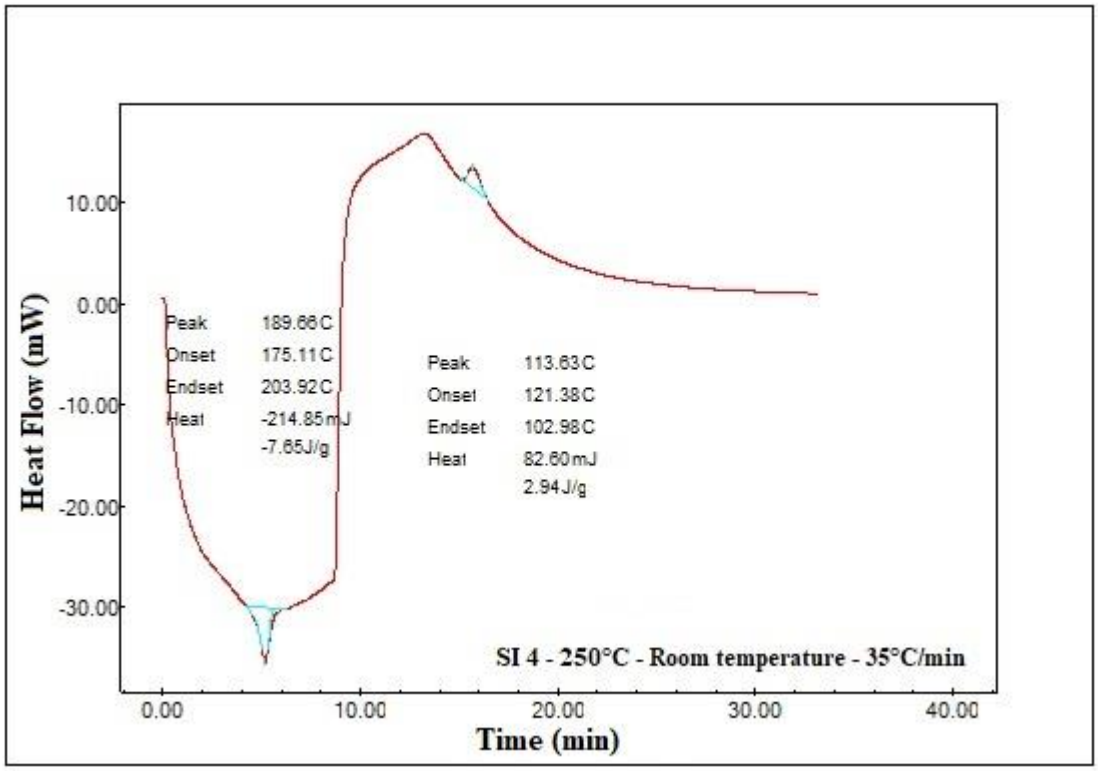

DSC of SI-4 quenched in iced water at a heating/cooling rate of 5, 15, 25 and 35 ˚C/min

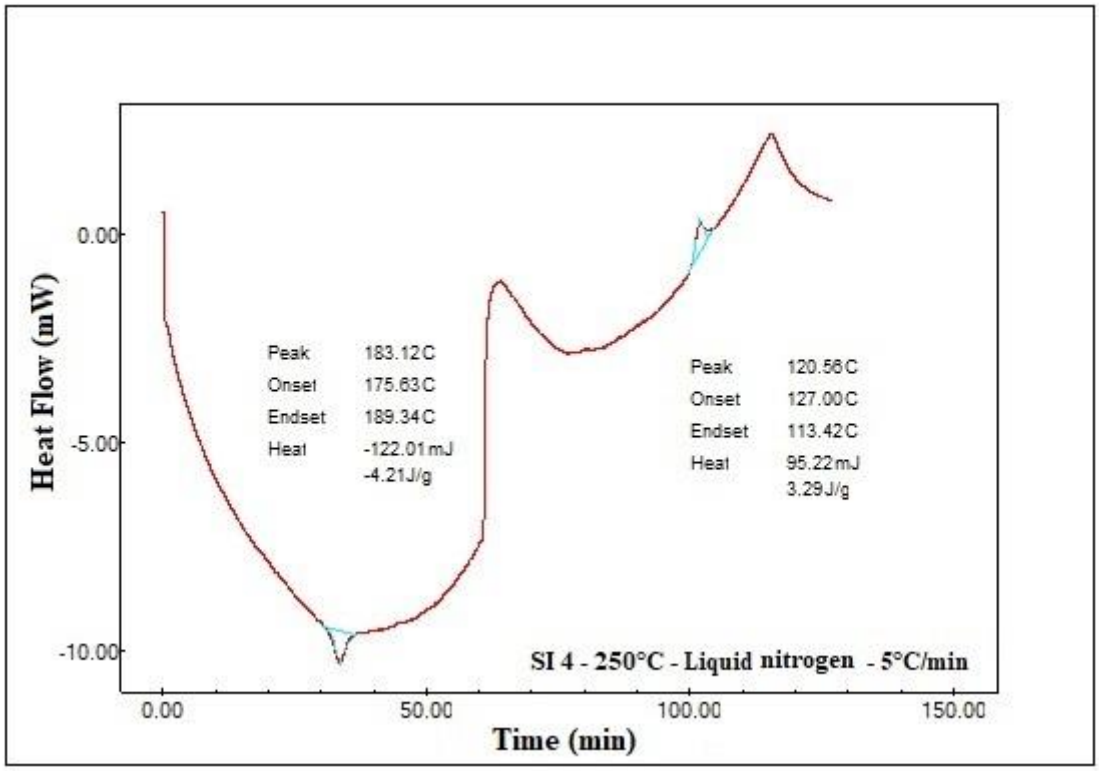
Heat Flow (mW)
0.00
-5.00
-10.00
Peak 183.12C
Onset 175.63C
Endset 189.34C
Heat -122.01mJ
-4.21J/g
Peak 120.56C
Onset 127.00C
Endset 113.42C
Heat 95.22mJ
3.29J/g
SI 4 - 250°C - Liquid nitrogen - 5°C/min
0.00
50.00
100.00
150.00
Time (min)

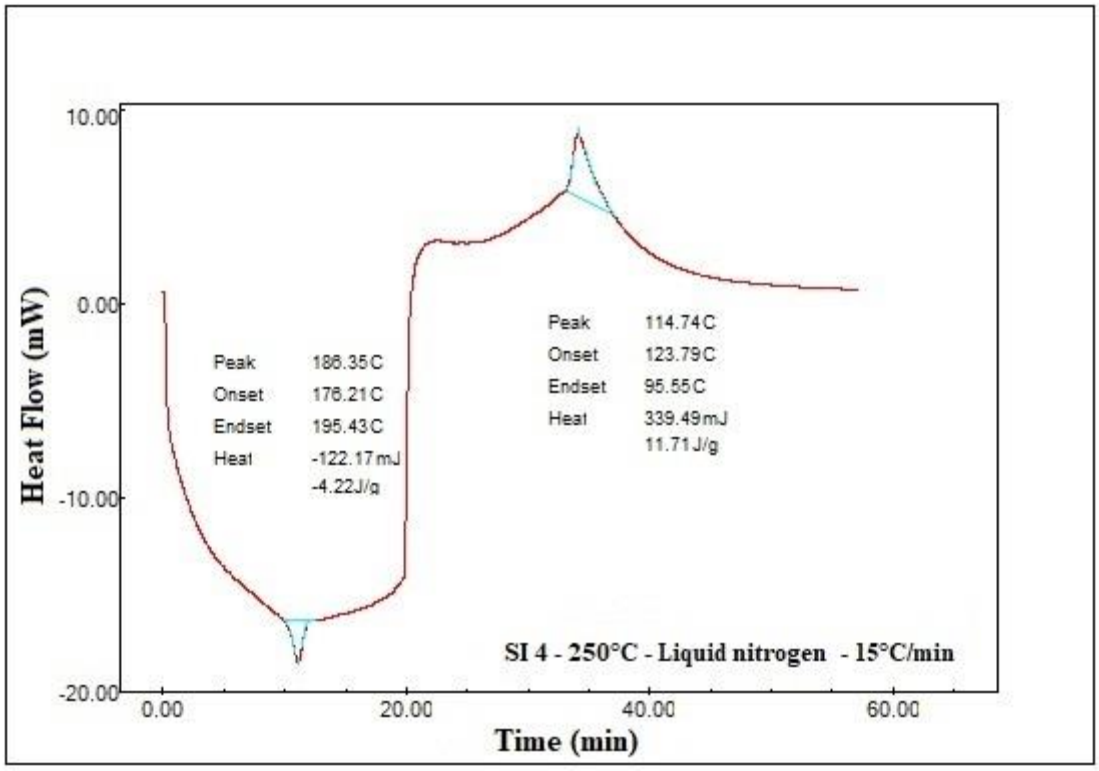
Heat Flow (mW)
10.00
0.00
-10.00
-20.00
Peak 186.35C
Onset 176.21C
Endset 195.43C
Heat -122.17mJ
-4.22J/g
Peak 114.74C
Onset 123.79C
Endset 95.55C
Heat 339.49mJ
11.71J/g
SI 4 - 250°C - Liquid nitrogen - 15°C/min
0.00
20.00
40.00
60.00
Time (min)

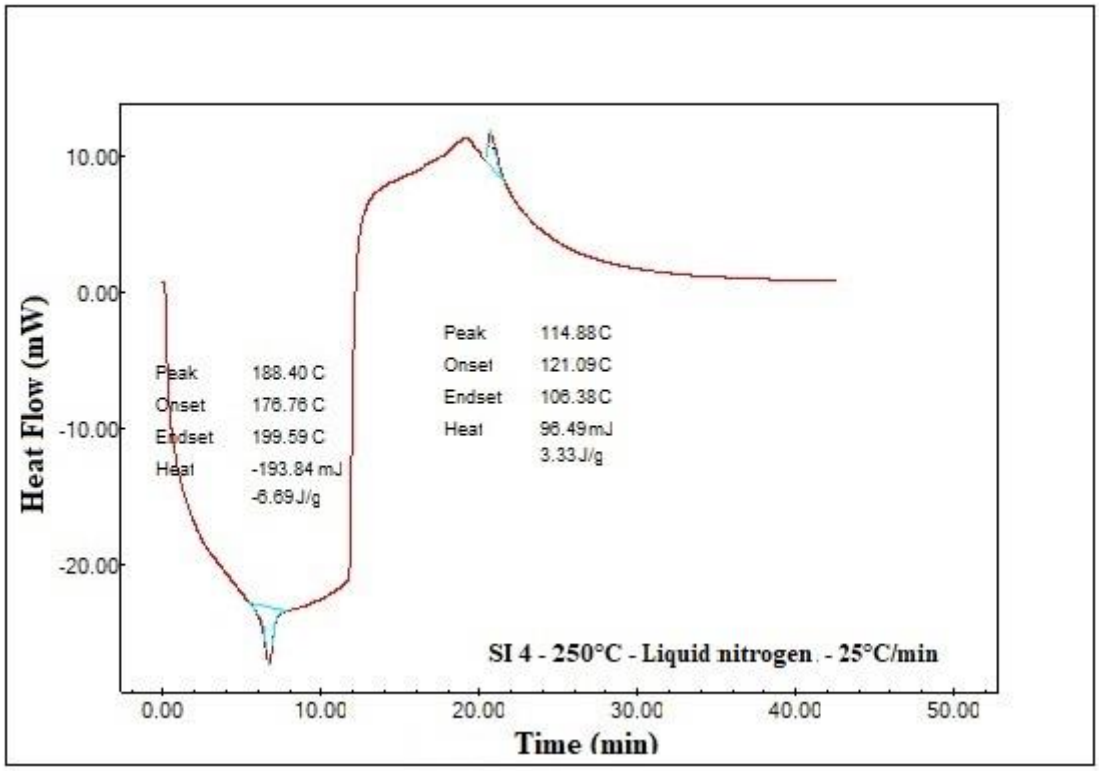

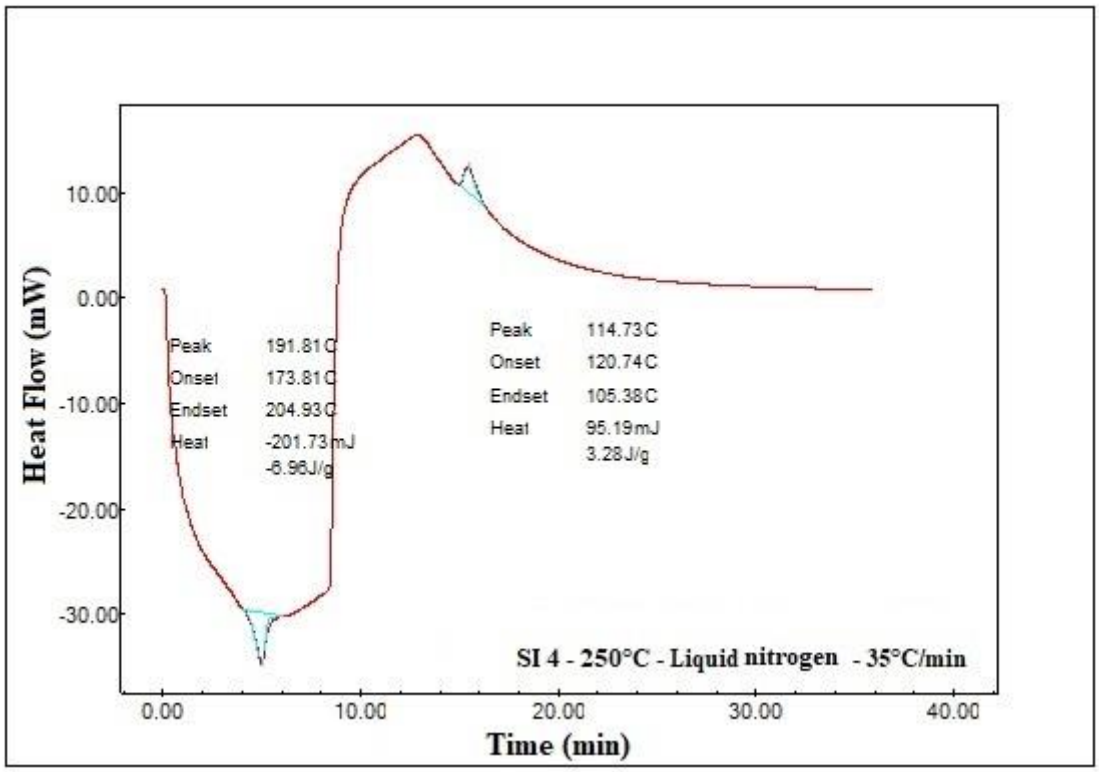

DSC of SI-4 quenched in liquid nitrogen at a heating/cooling rate of 5, 15, 25 and 35 ˚C/min

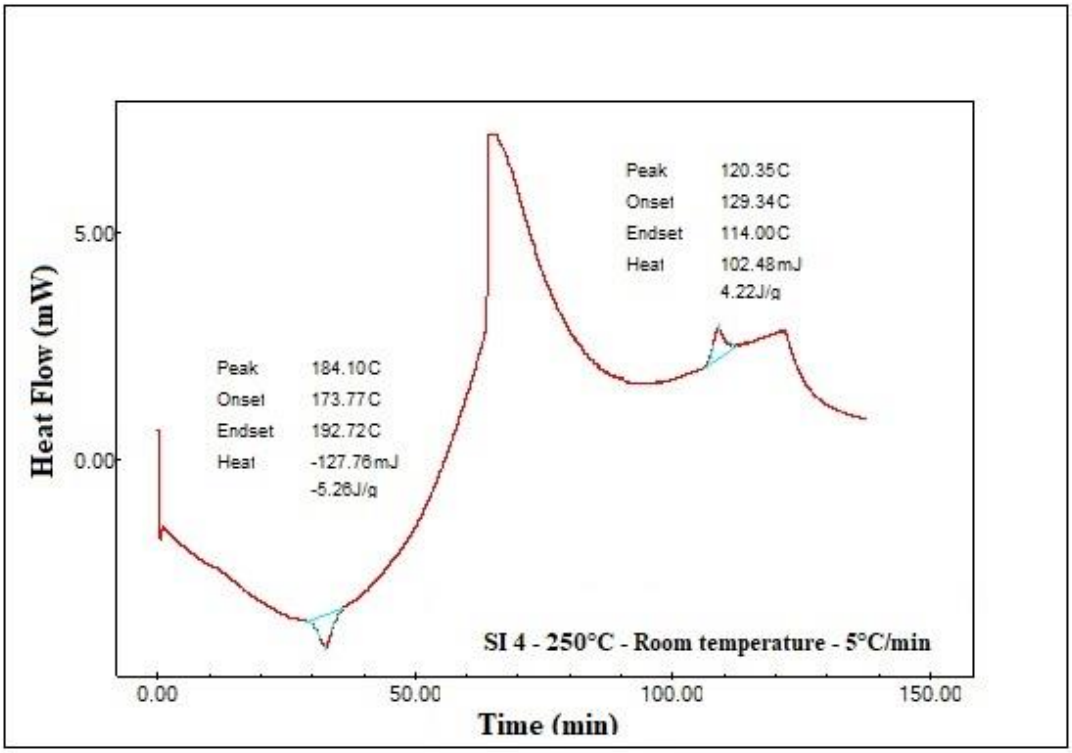
Peak 120.35 C
Onset 129.34 C
Endset 114.00 C
Heat 102.48 mJ
4.22 J/g
Peak 184.10 C
Onset 173.77 C
Endset 192.72 C
Heat -127.76 mJ
-5.26 J/g
5.00
0.00
Heat Flow (mW)
SI 4 - 250°C - Room temperature - 5°C/min
0.00
50.00
100.00
150.00
Time (min)

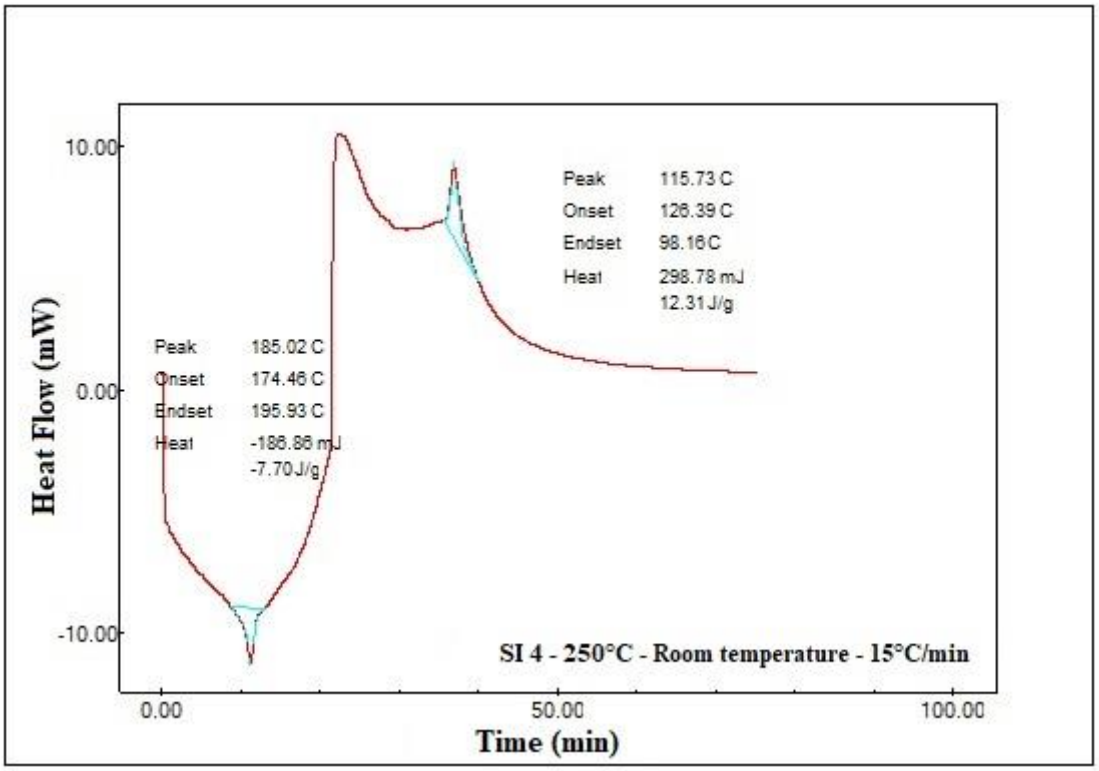
Peak 115.73 C
Onset 126.39 C
Endset 98.16 C
Heat 298.78 mJ
12.31 J/g
Peak 185.02 C
Onset 174.46 C
Endset 195.93 C
Heat -186.86 mJ
-7.70 J/g
10.00
0.00
-10.00
Heat Flow (mW)
SI 4 - 250°C - Room temperature - 15°C/min
0.00
50.00
100.00
Time (min)

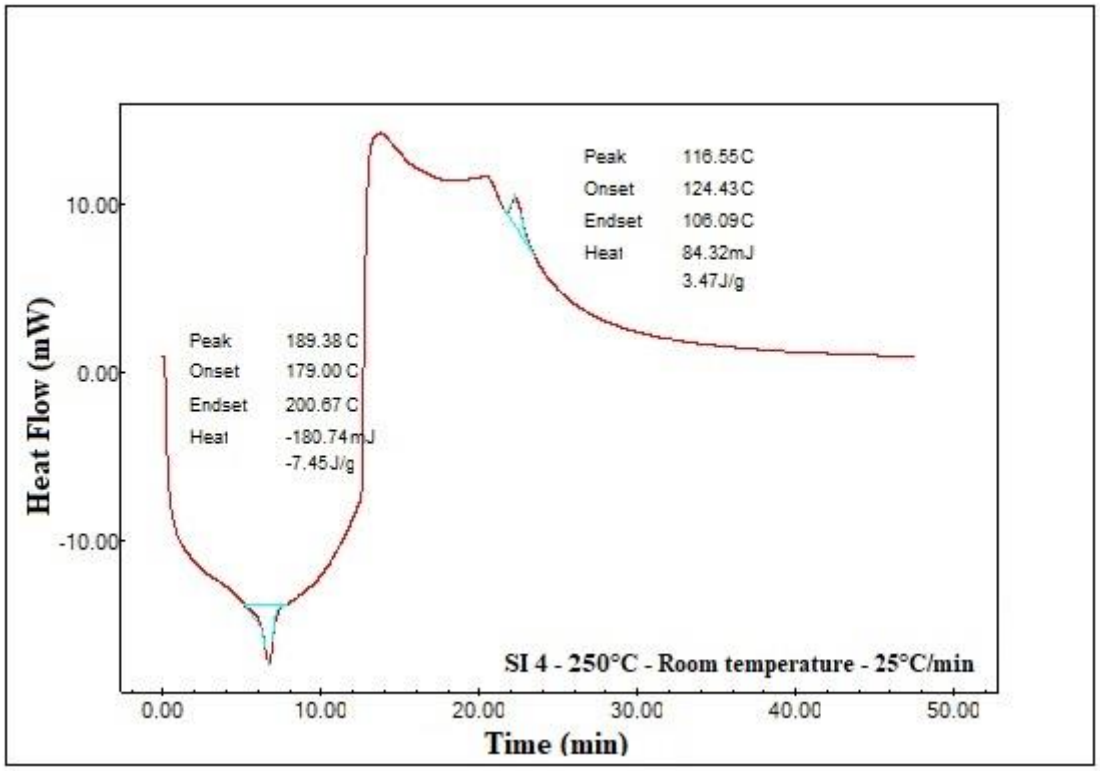

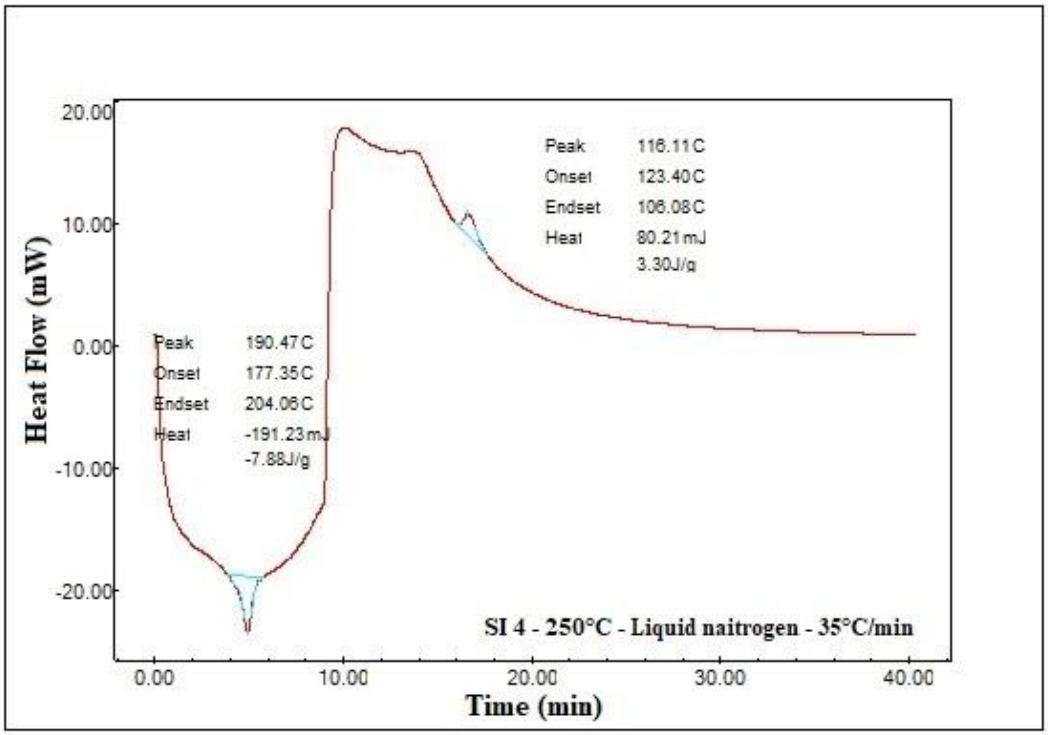

DSC of SI-4 quenched at room temperature at a heating/cooling rate of 5, 15, 25 and 35 ˚C/min

(C.V.)

Curriculum Vitae

PERSONAL INFORMATION:

Name: Sivar Aziz

Surname: Baiz

Date of Birth: 01.June.1992

Place of Birth: Ranya-Sulaimanyeh-Iraq

Nationality: Iraqi

Marital status: Engaged

Email address: Sivaraziz0@gmail.com

Mobile no.: 00964-7502008387

EDUCATION:

High-school: 5th AZAR Highschool-Ranya (2007-2009)

Undergraduate(BSc): Sulaimanyeh University-Faculty of Science-Physics Department (2010-2014)

LANGUAGES:

KURDISH: Native (Mather language)

ENGLISH: Advanced ([89/100] according to -Firat University-TOMER-English proficiency Exam)

ARABIC: Good

TURKISH: Good

EXPERIENCE:

- I worked in LEYBOLD -LD DIDACT company which is a German company for academic devices and set up of laboratories (2015-2017) and in (2018- current time).

PROJECTS:

Optical Properties of Galaxies using the Millennium Simulation program. Undergraduate project(2014).

COMPUTER PROGRAMMING AND SKILLS:

- Microsoft Office (Word, Excel, PowerPoint, etc.)
- FORTRAN
- ORIGIN for graphing

ACADEMIC PUBLICATIONS:

➢ Articles:

1. Canbay, C. A., Karaduman, O., Ünlü, N., **Baiz, S. A**., & Özkul, İ. (2019). Heat treatment and quenching media effects on the thermodynamical, thermoelastic and structural characteristics of a new Cu-based quaternary shape memory alloy. *Composites Part B: Engineering*, 106940.
2. Canan Aksu Canbay, **Sivar Aziz Baiz**, İskender Özkul, Aysegul Dere. (2019) The effect of e/a ratio on thermodynamic parameters and surface morphology of Cu–Al–Fe–X shape memory alloys. Journal of Thermal Analysis and Calorimetry
3. Karaduman, O., Ünlü, N., Canbay, C. A., Özkul, İ., & **Baiz S. A.** (2019). The Investigation of SME in a Cu-Al-Ni HTSMA. *Journal of Materials and Electronic Devices 2,*(1), 6-10.
4. Karaduman, Oktay, Canan Aksu Canbay, İskender Özkul, **Sivar Aziz Baiz**, and Nihan Ünlü. "The Production and Characterization of Ternary Heusler Shape Memory Alloy with A New Composition." *Journal of Materials and Electronic Devices* 2, no. 1 (2018): 16-19.
5. Nihan Ünlü, Canan Aksu Canbay, İskender Özkul, **Sivar Aziz Baiz**, Karaduman, Oktay. "THE INVESTIGATION OF SME IN Cu-Al BASED SMA." *Journal of Materials and Electronic Devices*, no. 1 (2018): 16-19.

➢ Conference Papers, Proceeding Book and Oral presentations:

1. **Baiz, S. A.**, Canbay, C. A., & Ozkul, I. (2018, November). The investigation of thermodynamic and structural parameters in Cu-Al-Fe-Mn SMAs. In *AIP Conference Proceedings* (Vol. 2042, No. 1, p. 020038). AIP Publishing.
2. **BAIZ, S**., CANBAY, C., & KARADUMAN, O. Classification and Applications of SMA. 5th International Conference on Materials Science and Nanotechnology for Next Generation (MSNG2018). Volume: Full-text book, page:357-359.

3. Canan Aksu Canbay, Nihan Unlu, **Sivar Aziz**, Oktay Karaduman A, Iskender Özkul. (2018). Mathematical Model for NiTi Alloy Thermal Process. 5th International Conference on Materials Science and Nanotechnology for Next Generation (MSNG2018). Volume: Full-text book, page:357-359.
4. Safiye Jameel BIROO, Canan AKSU CANBAY, **Sivar Aziz**, İskender Özkul. (2018).”Structural properties of CdO-ZnO Semiconductor Composite” International Engineering and technology symposium .Batman University.
5. Canan Aksu Canbay, İskender Özkul, Ece Kalay, Aysegul Dere, **S.Aziz Baiz**. (2019). “Force Effect on Martensite Transformation Temperature” .OEMT, Dubai.